

FLUORESCENCE IMAGING FOR NUCLEAR ARMS CONTROL VERIFICATION

A Dissertation

by

JESSICA SHAWN FEENER

Submitted to the Office of Graduate and Professional Studies of  
Texas A&M University  
in partial fulfillment of the requirements for the degree of

DOCTOR OF PHILOSOPHY

Chair of Committee,	William S. Charlton
Committee Members,	Marvin L. Adams
	David R. Boyle
	Charles Hermann
Head of Department,	Yassin A. Hassan

August 2014

Major Subject: Nuclear Engineering

Copyright 2014 Jessica Shawn Feener

## ABSTRACT

Nuclear disarmament is a highly debated subject. Proponents argue that political conditions for nuclear disarmament are ripe. Opponents reason that dismantlement could create instability leading to a higher probability of nuclear war or large-scale conventional war. Verification of disarmament can help alleviate instabilities and as nuclear arsenals decrease, verifying actual warheads and not just delivery vehicles will become more important. Current techniques that could be used in warhead verification have the ability to reveal sensitive information about the warhead and thus require an information barrier.

This research developed a proof-of-principle concept for a new technique to address the need of nuclear warhead verification for arms control treaties. Specifically, this technique uses fluorescence imaging to determine fissile material attributes in verifying, during the dismantlement process, an uncanned nuclear warhead or warhead component without revealing sensitive information. This could potentially reduce the need for an information barrier.

Experiments were performed using a Princeton Instruments PIXIS: 1024B/BUV back-illuminated CCD camera to image the fluorescence produced by the decay of nuclear material. The Monte Carlo simulation tool GEANT4 was used to model the experimental setups and to compare with the experimental results. The results verified the proof-of-concept of fluorescence imaging for use in nuclear arms control treaty verification.

Fluorescence imaging would be most beneficial for assessing the fissile material attributes of U enrichment (greater than a threshold) and symmetry. It also contributes valuable data for verifying the presence of fissile material, presence of Pu, presence of U, mass greater than a threshold, Pu age, and  $^{239}\text{Pu}$  to  $^{240}\text{Pu}$  ratio greater than a threshold. Fluorescence imaging may also be beneficial to the “absence of oxide” attribute, but additional experiments are needed to confirm this assumption. Additionally, it was concluded that the only potential for revealing presumably sensitive information is the ability to provide too much image detail on external surfaces of Pu components. However, simple steps could be taken to prevent the imaging system from acquiring too much detail and thus eliminate the need for an information barrier.

## DEDICATION

To my family.

## ACKNOWLEDGEMENTS

I would like to express gratitude my advisor and committee chair, Dr. William Charlton, for his years of guidance and support during my time in graduate school. I would also like to thank my committee members, Dr. Adams, Dr. Boyle, and Dr. Hermann for their advice and assistance throughout the course of this research.

Thanks also go to my friends, colleagues and the department faculty and staff at Texas A&M University. Your friendship, mentoring, and challenges have made my time as a graduate student a rewarding experience.

Finally, I am grateful to my mother, father, and husband for their encouragement and love.

This research was performed under appointment to the Nuclear Nonproliferation International Safeguards Graduate Fellowship Program sponsored by the National Nuclear Security Administration's Next Generation Safeguards Initiative (NGSI).

## NOMENCLATURE

BG	Background
CCD	Charged Coupled Device
CSV	Comma Separated Variable
FMCT	Fissile Material Cutoff Treaty
GEANT4	GEometry ANd Tracking
H.D.Poly	High Density Polyethylene
HE	High Explosives
HEU	Highly Enriched Uranium
ICBM	Intercontinental Ballistic Missiles
LEU	Low Enriched Uranium
NNWS	Non-Nuclear Weapon State
NWS	Nuclear Weapon State
NPT	Nuclear Nonproliferation Treaty
PNI	Presidential Nuclear Initiatives
SALT	Strategic Arms Limitation Talks
SLBM	Submarine-Launched Ballistic Missiles
SORT	Strategic Offensive Reductions Treaty
START	Strategic Arms Reduction Treaty
UV	Ultra Violet

## TABLE OF CONTENTS

	Page
ABSTRACT .....	ii
DEDICATION .....	iv
ACKNOWLEDGEMENTS .....	v
NOMENCLATURE .....	vi
TABLE OF CONTENTS .....	vii
LIST OF FIGURES .....	ix
LIST OF TABLES .....	xiii
CHAPTER I INTRODUCTION .....	1
I.A. Motivation .....	1
I.B. Overview of Nuclear Weapons, Dismantlement, and Verification .....	2
I.C. Fluorescence Background Information and Theory .....	5
I.D. Objectives .....	10
CHAPTER II OVERVIEW OF NUCLEAR ARMS CONTROL TREATIES AND VERIFICATION METHODOLOGIES .....	12
II.A. Past, Present, and Future Nuclear Arms Control Agreements and Treaties .....	12
II.B. Fissile Material Verification Methodologies .....	16
II.C. Overview of Fissile Material Verification Technologies .....	18
CHAPTER III EXPERIMENTS .....	22
III.A. Imaging System .....	22
III.B. Sources and Other Experimental Material .....	24
III.C. General Set-up and Procedure .....	28
III.D. Image Analysis .....	30
III.E. Experimental Set-ups and Results .....	32
III.F. Experimental Conclusions Summary .....	65
CHAPTER IV SIMULATIONS .....	69
IV.A. Simulation Overview .....	69
IV.B. Simulation Results .....	74

IV.C. Simulation Remarks and Summary .....	93
CHAPTER V SUMMARY AND CONCLUSIONS .....	96
REFERENCES .....	102
APPENDIX A SUPPLEMENTAL INFORMATION .....	109
APPENDIX B SAMPLE GEANT4 GPS AND HEADER FILES .....	111
APPENDIX C SAMPLE PYTHON FILES .....	132



## LIST OF FIGURES

	Page
Figure 1. Schematic of the energy states of the 2P and 1N electronic-vibrational states of $N_2$ and $N_2^+$ .....	6
Figure 2. Nitrogen fluorescence spectrum between 300 and 400 nm .....	7
Figure 3. Quantum efficiency curve for the PIXIS: 1024B/BUV .....	23
Figure 4. Photograph of $^{210}Po$ source. ....	24
Figure 5. Photograph of depleted $UO_3$ in a plastic petri dish. ....	25
Figure 6. Photograph of U metal specimen next to half silver dollar and quarter. ....	25
Figure 7. Photograph of light-tight-black-box open.....	29
Figure 8. Photograph of light-tight-black-box closed. ....	29
Figure 9. Image process example 1. ....	31
Figure 10. Image process example 2. ....	32
Figure 11. Experimental Set-up: Specimen on source stand at 25 cm from camera lens. ....	33
Figure 12. Montage of the analyzed images from single U metal specimens, front facing. ....	34
Figure 13. Standard deviation and mean versus enrichment of the four highest enriched images from single U metal specimens, front facing .....	35
Figure 14. Standard deviation versus source strength of the four highest enriched images plus background from single U metal specimens, front facing.....	35
Figure 15. Experimental Set-up: Camera facing down and specimen lying on surface .....	38
Figure 16. Montage of the analyzed images from multiple U metal specimens, front facing .....	39

Figure 17. Standard deviation and mean versus added enrichment of images from multiple U metal specimens, front facing. ....	40
Figure 18. Standard deviation versus the added source strength of images from multiple U metal specimens, front facing. ....	41
Figure 19. Standard deviation and mean versus added enrichment of images from the single and multiple U metal specimens, front facing set-ups. ....	42
Figure 20. Experimental Set-up: Camera facing down and specimen sitting sideways .....	43
Figure 21. Close-up example of specimens sitting sideways configuration (shown as quarters).....	44
Figure 22. Montage of the analyzed images from multiple U metal specimens, side facing.....	44
Figure 23. Standard deviation and mean versus added enrichment of images from multiple U metal specimens, side facing.....	45
Figure 24. Standard deviation versus the added source strength of images from multiple U metal specimens, side facing.....	46
Figure 25. Standard deviation and source strength versus enrichment of images from multiple U metal specimens, side facing.....	47
Figure 26. Montage of UO <sub>3</sub> in petri dishes. ....	48
Figure 27. Standard deviation and mean versus UO <sub>3</sub> enrichment in a plastic petri dish. ....	49
Figure 28. Standard deviation versus UO <sub>3</sub> source strength in a plastic petri dish .....	50
Figure 29. <sup>210</sup> Po source upside down alone and in a plastic petri dish to show plastic scintillation.....	51
Figure 30. Natural UO <sub>3</sub> in metal dish.....	52
Figure 31. Experimental set-up: <sup>210</sup> Po source with H.D.Poly held ~4cm above.....	53
Figure 32. Montage of <sup>210</sup> Po source with different thicknesses of H.D.Poly.....	54

Figure 33. Standard Deviation and Mean for $^{210}\text{Po}$ source with different thicknesses of H.D.Poly. ....	56
Figure 34. Standard Deviation and Mean for $^{210}\text{Po}$ source with different thicknesses of H.D.Poly – bar graph. ....	57
Figure 35. Montage of $^{210}\text{Po}$ source with Fe foil, black plastic, and background. ....	59
Figure 36. Standard deviation and mean of $^{210}\text{Po}$ source with non-translucent materials. ....	60
Figure 37. Mean and standard deviation of beta and gamma sources. ....	61
Figure 38. Montage of $^{210}\text{Po}$ source at various distances. ....	62
Figure 39. Mean and standard deviation of $^{210}\text{Po}$ source at various distances. ....	63
Figure 40. Photograph of $^{210}\text{Po}$ source surrounded by polyethylene beads. ....	64
Figure 41. Montage of $^{210}\text{Po}$ source images at 100 cm alone for 5 minute (left) and in polyethylene beads for 30 minutes (right). ....	65
Figure 42. Screenshot of the 93% U metal specimen and associated plot profile. ....	71
Figure 43. Alpha energy distribution comparison from GEANT4 and experimental result. ....	72
Figure 44. Montage of the simulated images from single U metal specimens, front facing – each image has individual intensity scale ....	76
Figure 45. Montage of the simulated images from single U metal specimens, front facing – all images on the same intensity scale. ....	77
Figure 46. Normalized standard deviation, mean, and source strength versus enrichment from simulated images of single U metal specimens, front facing. ....	78
Figure 47. Normalized standard deviation, mean, and source strength with background added. ....	79
Figure 48. Simulated and experimental standard deviation versus enrichment for single U metal specimens, front facing. ....	81

Figure 49. Montage of the simulated images from multiple U metal specimens, front facing - each image has individual intensity scale. ....	83
Figure 50. Montage of the simulated images from multiple U metal specimens, front facing - all images on the same intensity scale.....	84
Figure 51. Normalized standard deviation, mean, and source strength versus enrichment from simulated images of multiple U metal specimens, front facing .....	85
Figure 52. Simulated and experimental standard deviation versus enrichment for multiple U metal specimens, front facing .....	85
Figure 53. Montage of the simulated images from multiple U metal specimens, side facing - each image has individual intensity scale. ....	87
Figure 54. Montage of the simulated images from multiple U metal specimens, side facing - all images on the same intensity scale. ....	88
Figure 55. Normalized standard deviation, mean, and source strength versus enrichment from simulated images of multiple U metal specimens, side facing .....	89
Figure 56. Simulated and experimental standard deviation versus enrichment for multiple U metal specimens, side facing.....	89
Figure 57. Montage of the simulated UO <sub>3</sub> in plastic petri dish.....	90
Figure 58. Normalized standard deviation, mean, and source strength versus enrichment from simulated images of UO <sub>3</sub> .....	91
Figure 59. Simulated and experimental standard deviation versus enrichment for UO <sub>3</sub> .....	91
Figure 60. Comparison of <sup>210</sup> Po source images.....	92

## LIST OF TABLES

	Page
Table 1. Specific Activities and Main Alpha Energy of Isotopes of Interest.....	10
Table 2. Status and Significant Dates of Nuclear Arms Control Agreements .....	13
Table 3. Treaty Limits and Verification Status of Nuclear Arms Control Agreements .....	14
Table 4. Isotopics of U Metal Specimens .....	26
Table 5. Number of Particles per Unit Time at Source Surface.....	27
Table 6. Ranges for 5.3 MeV Alpha Particles.....	28
Table 7. Mean and Standard Deviation Values from Single U Metal Specimens, Front Facing.....	34
Table 8. Mean and Standard Deviation Values from Multiple U Metal Specimens, Front Facing.....	40
Table 9. Mean and Standard Deviation Values from Multiple U Metal Specimens, Side Facing .....	45
Table 10. Mean and Standard Deviation Values from UO <sub>3</sub> in a Plastic Petri Dish .....	49
Table 11. Mean and Standard Deviation Values from UO <sub>3</sub> in a Metal Dish .....	52
Table 12. Mean and Standard Deviation Values of <sup>210</sup> Po with Different Thicknesses of H.D.Poly .....	55
Table 13. Mean and Standard Deviation Values for the <sup>210</sup> Po Source at Various Distances.....	62
Table 14. Percent Change in Mean for Different Values of Added Background .....	80
Table 15. Fissile Material Attribute Verification Summary.....	98

# CHAPTER I

## INTRODUCTION

### **I.A. Motivation**

Proponents of nuclear disarmament contended that political conditions for disarmament are ripe. Reasons to support this claim include the fact that the New Strategic Arms Reduction Treaty (START) is signed, ratified and entered into force and there is talk of further cuts in the size of the United States' and the Russian Federation's nuclear arsenals. Additionally, there is global pressure from Non-Nuclear Weapon States (NNWS) party to the Nuclear Nonproliferation Treaty (NPT) for Nuclear Weapon States (NWS) to uphold their nuclear disarmament obligations.<sup>1,2,3,4</sup> Opponents of nuclear disarmament argue that the deterrent value of nuclear weapons has created stability and that dismantlement could create instability leading to a higher probability of nuclear war or large-scale conventional war.<sup>5,6</sup> The willingness of a state to agree to (further) reductions in their nuclear arsenals will, as in any treaty, depend on how it envisions the benefits and consequences; "its ability to balance threats and opportunities against decreased nuclear capabilities."<sup>7</sup>

Verification of the disarmament and dismantlement process can help alleviate instability by ensuring that "all nuclear-armed states are fulfilling their commitments, giving each state added confidence that the threats of nuclear conflict are diminishing."<sup>7</sup> Additionally, as nuclear warhead numbers decrease, verifying actual warheads and warhead components and not just delivery vehicles will become more important as "any uncertainties in the arsenals of other states can become more destabilizing since the

number of weapons needed by them to pose a significant military threat becomes correspondingly smaller.”<sup>7</sup> Therefore, if techniques to verify warhead dismantlement to a high confidence level are proven, states would feel less vulnerable from (further) decreases in their nuclear arsenals. Verification also builds confidence, trust and transparency between states.

While confidence between states party to an arms control treaty is essential, transparency can lead to problems because of secrecy surrounding nuclear weapons. Some techniques that can be used to verify warhead dismantlement to a high confidence level can reveal sensitive information about the warhead. This sensitive information could include the mass and isotopics of the nuclear material, dimension of the nuclear cores, and detailed design of the engineered components. Technologies, such as information barriers, have been developed to protect sensitive information, but there is still some controversy surrounding this issue.<sup>8,9</sup> If a verification technology was developed that could verify a warhead, warhead component, or step in the dismantlement process without revealing sensitive information it would be an improvement on current techniques.

### **I.B. Overview of Nuclear Weapons, Dismantlement, and Verification**

In order to have a nuclear explosive device you must have fissile material, defined as material that is capable of undergoing fission after capturing thermal neutrons, and more specifically you must have special fissile material which includes Highly Enriched Uranium (HEU) and weapons grade plutonium (Pu). HEU is defined as uranium with a <sup>235</sup>U content greater than 20%. Most warheads would have enrichment

closer to 90%  $^{235}\text{U}$ . Weapons grade Pu typically contains more than 90%  $^{239}\text{Pu}$ .<sup>10</sup> Additionally, the fissile material must be in metallic form.

There are many different nuclear warhead designs, but there are three general warhead types: gun-type, implosion and thermonuclear. In a gun-type device, two subcritical components of HEU are combined using High Explosives (HE) to make a supercritical configuration. An implosion device uses HE (also known as the physics package) to implode a spherical ‘pit’ of HEU or weapons grade Pu into a supercritical configuration. A thermonuclear device combines an implosion device, known as the primary, with a secondary fusion device composed of uranium and lithium deuteride. Most modern weapons contain a thermonuclear warhead. Gun-type devices are essentially obsolete.<sup>6,11</sup>

The term nuclear warhead is rarely defined and often used interchangeably with nuclear weapon. In this work, nuclear weapon will be defined as a nuclear warhead plus its delivery vehicle. A nuclear warhead will be defined as the fissile material and other components (physics package, secondary, etc.) that make up the nuclear explosive device. A warhead component will be defined as all or some of the fissile material in the nuclear warhead.

As there are many warhead designs, the specific dismantlement of each is unique. Additionally, states operate their dismantlement systems differently. In spite of this, some commonalities can be made. In general, nuclear weapon dismantlement is a process that includes:

1. Retirement of a weapon and storage of the retired weapon



2. Transportation to a disassembly site
3. Weapon disassembly (nuclear warhead from delivery vehicle)
4. Warhead disassembly (fissile material from physics package)
5. Fissile material component storage and non-nuclear component disposition
6. Further disassembly of fissile material components and conversion into non-weapons usable material.

In general, “a warhead is considered to be fully dismantled when the HE is removed from the ‘pit’.”<sup>12</sup> To help safeguard against rapid re-arming, verification of the disassembly and conversion of fissile material components into non-usable weapons material is important.<sup>6</sup> There is also verification of weapon and fissile material stockpiles, production capabilities, and monitoring of fuel cycle facilities, but this is beyond the scope of weapon dismantlement verification.

The verification regime of the weapons dismantlement process will depend on what is agreed to by the states party to the treaty. Full scope weapon dismantlement verification would begin with a state declaring that a weapon is to be retired or that an already retired weapon is to be dismantled. Each step of the dismantlement process would be verified down to the conversion of fissile material to non-weapons useable form. On the other hand, states could agree to only verify one step in the dismantlement process, such as weapon disassembly or warhead disassembly. The earlier that verification is started, the higher the confidence that the item being verified is as declared.

Verification activities can include, but are not limited to, national technical means, item and facility inspections, tamper indicating tags and seals, and radiation detection. National technical means refers to systems such as reconnaissance satellites used to collect information for verifying compliance with treaty provisions.<sup>13</sup> Facility inspections can be planned or surprise visits and may allow the inspectors different levels of access. Inspectors may look for the presence or absence of certain processes or items. Tags and seals can be used to verify that once an item is inspected it has not been tampered with. Radiation detection is used to verify the removal of fissile material and is discussed in more detail in Chapter II.C. Additional information on verification activities can be found in references 6, 12, 14, 15, 16, and 17.

### **I.C. Fluorescence Background Information and Theory**

When charged atomic or nuclear particles pass through matter, they dissipate their energy in the excitation and ionization of the molecules (or atoms) in the surrounding material. Uncharged radiations, such as gamma rays or neutrons, produce secondary charged particles in their interaction through matter. The secondary charged particles will then deposit their energy through excitation and ionizations. The excited molecules de-excite radiatively through the emission of photons (light) or nonradiatively, known as quenching, mainly through heat.

Luminescence is the emission of light (visible or ultraviolet [UV]) with a characteristic spectrum, following the absorption of radiation. In organic molecules, it is an inherent molecular property and arises from the electronic structure of these molecules; luminescence is exhibited in the solid, liquid, and gas states. In contrast, the

luminescence of inorganic materials is a crystalline property, normally not exhibited in other phases.<sup>18</sup>

In this work, we are mainly concerned with luminescence from organic molecules. The fluorescence photons of interest are from the de-excitation of nitrogen molecules in air. Radiation from a source deposits its energy in the surrounding air by exciting and ionizing air molecules. Nitrogen molecules make up ~76% of air and emit photons in a band spectrum, where nearly all the photons are emitted in the near UV range with wavelengths between 300 and 400 nm.<sup>19,20</sup> This band structure is caused by the vibrational (and rotational) movements of the molecular nuclei which modify the energy states of the electrons. The electronic molecular state is split into several vibrational levels each having a rotational substructure. The fluorescence spectrum is created almost entirely from transitions of the second positive (2P) band system in  $N_2$  and the first negative (1N) band system of  $N_2^+$ .<sup>21</sup> This is shown schematically in Figure 1.

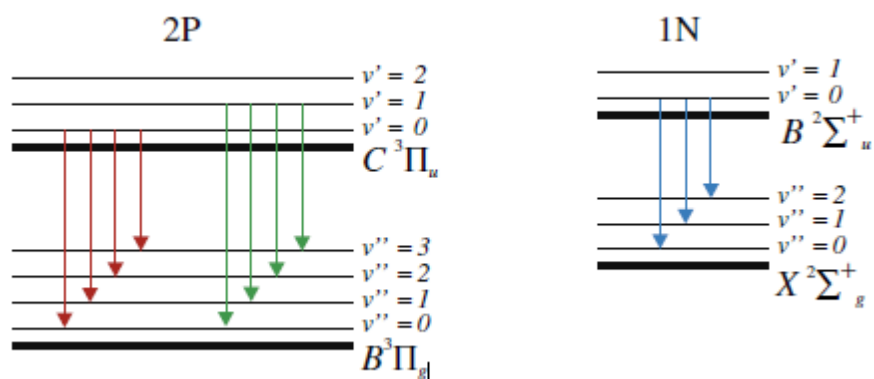


Figure 1. Schematic of the energy states of the 2P and 1N electronic-vibrational states of  $N_2$  and  $N_2^+$ .<sup>21</sup>

The electronic bands are established by all electronic-vibrational states having the same initial and final electronic state. The spectroscopic notation for this transaction is  $C^3\Pi_u(v') \rightarrow B^3\Pi_g(v'')$  for the 2P system and  $B^2\Sigma_u^+(v') \rightarrow X^2\Sigma_g^+(v'')$  for the 1N system where  $v'$  and  $v''$  are the initial and final vibrational levels, respectively. The corresponding spectral bands are shown in Figure 2 and are drawn in the same colors.

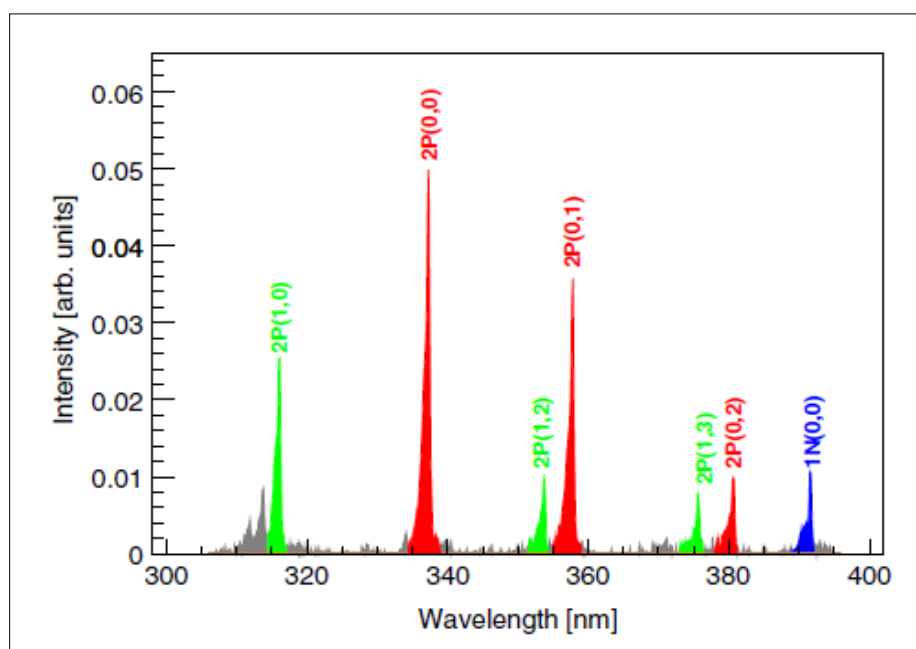


Figure 2. Nitrogen fluorescence spectrum between 300 and 400 nm.<sup>21</sup>

To image the fluorescence photons, an imaging system simply needs to have high sensitivity in the wavelength region of interest. Common image sensors are charge-coupled device (CCD) chips. The CCD chip is an array of semiconductor capacitors with each capacitor representing a pixel. Incident photons are converted into an electric charge proportional to the light intensity deposited in the pixel during an exposure. At

the end of the exposure, these charges are shifted from one pixel to another and collected to create an array of voltages. The image is the display of the electric distribution.<sup>22</sup>

Imaging fluorescence photons excited by radiation is considered a low-light application. Because solar and man-made light cover the same wavelength range as the molecular nitrogen fluorescence spectrum, images must be acquired in darkness. Additionally, dark current and background sources of fluorescence light should be minimized. Dark current is caused by electrons being thermally excited in a CCD pixel. Dark current is temperature and exposure time dependent. To minimize thermally excited electrons, CCDs can be cooled.

This imaging technique is used in ultra-high energy cosmic ray research for the detection and reconstruction of cosmic ray properties where beta particles are the main contributor to the fluorescence photons. This requires the use of fluorescence telescopes or satellites to image fluorescence photons at long distances due to the long range of the cosmic rays. In theory, this technique could also be used to image gamma sources but a very large field of view or large distance from the source to the camera would be needed due to the long mean free path of gamma rays in air.<sup>23,24,25,26</sup>

This research is interested in the fluorescence photons being created by the alpha particles emitted by the fissile material. Alpha particles deposit all their energy in a short range ( $\sim 3.6$  cm in air)<sup>27</sup>, producing many fluorescence photons near the source allowing for basic shape detection. The long distance traveled (mean free path equivalent<sup>a</sup> of 3.08

---

<sup>a</sup> The mean free path is defined as the average distance traveled by radiation before an interaction takes place. Photons at this energy will undergo radiative and nonradiative transfer between nitrogen molecules

km for 340 nm photons at sea level)<sup>28</sup> by fluorescence photons in air allows for imaging at various distances from alpha emitting material. Fluorescence light can also travel through translucent materials.

Additionally, a large number of fluorescence photons are produced per alpha particle. Reports in the literature vary between ~30 and ~760 photons per ~5 MeV alpha particle in air at atmospheric pressure, but the most reliable source (Reference 18) that lists ~760 photons per alpha.<sup>18,29,30,31</sup> The number of photons produced is proportional to the energy deposited per unit path length; the fluorescence varies with distance in a similar manner to the Bragg curve's ionization against distance.<sup>a</sup> If an alpha source is imaged in an atmosphere of 100% nitrogen, the number of photons produced increases by ~24% due to the elimination of oxygen molecules that contribute to quenching. Argon produces a similar number of photons between 300 and 400 nm per 5 MeV alpha particle (about 1000 photons). The light yields from N<sub>2</sub> and Ar are about 100 times greater than that from other gases. The total number of photons also increases with decreasing pressure, due to less collisional quenching.<sup>b,18</sup>

The specific activity and main alpha particle energy of the U, Pu, and other isotopes of interest are given in Table 1. The differences in specific activity should allow for differentiation of some materials and isotopic concentration. Specifically, the difference in the specific activity of <sup>235</sup>U, <sup>238</sup>U, and especially <sup>234</sup>U should allow for a

---

but attenuation due to this is negligible. The total atmospheric attenuation coefficient for 340 nm photons is 0.325 (km<sup>-1</sup>) at sea level; therefore, the equivalent mean free path is 3.08 km.

<sup>a</sup> See Figure A1 for an example Bragg curve.

<sup>b</sup> See Figure A2 for total number of photons at different pressures.

differentiation of U enrichment. This is because the two main processes that have been used to enrich U, gaseous diffusion and gas centrifuge, enrich  $^{234}\text{U}$  (to a greater proportion) as it enriches  $^{235}\text{U}$ . Additionally, the slight difference between the  $^{239}\text{Pu}$  and  $^{240}\text{Pu}$  specific activities may give some indication of the Pu quality ( $^{239}\text{Pu}$  to  $^{240}\text{Pu}$  ratio).

Table 1  
Specific Activities and Main Alpha Energy of Isotopes of Interest

Isotope	Specific Activity (BQ/g)	Main Alpha Energy (MeV)
$^{234}\text{U}$	$2.3 \times 10^8$	4.8
$^{235}\text{U}$	$8.0 \times 10^4$	4.4
$^{238}\text{U}$	$1.2 \times 10^4$	4.2
$^{238}\text{Pu}$	$6.3 \times 10^{11}$	5.5
$^{239}\text{Pu}$	$2.3 \times 10^9$	5.2
$^{240}\text{Pu}$	$8.4 \times 10^9$	5.2
$^{242}\text{Pu}$	$1.5 \times 10^8$	4.9
$^{210}\text{Po}$	$1.7 \times 10^{14}$	5.3
$^{226}\text{Ra}$	$3.7 \times 10^{10}$	4.8
$^{241}\text{Am}$	$1.3 \times 10^{11}$	5.5
$^{252}\text{Cf}$	$2.0 \times 10^{13}$	6.1

### I.D. Objectives

The primary objective of this research was to develop and assess the use of fluorescence imaging for warhead verification in nuclear arms control treaties. Specifically, to determine what fissile material attributes can be confirmed in an uncanned nuclear warhead or warhead component; and if it can do so without revealing

sensitive information.<sup>a</sup> This technique may have advantages over traditional verification detector systems by providing certain information needed for verification purposes while not revealing presumably sensitive information such as detailed geometrical or isotopic data. This verification technique could be applicable to both uranium and plutonium components and may eliminate the need for an information barrier if it is provably unable to discern classified information from a warhead or warhead component.

In order to assess the feasibility of fluorescence imaging for nuclear arms control verification, proof-of-concept experiments have been performed using an off-the-shelf imaging system. The experimental results were then compared to simulated results from the Monte Carlo transport code GEometry ANd Tracking (GEANT4)<sup>32</sup> to assess the accuracy of the model. The results of this research will determine if fluorescence imaging is a viable tool for nuclear warhead verification in arms control treaties.

---

<sup>a</sup> Fissile material attributes are explained in Chapter II.B. Uncanned nuclear warhead is specified because fluorescence photons cannot travel through non-translucent materials.



CHAPTER II  
OVERVIEW OF NUCLEAR ARMS CONTROL TREATIES AND VERIFICATION  
METHODOLOGIES

**II.A. Past, Present, and Future Nuclear Arms Control Agreements and Treaties**

The earliest efforts to halt the growth of nuclear arms began in 1964 when the United States proposed a verified freeze on the number of US and Soviet strategic nuclear offensive and defensive delivery vehicles. This eventually turned into the first Strategic Arms Limitation Talks (SALT I). Since then, the US and the Soviet Union have had a series of agreements to limit and reduce their nuclear weapon arsenals.<sup>33</sup> After the Soviet Union dissolved in 1991 negotiations continued with Russia.

A summary of the status and significant dates for the strategic nuclear arms control agreements SALT I and II, START I, II, and III, Strategic Offensive Reductions Treaty (SORT), and New START as well as the nonstrategic Intermediate-Range Nuclear Forces (INF) Treaty are given in Table 2. Table 3 gives the treaty limits and verification status for the same agreements. Not listed here is the nonstrategic Presidential Nuclear Initiatives (PNI). PNI was not an official treaty – it was a pledge by Washington and then Moscow, starting in 1991, to remove and reduce certain tactical nuclear weapons. While PNI did not specify limits, had no verification, and compliance with the commitments are uncertain, it is possible that up to 17,000 tactical nuclear weapons were removed from service, constituting the deepest reductions to date.<sup>34</sup>

Table 2  
Status and Significant Dates of Nuclear Arms Control Agreements<sup>33,35</sup>

Treaty	Status	Date				
		Signed	Ratified (U.S)	Entered Into Force	Implementation Deadline	Expiration
SALT I	Expired	5/26/72	8/3/72	10/3/72	NA	10/3/77
SALT II	Never Entered Into Force	6/18/79	NA	NA	NA	NA
INF	In Force	12/8/87	5/27/88	6/1/88	6/1/91	none
START I	Expired	7/31/91	10/1/92	12/5/94	12/5/01	12/5/09
START II	Never Entered Into Force	1/3/93	1/26/96	NA	NA	NA
START III	Never Negotiated	NA	NA	NA	NA	NA
SORT	Replaced by New START	5/24/02	3/6/03	6/1/03	NA	2/5/11
New START	In Force	4/8/10	12/22/10	2/5/11	2/5/18	2/5/21

Also not listed in these tables are arms control treaties such as those that seek to keep their region free of nuclear weapons; these are preventative and therefore do not limit or verify existing warheads. The NPT obligates NWS to "pursue negotiations in good faith on effective measures relating to cessation of the nuclear arms race at an early date and to nuclear disarmament, and on a treaty on general and complete disarmament

under strict and effective international control<sup>36</sup> but has no verification measures specified to monitor warhead disarmament.

Table 3  
Treaty Limits and Verification Status of Nuclear Arms Control Agreements<sup>33,35</sup>

	Deployed Warhead Limit	Deployed Delivery Vehicle Limit	Verification
SALT I	NA	US: 1366 USSR: 1690	Delivery Vehicles
SALT II	NA	2,250	Delivery Vehicles
INF	NA	All ground-launched ballistic and cruise missiles with ranges between 500 and 5,500 kilometers	Delivery Vehicles
START I	6,000	1,600	Delivery Vehicles
START II	3,000-3,500	NA	Conversion of delivery vehicles to conventional roles
START III	2,000-2,500	NA	NA
SORT	1,700-2,200	NA	None
New START	1,550	700; 800 including non-deployed	Delivery Vehicles

START I was the first treaty to actually establish an aggregate limit on strategic nuclear warheads. While none of these treaties have verification measures to verify actual warheads, the verification measures of START I are the basis for the only nuclear

arms control treaty currently in force and being implemented that sets a number to reduce existing, strategic weapons – New START.<sup>35,33,37</sup>

New START was signed by the U.S. and Russia in 2010 and entered into force in 2011. New START is a legally binding agreement that reduces strategic nuclear warheads and strategic delivery vehicles. The treaty text states that “verification of conversion or elimination in accordance with this treaty shall be carried out by national technical means ... and inspection activities.”<sup>38</sup>

‘Inspection activities’ can take place at bases, declared facilities, and formerly declared facilities to confirm the declared number and types of Intercontinental Ballistic Missiles (ICBMs), Submarine-Launched Ballistic Missiles (SLBMs), and heavy bombers, their number of reentry vehicles or armaments, their conversion or elimination, and the absence of any undeclared items. The only radiation detection equipment allowed in inspections are neutron detectors to confirm that non-nuclear objects are in fact non-nuclear.<sup>13</sup> These inspection activities are only geared towards the verification of delivery vehicles – ICBMs, SLBMs, or heavy bombers – not the actual nuclear warhead.

Future treaties are likely to have increasing levels of verification. For example, the Fissile Material Cutoff Treaty (FMCT) is expected to have a “non-discriminatory, multilateral and internationally and effectively verifiable treaty banning the production of fissile material for nuclear weapons or other nuclear explosive devices.”<sup>39</sup> While actual nuclear warhead verification has yet to be included in a treaty, a number of studies have been performed on how nuclear warheads, warhead components, or dismantlement verification could be performed and the technologies that could be used. An overview of

fissile material verification methodologies and radiation technologies will be discussed in the following two sections. More information on the actual implementation of verification measures can be found in a number of references (6,7,10,12,14,15,16,17).

### **II.B. Fissile Material Verification Methodologies**

Because of the secrecy surrounding nuclear weapons, most design information is considered sensitive and therefore protected by the state. However, treaty partners can agree to exchange any information they choose. Therefore, what information will be considered sensitive and non-sensitive in treaty verification is just educated speculation. If NNWSs become involved in verification, such as the work initiated in the U.K. Norway Initiative, NWSs need to ensure they are not proliferating nuclear weapons information to NNWSs; this would be a violation of the NPT.<sup>6</sup> It is generally agreed that this sensitive information would include the mass and isotopics of the nuclear material, dimension of the nuclear cores, and detailed design of the engineered components.

To protect sensitive information, studies have suggested two general approaches for warhead verification; the template approach and attribute approach. The template approach compares the radiation signature from a known standard to the declared item. A reference signature is taken directly from an item that has been authenticated as declared (the known standard). Thereafter, each item to be verified is measured and the signature is compared to that of the reference signature. All signatures need to be protected by an information barrier due to the fact that these measurements would most likely contain classified data.<sup>40</sup> A new approach under investigation combines template matching and modern cryptography, known as zero-knowledge protocol, to attempt to

eliminate the need for information barriers. More information on zero-knowledge protocol can be found in reference 41.

The attribute approach confirms intrinsic characteristics of a weapon or weapon component, such as:

- Presence of fissile material
- Presence of Pu
- Presence of U
- Mass (of fissile material, Pu, or U) greater than a threshold
- Symmetry
- Pu age (time since separation of Am from Pu greater than 25 years)
- Absence of oxide
- $^{240}\text{Pu}$  to  $^{239}\text{Pu}$  ratio greater than a threshold (quality of Pu measure)
- Enrichment of U greater than a threshold
- Presence of high explosives
- Mass of high explosives greater than a threshold

While the actual attributes are unclassified, current technologies to confirm these attributes have the potential to reveal sensitive information and thus require an information barrier. Some attribute measurement systems seek to verify all these attributes while others argue that simply verifying the presence of fissile material and high explosives is sufficient.<sup>42,43</sup> The objective of this work is to assess the fissile material attributes where fluorescence imaging would be useful in verifying an uncanned

nuclear warhead or warhead component and evaluate if it can do so without revealing presumably sensitive information about these components.

### **II.C. Overview of Fissile Material Verification Technologies**

Most fissile material verification technologies rely on gamma-ray and neutron measurements. The neutron and gamma radiation signatures for metallic HEU and weapons-grade Pu are unique, making it possible to verify them nondestructively. Nondestructive techniques measure the radiation spontaneously emitted or induced from the material and do not alter the physical or chemical state. Destructive techniques require sampling the material and analyzing the sample in a lab with chemical procedures that alter the state of the material. While destructive techniques are typically more precise than nondestructive techniques, they will most likely not be used in arms control verification. They are expensive, time consuming, require a sample of the material, and can reveal very detailed information about the material.

The following is a brief overview of gamma-ray and neutron detection and what these measurements can conclude about the material measured. For a full overview of radiation detection and measurements see references 44 and 45. Additionally, reference 10 goes through technologies that can be used to confirm each attribute.

#### *Gamma-Ray Measurements*

There are essentially three broad categories of gamma-ray measurements: gamma-ray spectroscopy, gross gamma counting, and gamma-ray imaging. These are discussed briefly below.

Gamma-ray spectroscopy is the most widely used gamma-ray measurement. Gamma-ray spectroscopy can be used to determine the fractional abundance of isotopes in a material by analyzing the energy spectrum of the detected gamma-rays. This can be used to confirm the presence of U and the enrichment can be deduced from the relative intensity of the 186 keV gamma-ray from  $^{235}\text{U}$ . The presence of Pu and the isotopic composition of the Pu can also be determined. The isotopic composition can then be used to determine the  $^{240}\text{Pu}$  to  $^{239}\text{Pu}$  ratio. The Pu age can be determined from the  $^{241}\text{Am}$  content. Additionally, the absence of oxide can be confirmed by the absence of the 870.7 keV peak emitted during de-excitation of the first excited state of  $^{17}\text{O}$ , that is only present in non-metallic forms.<sup>10,45</sup> Because gamma-ray spectroscopy can reveal isotopics of the nuclear material, it will most likely require an information barrier if it is to be used in warhead verification.

Gross gamma counting reveals relatively little about the material and will probably not require an information barrier. By assuming a general isotopic composition of HEU and weapon grade Pu, the approximate number of photons emitted over a period of time can be calculated if the approximate surface area visible to the detector of the item being measured is known. Due to the strong absorption of photons in metallic U and Pu, and therefore a short mean free path, only a small volume of the material is 'visible' to the detector. Infinite thickness is approximately 7 mean free paths, which is 0.26 cm for a 186 keV gamma-ray in Uranium metal. If the thickness of the sample is larger than the infinite thickness of the photons in the sample material, all samples of the same physical composition would present the same visible volume to the detector.



Therefore, gamma-ray measurements often only sample the surface of the material and cannot reveal material mass. But gross gamma-ray counting could differentiate between nuclear materials and U enrichment if the surface area visible to the detector of the item being measured is known.<sup>45</sup>

Gamma-ray imaging, with or without spectroscopy, is another technology that can be used in fissile material verification. Imaging with spectroscopy has the ability to differentiate between gamma-ray emitting materials but could also reveal isotopics. Thus, an information barrier is required. Gamma-ray imaging without spectroscopy, similar to gross gamma-ray counting, would not reveal isotopics. If the image resolution is capable of showing detailed design information, the resolution can be decreased in an easily verifiable manner. Pairing gross gamma-ray counting and gamma-ray imaging without spectroscopy with other non-sensitive techniques may increase verification effectiveness and will be discussed further in Chapter V.<sup>10,46</sup>

### *Neutron Measurements*

Differing from gamma-rays, neutrons can travel through high Z material allowing them to be detected from the whole sample. Generally speaking, the energy of the detected neutron is not readily collected, making isotope specific identification unapparent.<sup>a</sup> The two main neutron measurements are gross counting and coincidence counting. Gross neutron counting responds to all neutrons while coincidence counting discriminates between neutrons emitted randomly in time from ( $\alpha$ ,n) reactions and those

---

<sup>a</sup> The pulse-height spectra of neutron proportional counters contains only weak signatures of the energy of the detected neutron. Energy information may be obtained through the design of moderating materials surrounding the detectors.

neutrons from spontaneous or induced fission in which multiple neutrons are emitted in coincidence.

In general, when chemical form and isotopic composition is known, total neutron counting can be used to determine U or Pu assay (amount). Regardless of chemical form, coincidence counting can be used to determine the total quantity of U or Pu if the isotopic composition is known. This is possible because coincidence counting is only sensitive to coincident neutrons and thus only those isotopes that fission. The quantity of these isotopes can be determined even if the chemical form of the material yields additional single neutrons from ( $\alpha$ ,n) reactions.

In materials where one of the three neutron sources is dominate [( $\alpha$ ,n), spontaneous fission, induced fission], passive gross neutron counting can be used for assay. This is the case for U and Pu metal where spontaneous fission from  $^{238}\text{U}$  or  $^{240}\text{Pu}$  respectively, is dominate. In HEU metal, the neutron production rate is small due to the small percentage of  $^{238}\text{U}$  (~42 n/s for a 10 kg U sample enriched to 69.58%  $^{235}\text{U}$ ),<sup>45</sup> therefore active techniques are often used to determine HEU metal assay. In Pu metal, the neutron production rate is a signature for the effective  $^{240}\text{Pu}$  mass.

Gross neutron measurements can determine symmetry by comparing measurements at incremental rotations. Additionally, when isotopic composition is known it can determine material mass and absence of oxide [due to ( $\alpha$ ,n)]. If isotopic content is not known, these attributes are not as straight forward to determine. This will be discussed further in Chapter V along with combining gross neutron with gross gamma and fluorescence imaging.

## CHAPTER III

### EXPERIMENTS

A series of experiments were performed to test the assumptions of the imaging technique. The experiments include set-ups with U metal specimens,  $^{210}\text{Po}$ ,  $\text{UO}_3$ , gamma-ray and beta emitting sources, and translucent and non-translucent materials. The overall goal of the experiments was to determine what the imaging system could and could not see, what it could differentiate between, and to observe the characteristics and transmission of fluorescence photons. It is expected that the images would correlate to the alpha particle source strength, producing brighter images with stronger alpha sources. Additionally, as the flux of fluorescence photons on the lens is reduced due to distance or attenuation, the image brightness should decrease proportionally.

#### **III.A. Imaging System**

##### *Princeton Instruments PIXIS: 1024B/BUV*

A Princeton Instruments PIXIS: 1024B/BUV back-illuminated CCD was used to acquire all images. The camera is air cooled allowing for long exposure times with low electronic noise (typical dark current of 0.0004 e-/p/sec at  $-70^\circ\text{C}$ ). The CCD format is 1024 x 1024 imaging pixels, each pixel having an area of 13 x 13  $\mu\text{m}$ . The BUUV camera has a high sensitivity in the 300 – 400 nm range as shown in blue on the quantum efficiency curve in Figure 3. A fused silica lens was used to allow passage of UV photons. Full specifications can be found in reference 47. The Princeton Instruments WinView software was used for data acquisition.

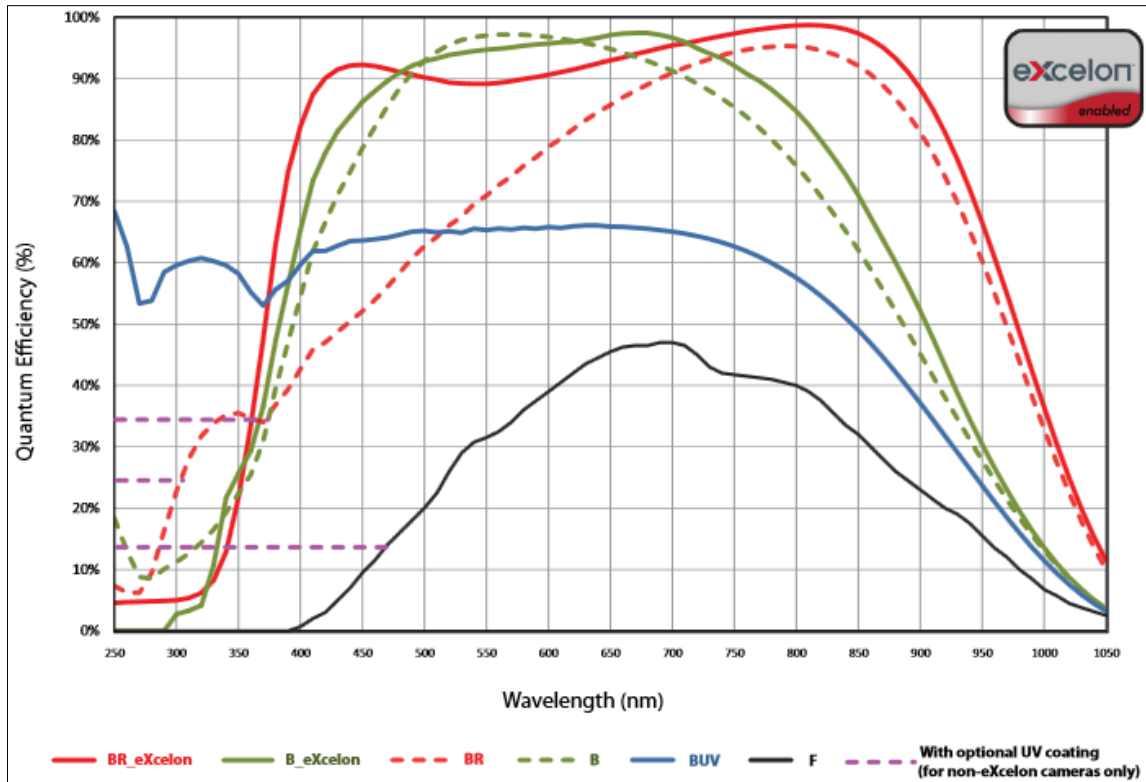


Figure 3. Quantum efficiency curve for the PIXIS: 1024B/BUV (shown in blue).

The PIXIS: 1024B/BUV camera has one of the highest quantum efficiencies in the region of interest and was successful in imaging the low light application of fluorescence photons created from nuclear materials. The camera used in the experiments was a demo camera loaned by Princeton Instruments for two weeks. During experiments it had to be recalibrated twice due to significant fluctuations in the dark current. This is not typical behavior for these cameras, and it can be assumed that a dedicated camera would acquire images with reduced dark current fluctuations and achieve better results.

### III.B. Sources and Other Experimental Material

A number of alpha emitting sources of different intensities and chemical form were imaged in the experiments. Beta and gamma-ray sources were also imaged to confirm the non-sensitivity of the imaging systems to these radiations. The alpha sources included a 5 mCi  $^{210}\text{Po}$  source, 10 grams of depleted  $\text{UO}_3$  (0.2%  $^{235}\text{U}$ ), 10 grams of natural  $\text{UO}_3$ , and eight U metal specimens with enrichments ranging from 0.2% to 93%. A photograph of the  $^{210}\text{Po}$  source is shown in Figure 4. It has a total diameter of  $\sim 1.5$  cm and an opening of  $\sim 0.75$  cm. The  $\text{UO}_3$  was imaged in a plastic petri dish with a diameter of  $\sim 9$  cm. A photograph of 10 grams of depleted  $\text{UO}_3$  in a plastic petri dish is shown in Figure 5. The U metal specimens are 41 g cylinders all having a 3 cm diameter and 0.3 cm thickness. A photograph of a U metal specimen is shown in Figure 6 next to a silver half dollar and quarter for size reference. Table 4 gives the isotopic percentages of each of the U metal specimens.



Figure 4. Photograph of  $^{210}\text{Po}$  source.



Figure 5. Photograph of depleted  $\text{UO}_3$  in a plastic petri dish.



Figure 6. Photograph of U metal specimen next to half silver dollar and quarter.

Table 4  
Isotopics of U Metal Specimens

Enrichment %	Isotope %		
	<sup>234</sup> U	<sup>235</sup> U	<sup>238</sup> U
0.2 (DU)	<0.002	0.189	99.808
0.7 (NU)	0.006	0.712	99.282
4.7	0.051	4.735	95.19
19.4	0.169	19.365	80.197
20.8	0.228	20.762	78.912
54.9	0.453	54.861	44.34
70.5	0.778	70.485	28.414
93.2	1.004	93.16	5.431

The beta sources used for testing included a combination of low activity beta sources (consisting of C-14, Pb-210, Tc-99, Pm-147, Sr-90, and Cl-36 with a total activity of 0.131  $\mu$ Ci). Similarly, the gamma sources were a combination of two Cs-137 and one Co-60 with a total activity of 17.6  $\mu$ Ci.

Table 5 lists all the sources used, along with the number of particles per unit time at the surface of the source (reaching air). For the U metal specimens and UO<sub>3</sub>, the number of alpha particles per unit time was calculated using the computer code SOURCES 4A which gives the alphas/second-cm<sup>2</sup>. This result was multiplied by the surface area of the source to acquire the total source strength.<sup>48</sup> Note that the source strength of particles reaching the air is greater for the UO<sub>3</sub> than for the metal of the same enrichment. This occurs because the 10 grams of oxide is spread out over a greater area,

and the high density of U metal prevents most of the alpha particles from reaching the air.

Table 5  
Number of Particles per Unit Time at Source Surface

Source	Rate of particles (beta, gamma or alpha) expected to reach air (particles/sec)
“Beta” Sources	4.85E+03
“Gamma” Sources	6.51E+05
<sup>210</sup> Po	1.85E+08
Depleted UO <sub>3</sub>	4.68E+03 *
Natural UO <sub>3</sub>	7.51E+03 *
U Metal Sources (Enrichment in %)	
0.2 (DU)	1.1485E+03
0.7 (NU)	1.8479E+03
4.7	9.6384E+03
19.4	3.0236E+04
20.8	4.0289E+04
54.9	7.9826E+04
70.5	1.3553E+05
93.2	1.7476E+05

\* Source strength shown is for UO<sub>3</sub> in petri dish.

A number of High Density Polyethylene (H.D.Poly) pieces and iron foils were used to observe the transmission of fluorescence photons through translucent and non-translucent material. Table 6 gives the alpha particle ranges for H.D.Poly, Fe, and air for 5.3 MeV alpha particles.



Table 6  
Ranges for 5.3 MeV Alpha Particles

Material	Alpha Range (cm)
Air	3.96
H.D.Poly	3.58E-03
Fe	1.07E-03

### III.C. General Set-up and Procedure

All experiments were performed in a light-tight-black-box 1.5 m by 1 m by 1 m. The inside of the box was lined with the black plastic used in dark rooms. A photograph of the box is shown in Figure 7. Each time the PIXIS camera was turned on, it was allowed to cool to normal operating temperature of  $-70^{\circ}\text{C}$ . Before each set of experiments, several dark images were acquired to confirm normal dark current conditions. The black-box was then closed, as shown in Figure 8, and a background image was acquired. The black box was opened, a source was placed inside, and an image was acquired with light to determine placement of the source. Several more dark images were taken to clear any residual image on the CCD. The black box was then closed and the image with the source present was acquired for a specified acquisition time.



Figure 7. Photograph of light-tight-black-box open.<sup>49</sup>



Figure 8. Photograph of light-tight-black-box closed.

### III.D. Image Analysis

The acquired images were 32-bit Tagged Image File Format (TIFF), and all image analysis was done in Image J.<sup>50</sup> The two calculated values used as the quantitative bases for the analysis and conclusions are the image mean and standard deviation; these are calculated from the gray values of the pixels in the full 32-bit, unprocessed, raw image. The graphs given in the results will show the standard deviation and the mean, with error bars equal to the standard deviation.

The images shown in the results have been processed and put into a montage for easy comparison. The image processing was only used to make it easier for the human eye to process and not for quantitative analysis. To process the image, it is first converted to a 16-bit image. The histogram of each image is then equalized to enhance contrast. A background image with the same exposure time and histogram equalized is subtracted. A color table is applied to the grayscale image to produce a pseudocolor image. The image is then saved as a Portable Network Graphics (PNG) so that it can be manipulated.

To show how this process changes what the image looks like, Figure 9 shows a montage of two images, one background (BG) and one with a source, unaltered (left), with the histogram equalized (middle), then with a color table applied to the equalized histogram(right); nothing has been subtracted from these images. Figure 10 then shows the same source image equalized with a background equalized image subtracted (the middle images in Figure 9) in part (a) and with a color table in part (b). This procedure is

how most images in the results are processed. Part (a) in Figure 10 can be equalized again as shown in part (c) and a color table applied as shown in part (d).

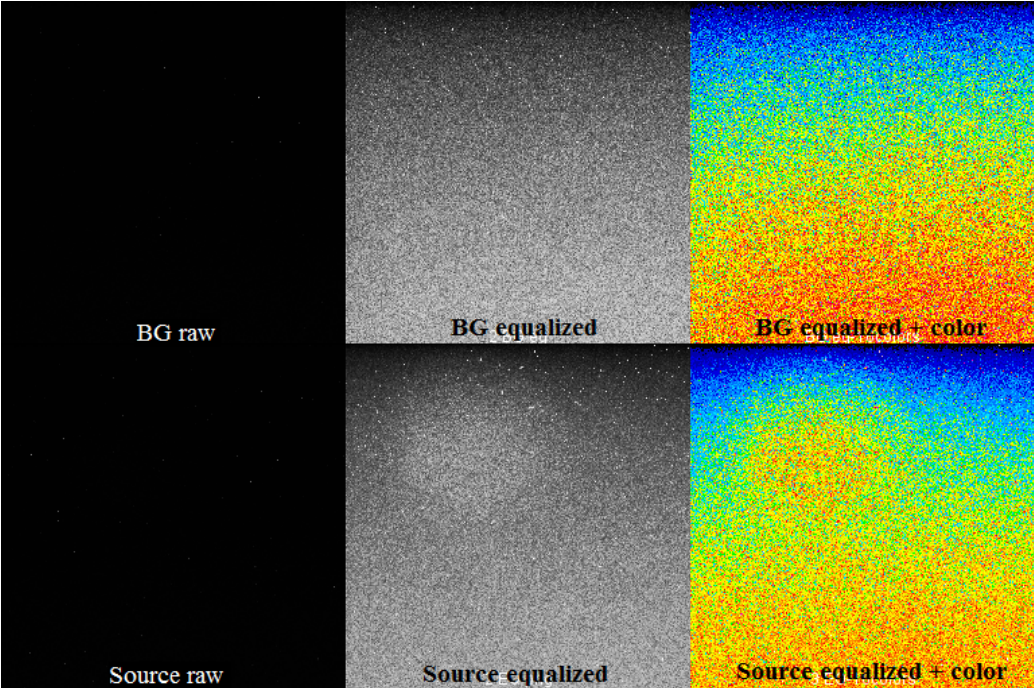


Figure 9. Image process example 1.

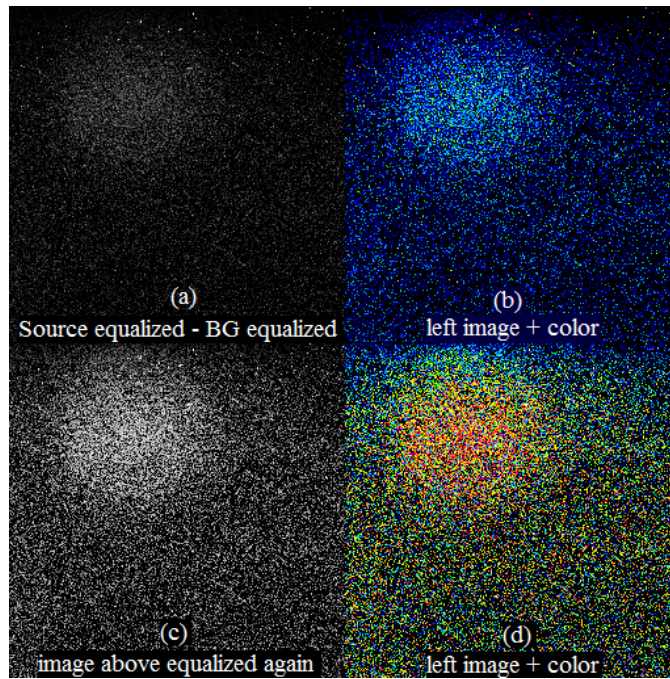


Figure 10. Image process example 2.

Except for images where the source location is obvious, the location of the sources is outlined in yellow. One thing that should be noted is that changing image format and compressing image data can result in the loss of some visual detail. While the consequences of this lost detail is minimal for the images shown in this dissertation, the full sized TIFF images make it easier for finding bright spots and other details.

### III.E. Experimental Set-ups and Results

#### *Single U Metal Specimens, Front Facing*

U metal specimens were imaged on a source stand at 25 cm from the camera lens, one at a time with the front (round) face facing the lens, as shown in Figure 11. Six images with 60 minute exposure times were taken in this set-up: a quarter and five U metal specimens with enrichments of 0.7%, 4.5%, 20.8%, 54%, and 93%. A montage of



the images is shown in Figure 12. This montage shows that the 54% and 93% enriched U specimens can be clearly identified. The same cannot be said about the specimens at 20.8% enriched and below.

The mean and standard deviation values for the four highest enrichment samples and background measurement with the same acquisition time are given in Table 7. A plot of the four highest enrichment samples values versus enrichment is shown in Figure 13. A plot of the standard deviation versus source strength for these images plus the background measurement is shown in Figure 14. The source strength graphed here is half the total source strength as the camera only views half the source.

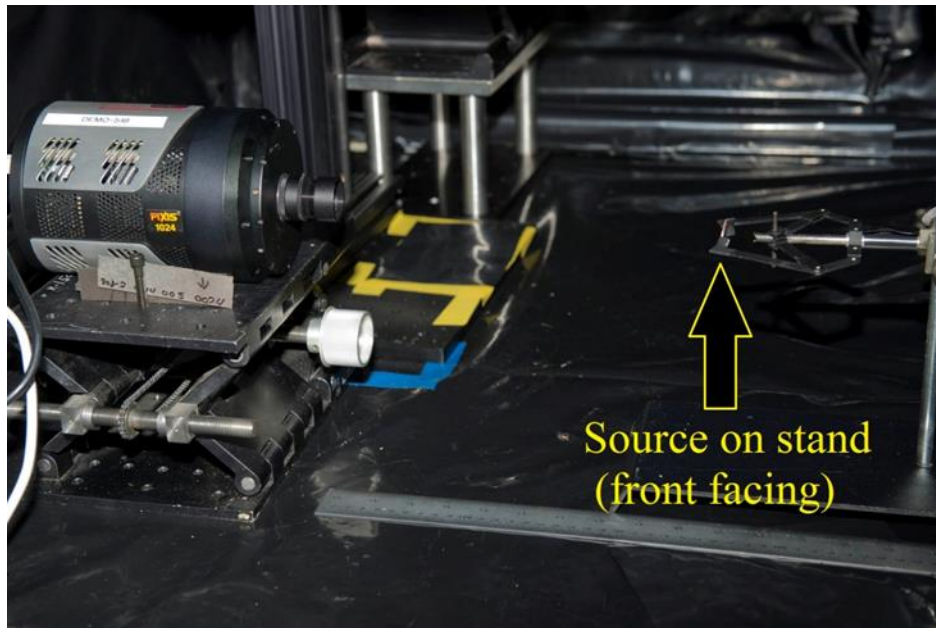


Figure 11. Experimental Set-up: Specimen on source stand at 25 cm from camera lens.<sup>a</sup>

---

<sup>a</sup> Image originally appeared in: J. S. Feener and W. S. Charlton, "Initial Results of Nuclear Fluorescence Imaging for Arms Control Verification," Proceedings of the 54th Institute of Nuclear Material Management Annual Meeting, Palm Desert, CA, July, 2013; and is reprinted with the permission of the Institute of Nuclear Materials Management.

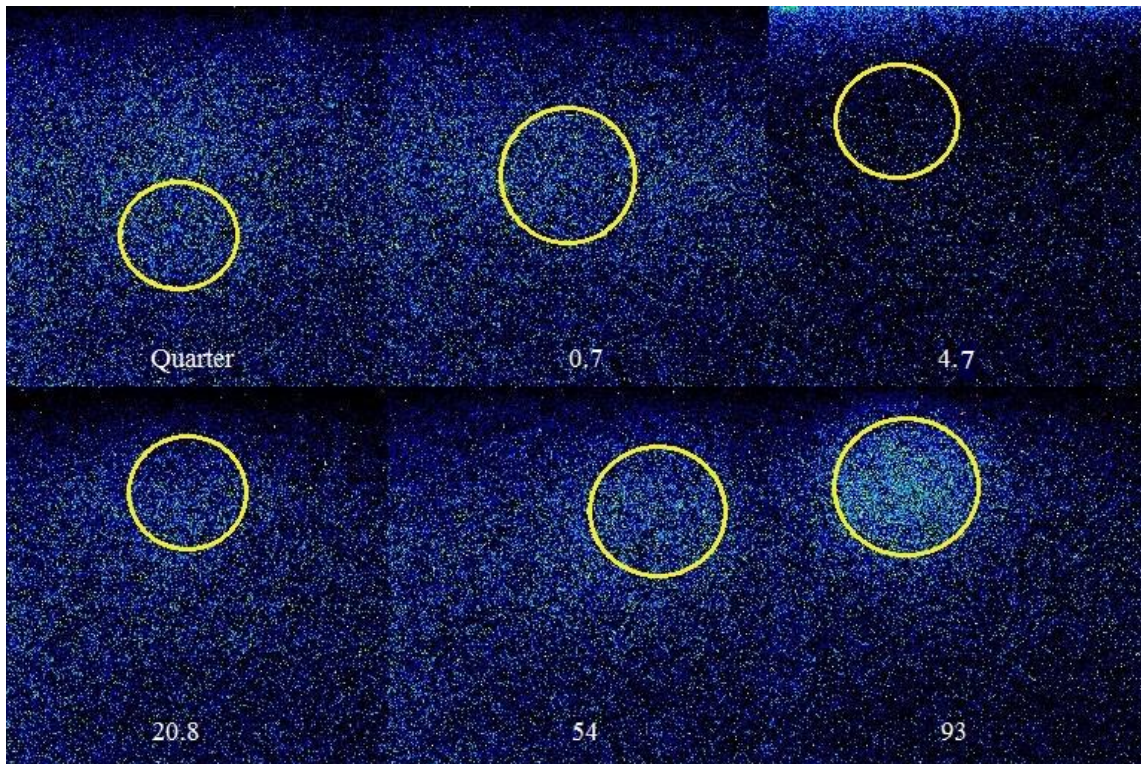


Figure 12. Montage of the analyzed images from single U metal specimens, front facing.<sup>a</sup>

Table 7

Mean and Standard Deviation Values from Single U Metal Specimens, Front Facing

Source	BG	4.7	20	54	93
Mean	463.824	9.474	46.164	137.084	237.533
StdDev	36.907	55.941	63.475	65.485	83.984

---

<sup>a</sup> Image originally appeared in: J. S. Feener and W. S. Charlton, "Initial Results of Nuclear Fluorescence Imaging for Arms Control Verification," Proceedings of the 54th Institute of Nuclear Material Management Annual Meeting, Palm Desert, CA, July, 2013; and is reprinted with the permission of the Institute of Nuclear Materials Management.

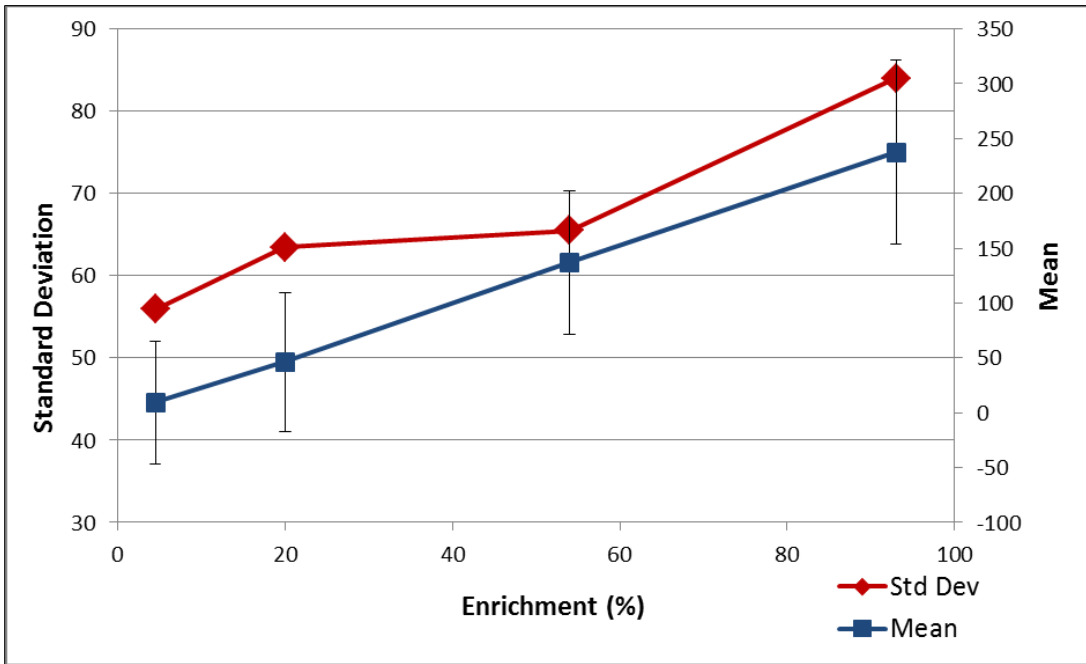


Figure 13. Standard deviation and mean versus enrichment of the four highest enriched images from single U metal specimens, front facing.

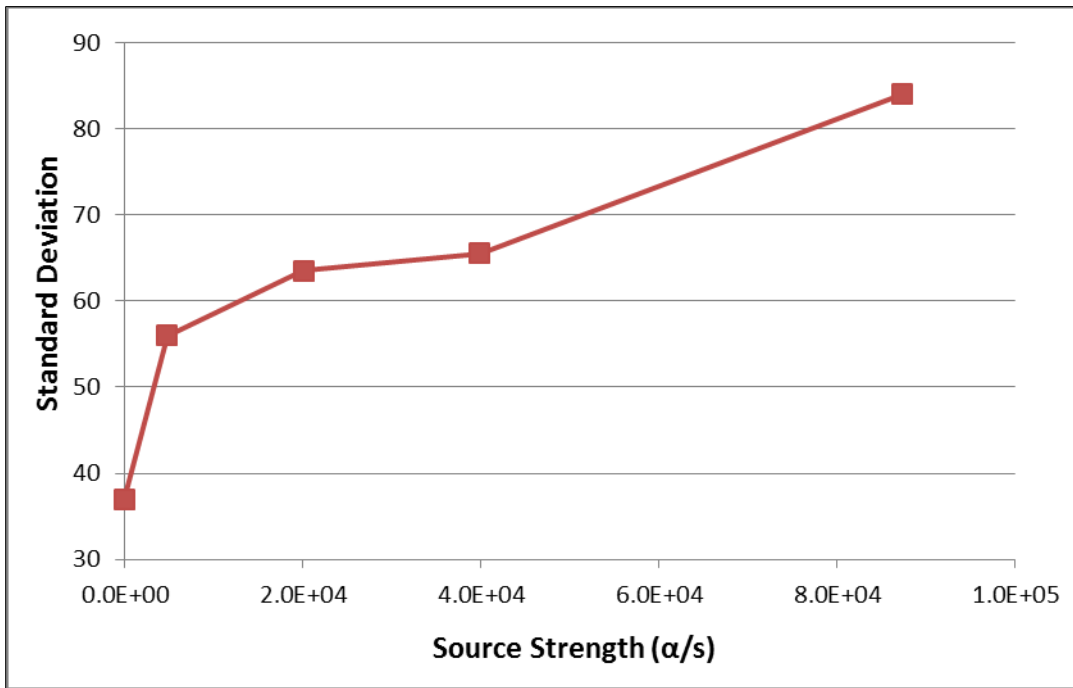


Figure 14. Standard deviation versus source strength of the four highest enriched images plus background from single U metal specimens, front facing.



Figure 13 and Figure 14 show the mean and standard deviation both track the enrichment, and therefore source strength fairly linearly. The standard deviation is a measure of the variation of pixel values from the average. Therefore, as long as the background and dark current is similar in each image being compared or evenly distributed in any one image, the standard deviation will increase with the greater number of UV photons from the source that hit the CCD. This is advantageous because the standard deviation can be used even if the image mean is unreliable due to variance in the dark current or background image (as seen by the large background mean value in Table 7). In other words, a bright spot on an image will be revealed by the standard deviation regardless of the intensity of the background and dark current, as long as the background and dark image is evenly distributed or similar when comparing images.

The values of the mean and standard deviation of the 4.7% and 20.8% enriched specimens in Table 7 are worth noting. The standard deviation is greater than the mean value, which is due to the acquisition software automatically subtracting a background (some acquisition software will perform an automated background subtraction). Thus, even if the background subtraction is not known, the standard deviation still gives valuable information as discussed above.

#### *Multiple U Metal Specimens, Front Facing*

Multiple U specimens lying flat on a surface 25 cm from the camera lens with the camera imaging downward were imaged in this set-up, as shown in Figure 15. Four images were acquired with 60 minute exposures. A montage of the four images in this set of experiments is shown in Figure 16. Each specimen is labeled with its enrichment,

and the sum of the enrichments of the specimens within the image is labeled at the bottom. Similar to the results from single U metal specimens, front facing, the 54%, 70%, and 93% enriched U specimens create bright spots allowing their location to be identified. The specimens at 20.8% enriched and below do not create clear bright spots.

The mean and standard deviation values for these four images plus a background measurement with the same acquisition time are given in Table 8. A plot of these values versus the enrichment sums, labeled “added enrichments”, is shown in Figure 17. Throughout the dissertation, the enrichment sums will be referred to as added enrichment. The graph of the standard deviation versus the added source strengths is shown in Figure 18. The first point in both graphs is the background measurement. The source strength shown is the summed source strengths of the specimens in the image (half the total strength as the camera only views half the source).

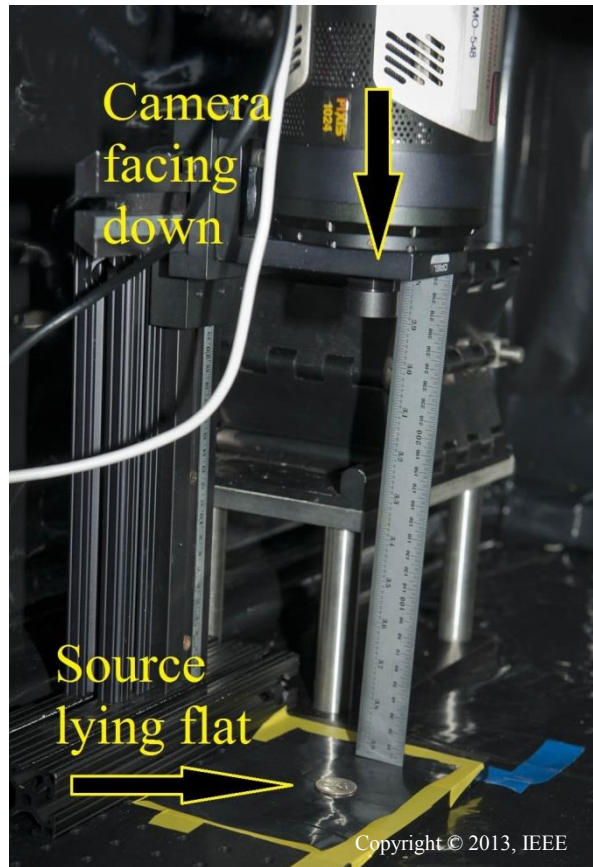


Figure 15. Experimental Set-up: Camera facing down and specimen lying on surface.<sup>49</sup>

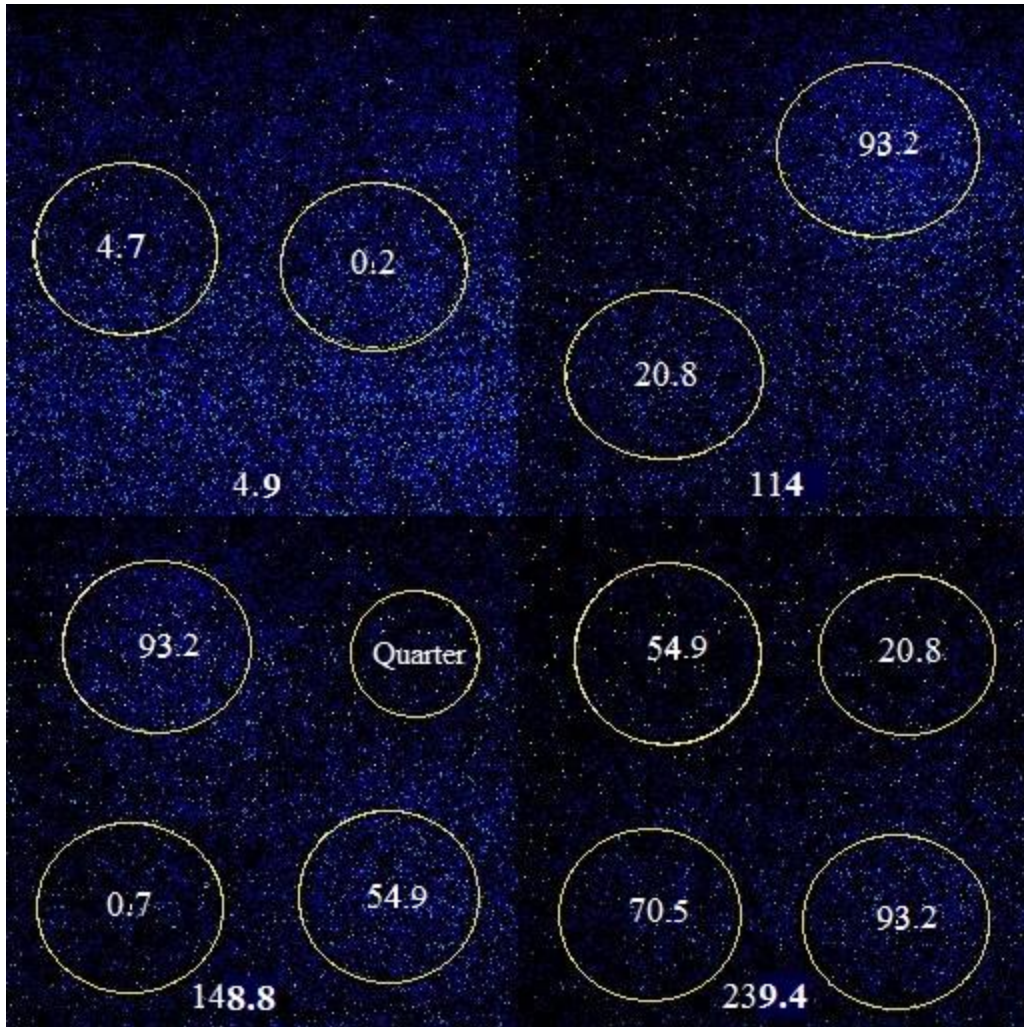


Figure 16. Montage of the analyzed images from multiple U metal specimens, front facing.<sup>a</sup>

---

<sup>a</sup> Image originally appeared in: J. S. Feener and W. S. Charlton, "Initial Results of Nuclear Fluorescence Imaging for Arms Control Verification," Proceedings of the 54th Institute of Nuclear Material Management Annual Meeting, Palm Desert, CA, July, 2013; and is reprinted with the permission of the Institute of Nuclear Materials Management

Table 8

Mean and Standard Deviation Values from Multiple U Metal Specimens, Front Facing

Added Enrichments	BG	4.9	114	148.8	239.4
Mean	234.177	119.172	325.873	392.307	362.424
StdDev	45.306	64.519	90.347	101.579	127.349

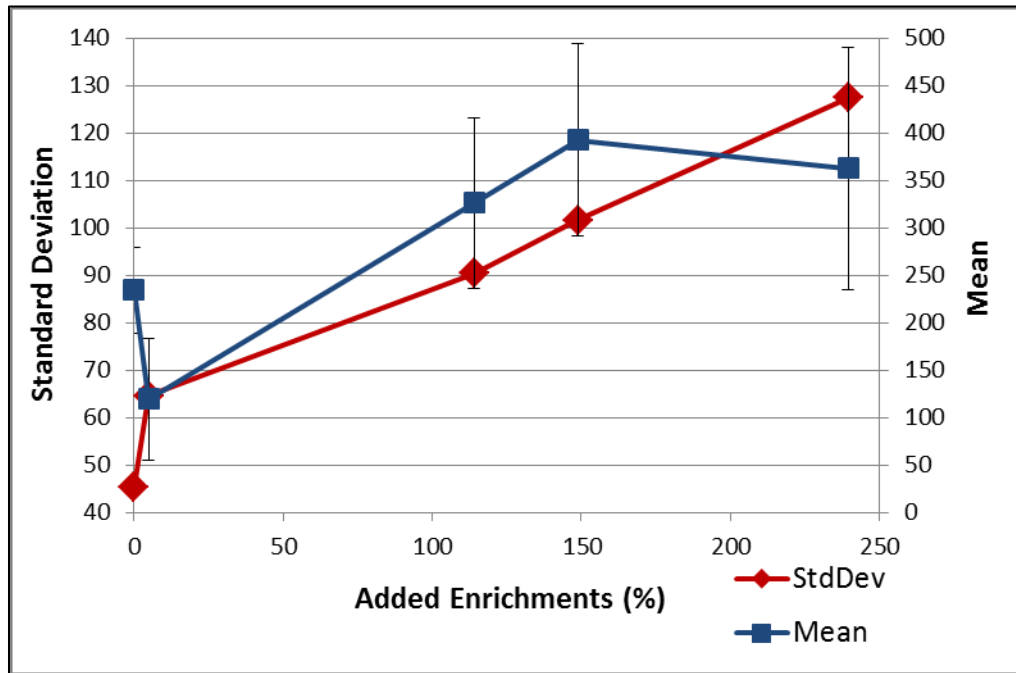


Figure 17. Standard deviation and mean versus added enrichment of images from multiple U metal specimens, front facing.

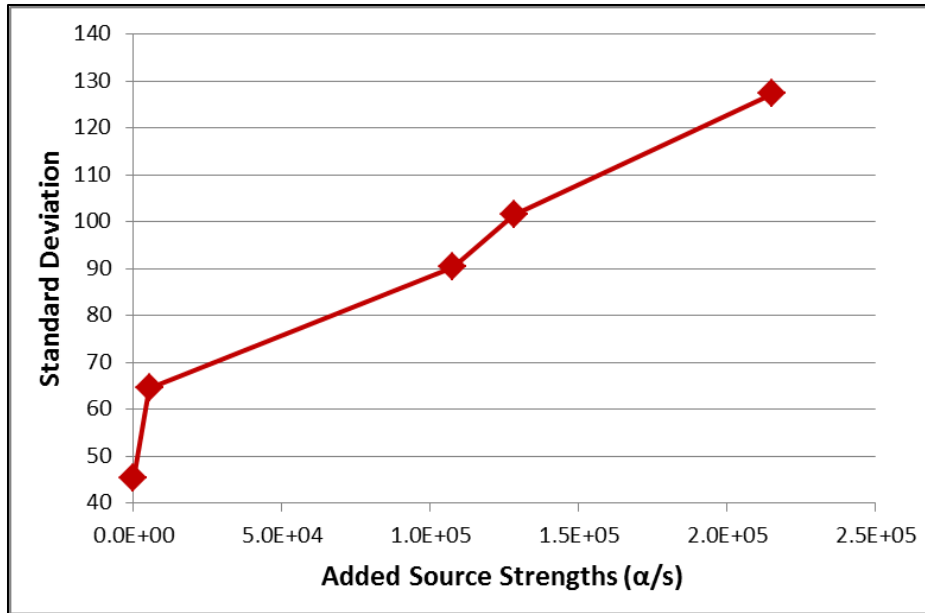


Figure 18. Standard deviation versus the added source strength of images from multiple U metal specimens, front facing.

These graphs show that the standard deviation increases linearly with enrichment and source strength, while the mean can fluctuate. Like the previous experimental set-up, this is because the increased source strength creates bright spots, increasing the standard deviation while the mean varies with background. To further illustrate this effect, the mean and standard deviation versus enrichment from this experimental set-up (multiple, front facing) and the previous experimental set-up (single, front facing) are shown in Figure 19. While the experimental set-ups are slightly different, the standard deviation increases more linearly with enrichment than the mean.

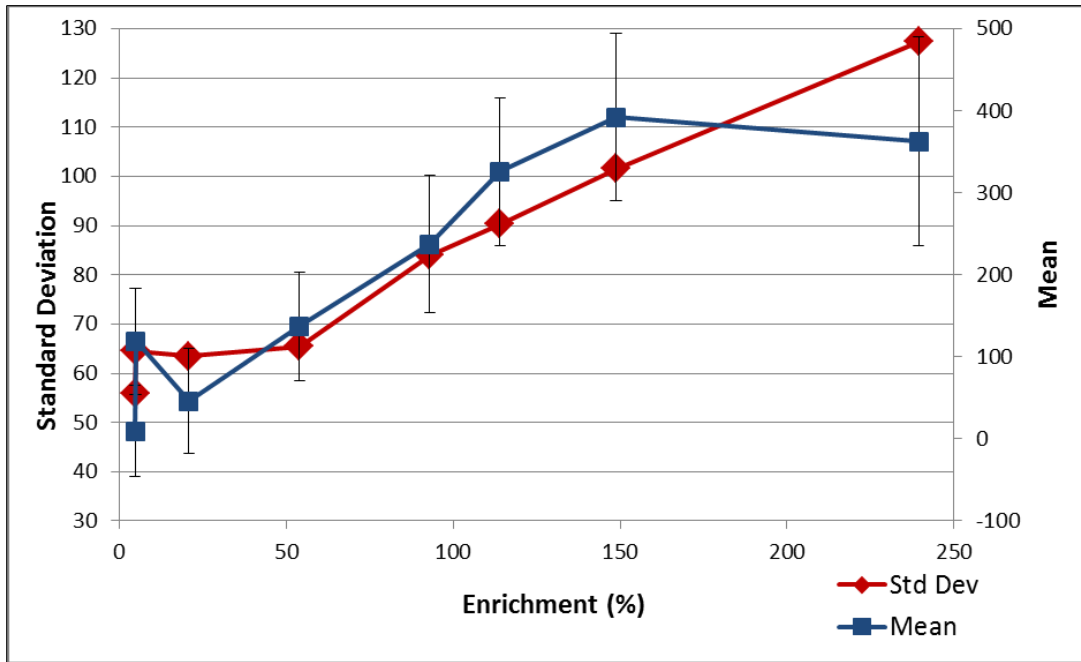


Figure 19. Standard deviation and mean versus added enrichment of images from the single and multiple U metal specimens, front facing set-ups.

#### *Multiple U Metal Specimens, Side Facing*

In this set of experiments, two U metal specimens sitting sideways were imaged in different configurations at 25 cm from the camera lens with the camera imaging downward, as shown in Figure 20. A close-up photograph of one configuration of the specimens sitting sideways is shown in Figure 21. Five images were acquired with 60 minute exposure times. A montage of the five images in this set of experiments is shown in Figure 22. Each specimen is labeled with its enrichment, and the sum of the enrichments of the specimens within the image is labeled at the bottom. Like the other U metal images, the 54%, 70%, and 93% enriched U metal specimens create clear bright spots allowing their location to be identified, while the specimens at 20.8% enriched and below do not create bright spots.

The mean and standard deviation values for these five images plus a background measurement with the same acquisition time are given in Table 9. A plot of these values versus the added enrichments is shown in Figure 23. The graph of the standard deviation versus the added source strength is shown in Figure 24. The first point in both graphs is the background measurement. The source strength shown is the summed source strengths of the specimens in the image.

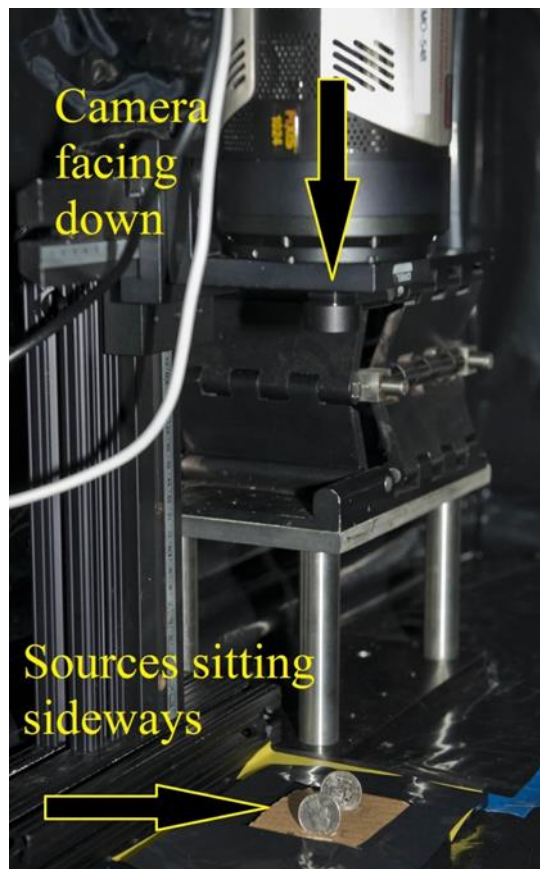


Figure 20. Experimental Set-up: Camera facing down and specimen sitting sideways.<sup>a</sup>

---

<sup>a</sup> Image originally appeared in: J. S. Feener and W. S. Charlton, "Initial Results of Nuclear Fluorescence Imaging for Arms Control Verification," Proceedings of the 54th Institute of Nuclear Material Management Annual Meeting, Palm Desert, CA, July, 2013; and is reprinted with the permission of the Institute of Nuclear Materials Management





Figure 21. Close-up example of specimens sitting sideways configuration (shown as quarters).<sup>a</sup>

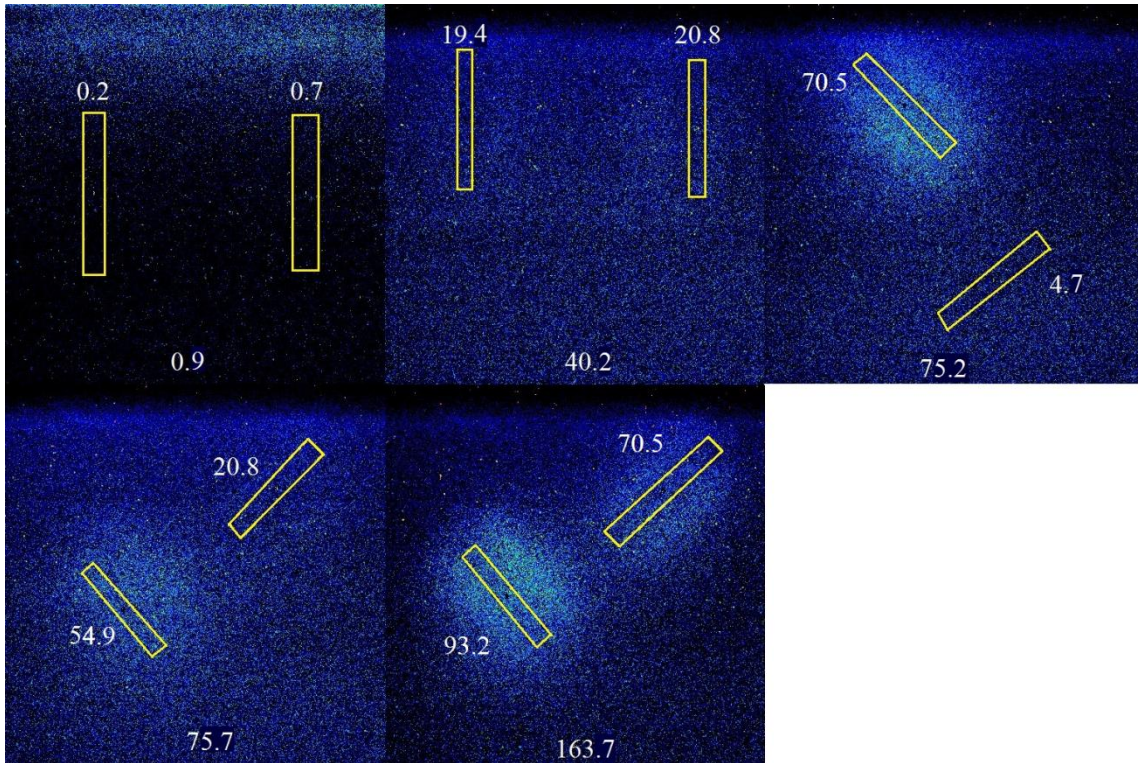


Figure 22. Montage of the analyzed images from multiple U metal specimens, side facing.<sup>a</sup>

---

<sup>a</sup> Image originally appeared in: J. S. Feener and W. S. Charlton, "Initial Results of Nuclear Fluorescence Imaging for Arms Control Verification," Proceedings of the 54th Institute of Nuclear Material Management Annual Meeting, Palm Desert, CA, July, 2013; and is reprinted with the permission of the Institute of Nuclear Materials Management

Table 9

Mean and Standard Deviation Values from Multiple U Metal Specimens, Side Facing

Added Enrichments	BG	0.9	40.2	75.2	75.7	163.7
Mean	457.294	220.564	194.115	143.82	225.896	100.098
StdDev	45.306	33.257	57.034	67.907	56.28	61.45

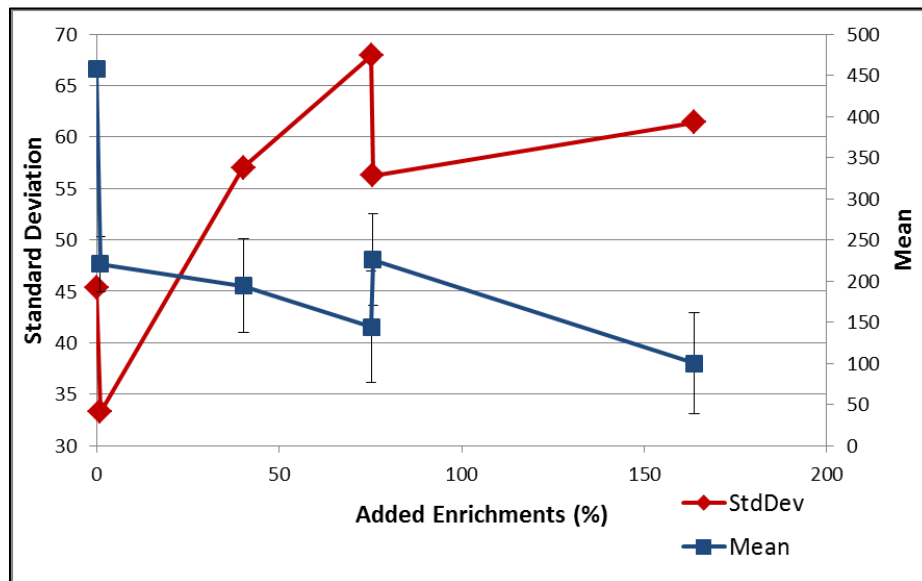


Figure 23. Standard deviation and mean versus added enrichment of images from multiple U metal specimens, side facing

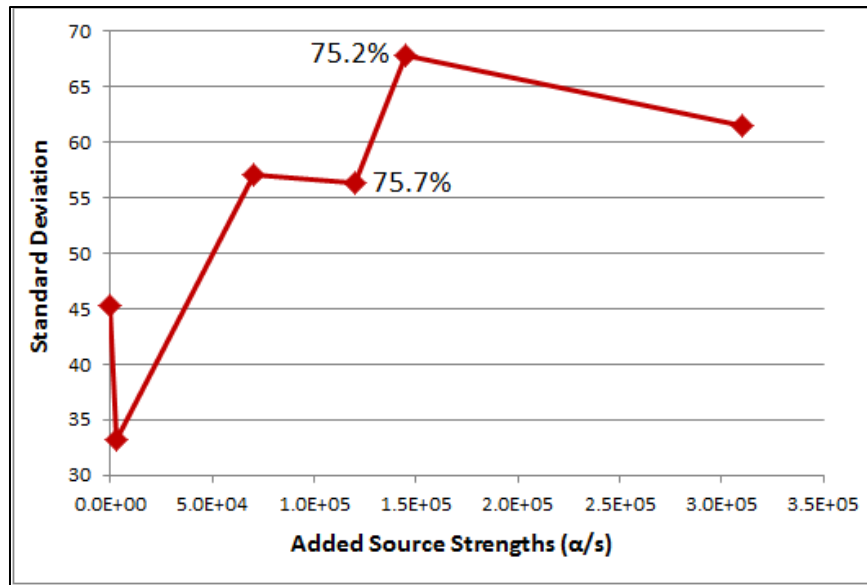


Figure 24. Standard deviation versus the added source strength of images from multiple U metal specimens, side facing.<sup>a</sup>

The mean in Figure 23 varies as it has done in the previous two U metal set-ups. However, the standard deviation does not increase as nicely with enrichment and source strength, shown in Figure 24, as the previous U metal set-ups. One thing to note is that the source strength of the added 75.2% (sum of the 70.5% and 4.7%) image is greater than the 75.7% (sum of the 54.9% and 20.8%) image source strength due to the increased total  $^{234}\text{U}$  content (proportionally the  $^{235}\text{U}$  content is less while the  $^{234}\text{U}$  content is more). Therefore, the 75.2% and 75.7% points are switched in these two plots since the x-axis in Figure 23 increases with enrichment and Figure 24 increases with source

---

<sup>a</sup> Note that the source strength for the combined 75.2% enriched is greater than the combined 75.7% enriched; therefore, these two points are switched from Figure 23 and Figure 24 as their x-axis increase with added enrichment.

strength. Figure 25 graphs both the standard deviation and source strength versus the added enrichments to visualize their change with enrichment together.

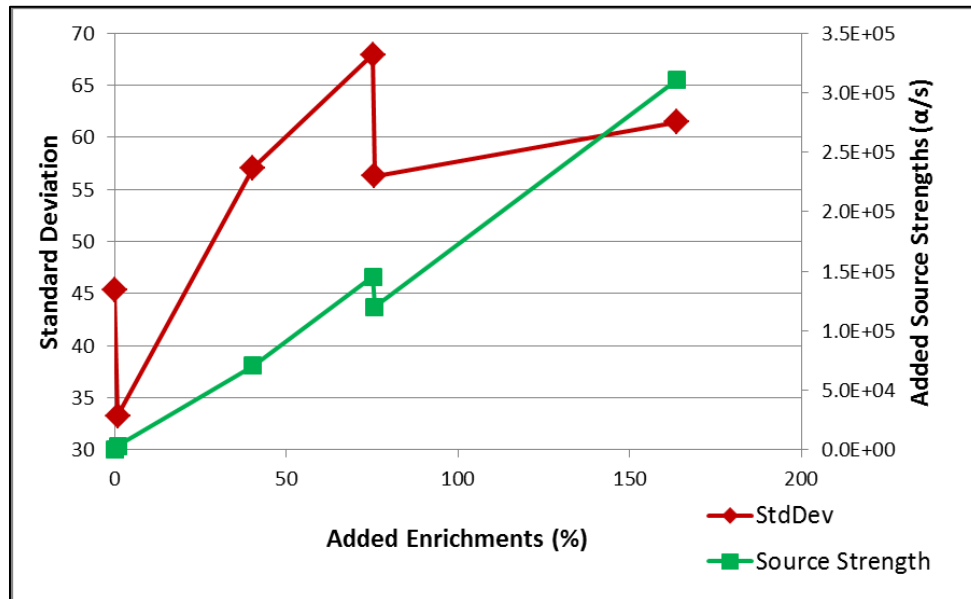


Figure 25. Standard deviation and source strength versus enrichment of images from multiple U metal specimens, side facing.

The drop in standard deviation from the added 75.2% to the 75.7% image could be due to the fact that the alpha source strength is greater for the added 75.2% image. Another explanation for why the standard deviation is greater for the added 75.2% than the 75.7% and 163.7% is that the 75.2% has one bright spot due to the 70% U metal specimen (the 4.7% U metal specimen doesn't create much of a bright stop), while the other two images have two bright spots. The two bright spots will increase the overall average, decreasing the variation between the average of pixel values and bright spot pixel values, therefore decreasing standard deviation. There is not a good explanation for

the drop in standard deviation between the background and added 0.9% image. The 0.9% image is darker than all other images acquired; this could be due to abnormal camera behavior. The standard deviation values are discussed more in Chapter IV where this experimental set-up is simulated.

### *UO<sub>3</sub> and Plastic Scintillation*

Depleted UO<sub>3</sub> and natural UO<sub>3</sub> were imaged in plastic petri dishes for 60 minute exposure times. The dishes were 25 cm from the lens with the camera facing down, similar to the experimental setup shown in Figure 15. A montage of the results including a background image (where salt was placed in the petri dish) is shown in Figure 26.

The mean and standard deviation values for the salt and UO<sub>3</sub> are given in Table 10. A plot of these values versus enrichment is shown in Figure 27. The graph of the standard deviation versus source strength is shown in Figure 28. In both of these plots, the first point is the background (salt in the petri dish) with the same acquisition time.

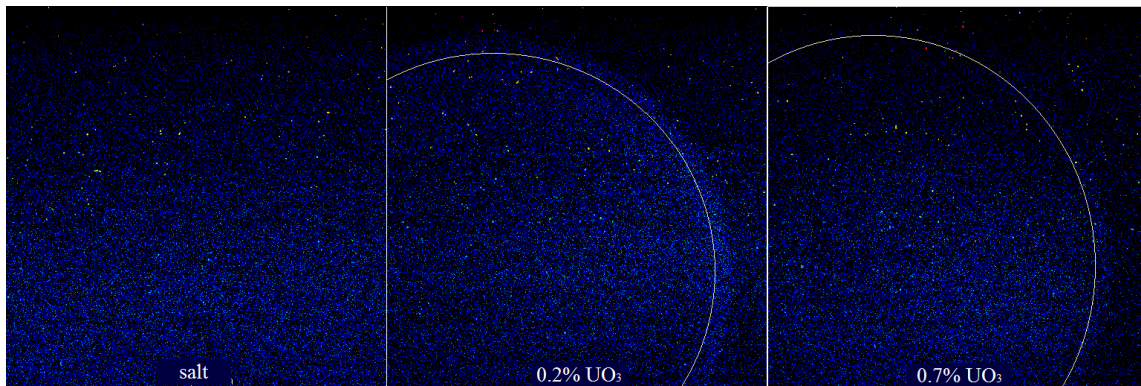


Figure 26. Montage of UO<sub>3</sub> in petri dishes.

Table 10  
 Mean and Standard Deviation Values from  $\text{UO}_3$  in a Plastic Petri Dish

Source	Salt	0.2%	0.7%
Mean	325.605	327.569	395.789
StdDev	39.837	50.492	52.417

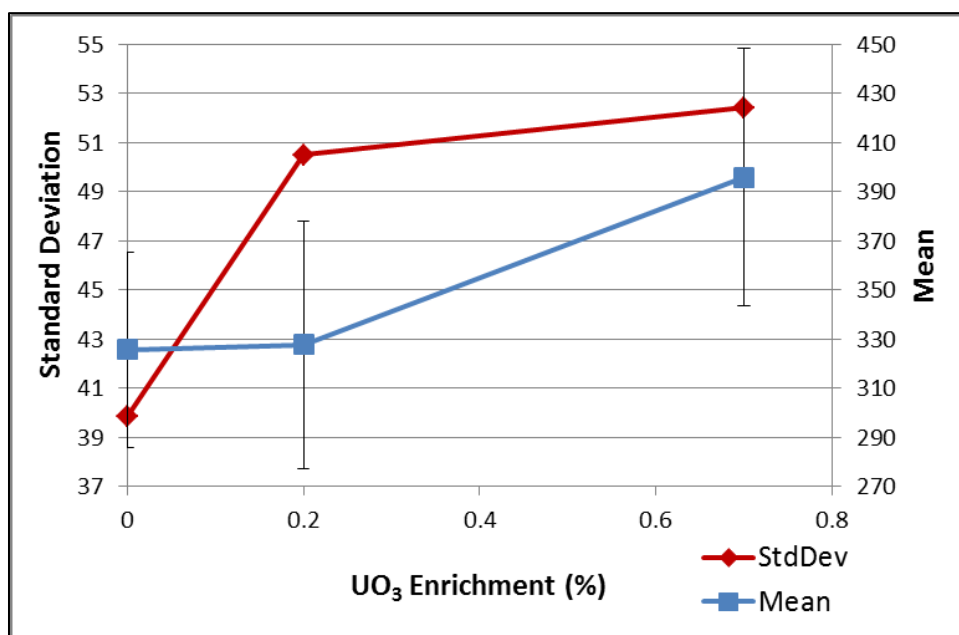


Figure 27. Standard deviation and mean versus  $\text{UO}_3$  enrichment in a plastic petri dish.

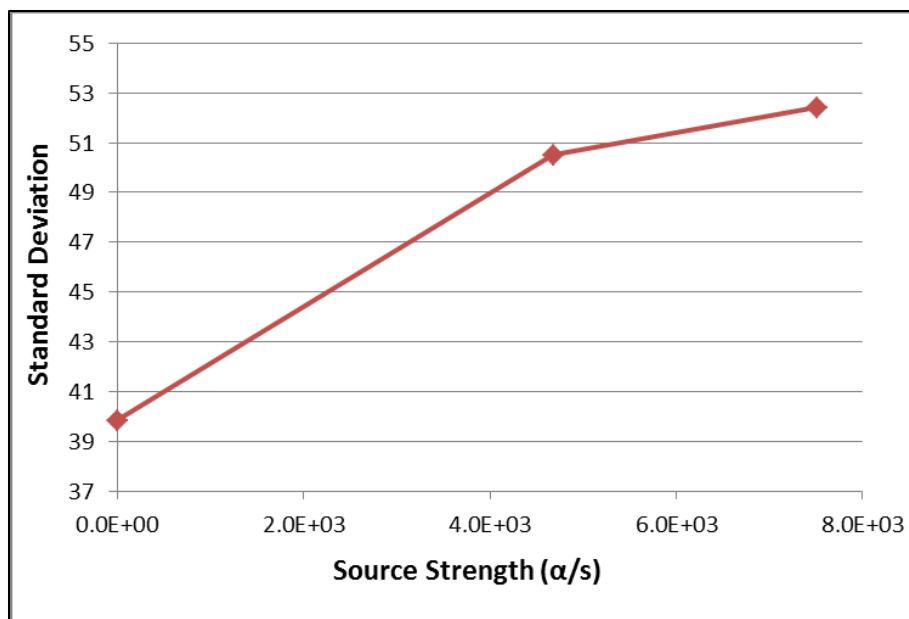


Figure 28. Standard deviation versus  $UO_3$  source strength in a plastic petri dish.

As with the U metal experiments, the standard deviation follows the  $UO_3$  source strength better than the mean. It was noticed that the edges of the petri dishes were lighting up, which is why salt was placed in a petri dish and imaged for the same amount of time. This step was taken to ensure some unknown phenomenon was not happening with the petri dish. When the petri dish containing salt was imaged, the edges did not light up, suggesting the alpha particles from the  $UO_3$  were causing scintillation in the plastic.

To test this theory, the  $^{210}Po$  source was placed upside down and imaged alone and inside a petri dish with an exposure time of 5 minutes. Figure 29 shows the results of these 2 images. Again the petri dish glows, confirming increased photons due to scintillation of the plastic of the petri dish from the alpha particles.



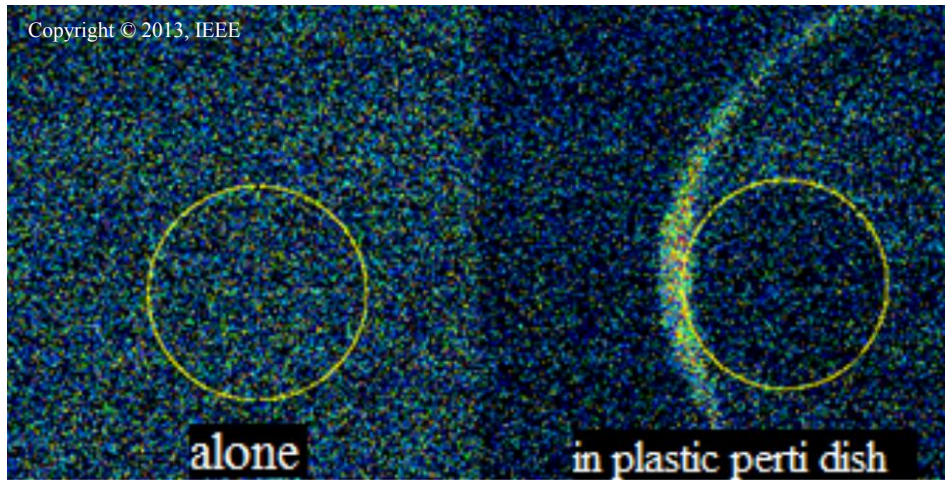


Figure 29.  $^{210}\text{Po}$  source upside down alone and in a plastic petri dish to show plastic scintillation.<sup>49</sup>

The natural  $\text{UO}_3$  was also imaged in a metal dish to confirm the imaging system could identify  $\text{UO}_3$  without the extra scintillation photons in the plastic petri dish. The experimental setup and exposure time is the same as when measured in the plastic petri dish. The natural  $\text{UO}_3$  could also be observed in the metal dish and is shown in Figure 30. The values of the mean and standard deviation of salt and natural  $\text{UO}_3$  imaged in the metal dish are given in Table 11. As when measured in the petri dish, the standard deviation increases with source strength.



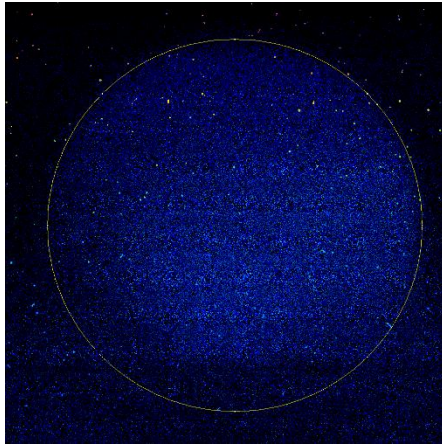


Figure 30. Natural  $\text{UO}_3$  in metal dish.

Table 11  
Mean and Standard Deviation Values from  $\text{UO}_3$  in a Metal Dish

Source	Salt	0.7
Mean	340.235	342.518
StdDev	45.757	50.539

*UV Photon Transmission through Translucent Material*

To examine UV photon transmission through translucent material, the  $^{210}\text{Po}$  source was imaged alone and with eight different thicknesses of H.D.Poly, including 0.079, 0.159, 0.318, 0.635, 1.27, 2.54, 5.08, and 7.62 cm thicknesses (1/32, 1/16, 1/8, 1/4, 1/2, 1, 2, and 3 inch thicknesses respectively). Five-minute exposure times were used. The distance between the lens and the source was 26 cm and the H.D.Poly was held by a plastic cylinder ~4 cm above the source as shown in Figure 31. Figure 32 shows a montage of these images, including a background image with the same exposure time for comparison. In the image with no H.D.Poly, the metal grating can clearly be

seen. The edge of the cylinder is also lit up which is most likely due to scintillation in the plastic (as discussed above). The images become blurred with increased thickness of H.D.Poly until a difference cannot be seen between background and an image with source.

Table 9 gives the mean and standard deviation values for each of these images. Figure 33 shows a scatter plot of these values. The last point in the graph is the background measurement with the same exposure time.

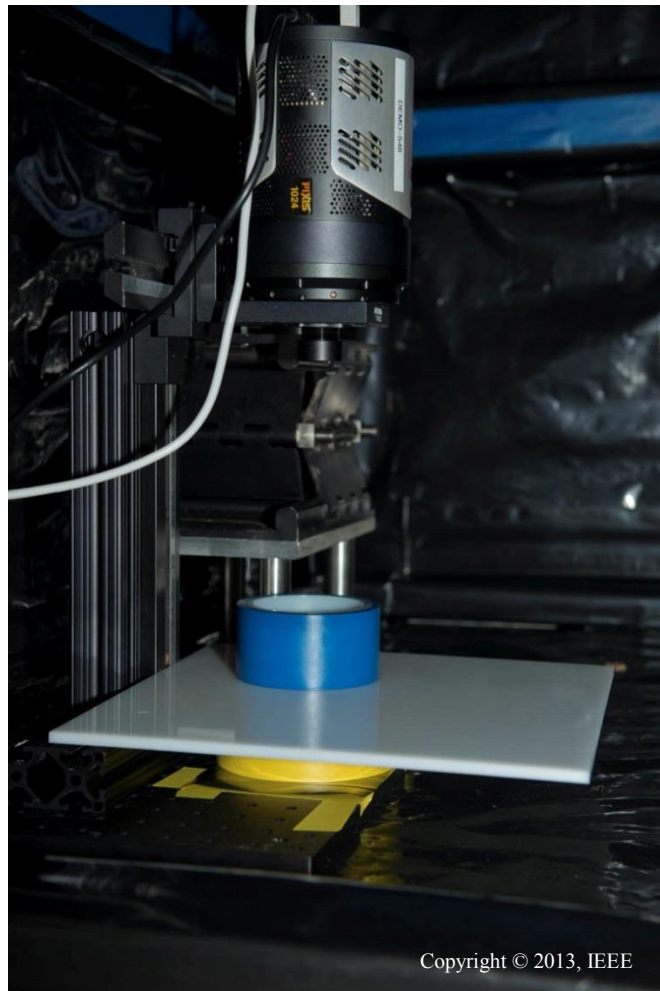


Figure 31. Experimental set-up:  $^{210}\text{Po}$  source with H.D. Poly held  $\sim 4\text{cm}$  above.<sup>49</sup>



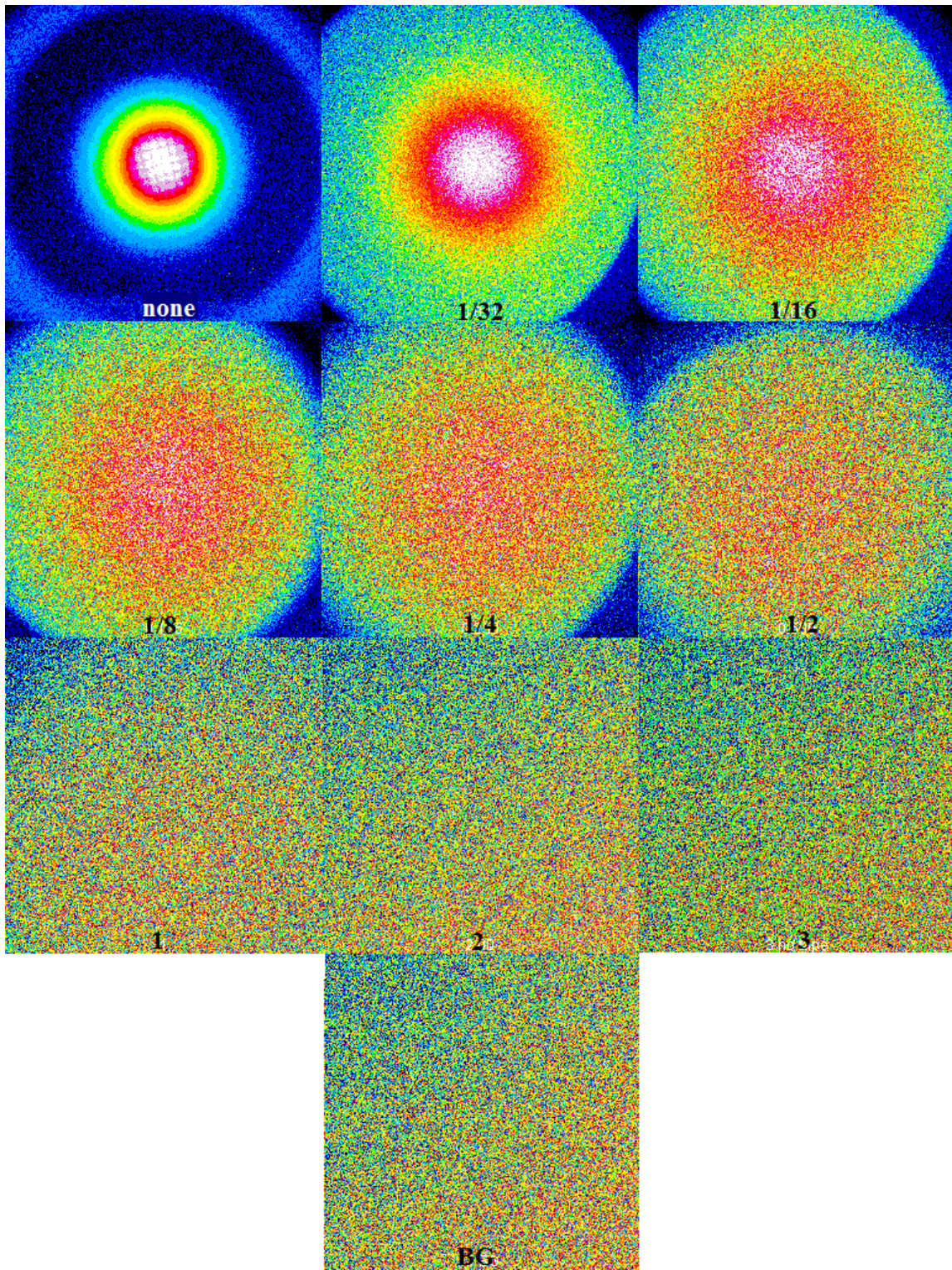


Figure 32. Montage of  $^{210}\text{Po}$  source with different thicknesses of H.D.Poly.

Table 12  
 Mean and Standard Deviation Values of  $^{210}\text{Po}$  with Different Thicknesses of H.D.Poly

H.D.Poly Thickness (inches)	Mean	StdDev
none	311.065	327.062
1/32	330.999	39.78
1/16	316.947	24.446
1/8	297.931	20.591
1/4	283.968	13.927
1/2	234.174	16.904
1	214.561	7.898
2	209.692	7.507
3	211.774	13.893
BG	217.55	12.573

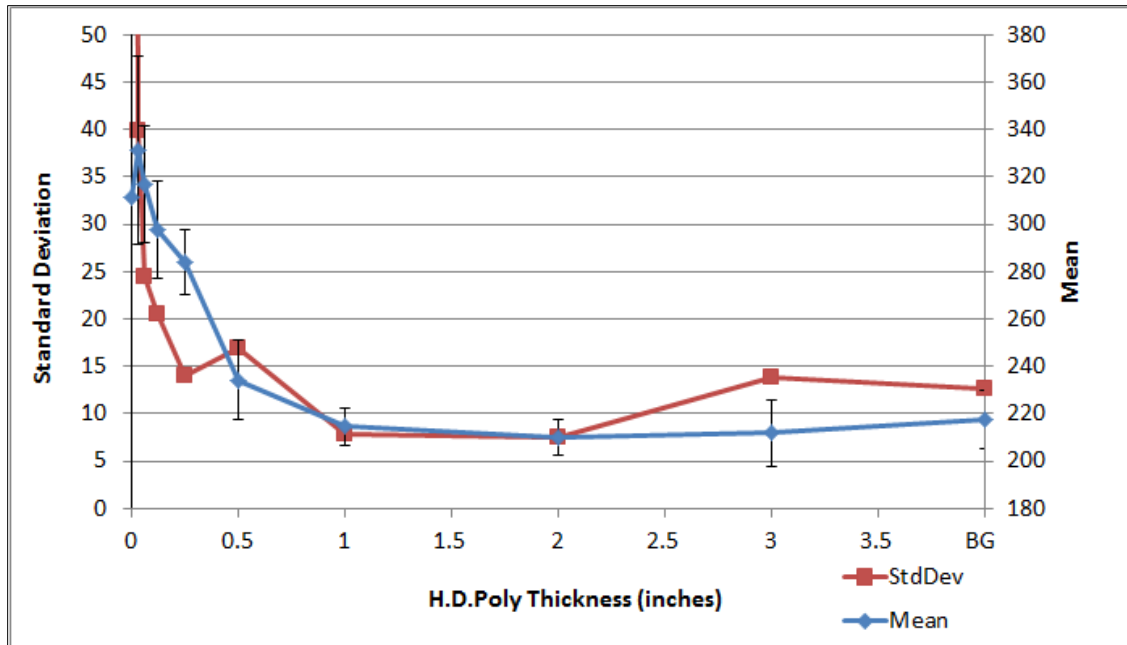


Figure 33. Standard Deviation and Mean for  $^{210}\text{Po}$  source with different thicknesses of H.D.Poly.<sup>a</sup>

Because of the multiple data points less than 0.5 cm of H.D.Poly thickness, and the standard deviation extending beyond the range of the graph, the data points are also plotted in a bar graph in Figure 34. Here, although the x-axis does not increase proportionally with the thickness of the H.D.Poly, each data point can be seen more clearly.

<sup>a</sup> The standard deviation for no H.D.Poly extends beyond the graph. The last point is the background (BG) data.



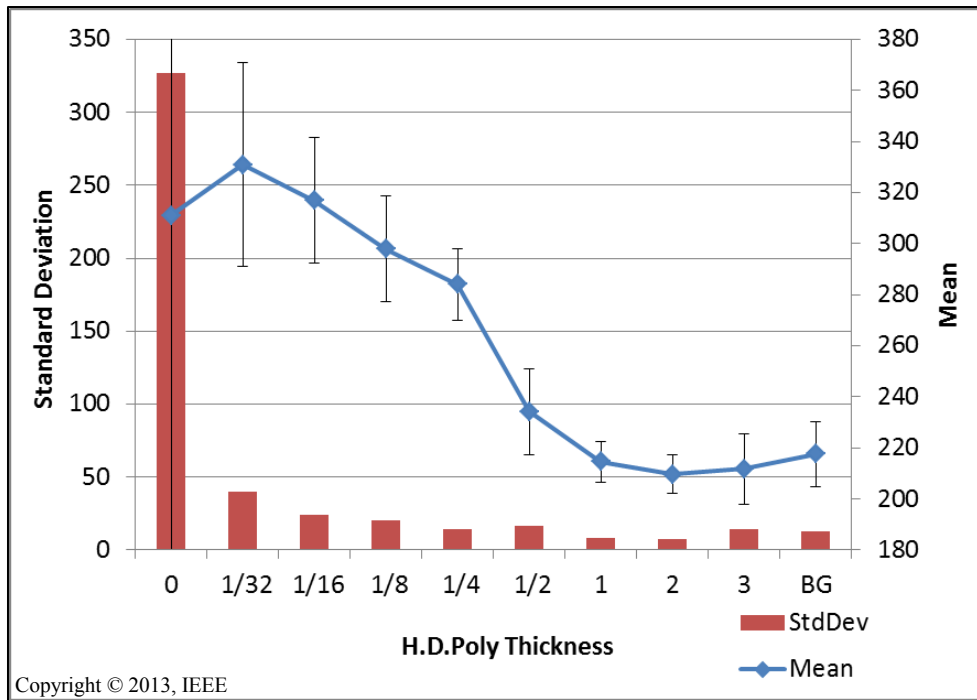


Figure 34. Standard Deviation and Mean for  $^{210}\text{Po}$  source with different thicknesses of H.D.Poly – bar graph.<sup>a,49</sup>

Here it is the mean, not the standard deviation, that follows the H.D.Poly thickness. Because these are shorter exposure times with a strong source, the background and dark current have little effect on the image. Therefore, the mean, which is just the average pixel value, will follow the number of photons impinging on the CCD.

The means from the 1/32” and 1/16” H.D.Poly thickness increase slightly from 0 H.D.Poly. This rise could be due to increased scintillation photons produced by alpha particles interacting with the H.D.Poly (the source was ~4cm from the H.D.Poly – very close to the range of 5.3 MeV alpha particles in air from  $^{210}\text{Po}$ ). At 1/8” and above, the

<sup>a</sup> The standard deviation error bar on the mean for no H.D.Poly (0 thickness) extends beyond the graph.

increased thickness of the H.D.Poly starts attenuating more photons than it produces, causing the mean to decrease until it falls within background levels. While the graph indicates that images with a 1/2" or more H.D.Poly falls within background, you can still make out the edges of the cylinder at 1" H.D.Poly thickness.

#### *UV Photon Transmission through Non-Translucent Material*

To examine UV photon transmission through non-translucent material, the  $^{210}\text{Po}$  source was imaged with black plastic between the source and camera lens. Nothing above background was observed; therefore, iron foils were placed directly on top of the source to confirm that only alpha particles penetrating the foil are creating UV photons observed by the camera. The 3 foil thicknesses were 0.005 mm (thin enough for 5.3 MeV alphas to penetrate), 0.01 mm, and 0.025 mm (optically thick to 5.3 MeV alphas). Thirty minute exposure times were used in this series of experiments. Figure 35 shows a montage of the  $^{210}\text{Po}$  source with 0.005 mm Fe, 0.01 mm Fe, black plastic, and background. As expected, when the alpha particles penetrate the foil, the source is clearly seen (Figure 35 0.005 mm Fe foil). When the alpha particles are unable to penetrate the foil or the UV photons are blocked by a non-translucent material, the source is not seen by the camera (Figure 35 0.01 mm Fe foil and black plastic, respectively).

Figure 36 plots the standard deviation and mean of the 3 Fe foils, the black plastic, and the background. The mean of the images doesn't convey much information about the images. Instead, the standard deviation is significantly greater for the one image in which the source can be seen. Similar to the U metal specimen experiments,

these are longer exposure times with a weaker source (due to the Fe foil shielding).

Thus, the standard deviation will reveal any bright spots in an image.

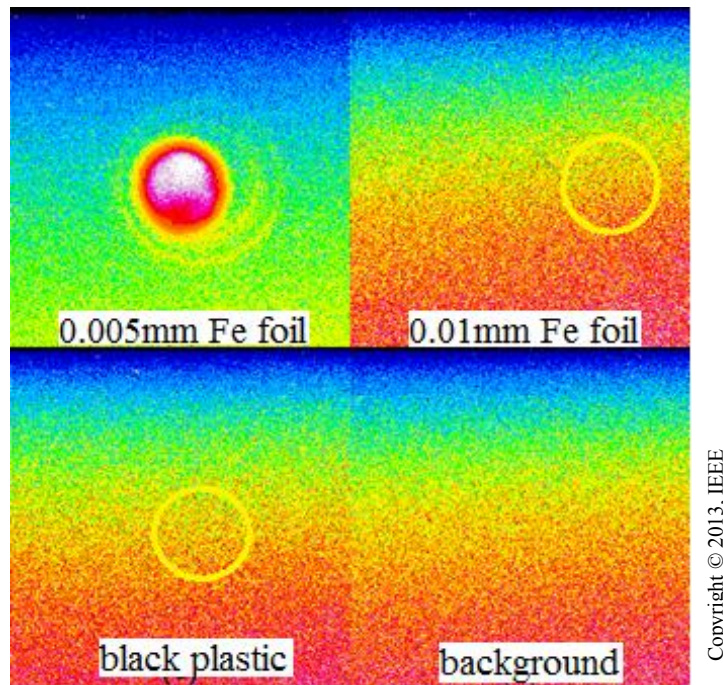


Figure 35. Montage of  $^{210}\text{Po}$  source with Fe foil, black plastic, and background.<sup>49</sup>



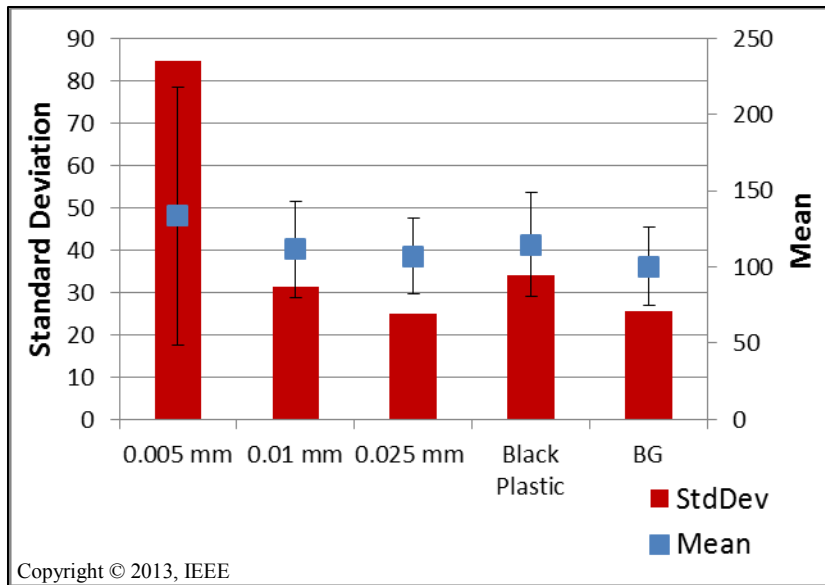


Figure 36. Standard deviation and mean of  $^{210}\text{Po}$  source with non-translucent materials.<sup>49</sup>

### *Beta and Gamma-ray Emitting Sources*

Several 60-minute acquisition time measurements were taken with the “beta” sources at 25 cm from the camera lens, but nothing above background was observed. Therefore, the sources were moved to 1 m from the camera lens to see if the increased field-of-view would be able to capture the approximate source location. Again, nothing above background was seen. Similarly, the “gamma” sources were imaged at 1 m from the camera lens with an exposure time of 60 minutes; nothing above background was observed. A plot of the mean and standard deviation for these configurations is shown in Figure 37. The mean and standard deviation both oscillate around background levels further indicating the imaging system could not observe these sources. One explanation is that the sources are just too weak or there needs to be a greater field-of-view to capture increased UV photon activity due to the long range beta particles and gamma-

rays. The more likely explanation is that this imaging system is not sensitive to these radiations.

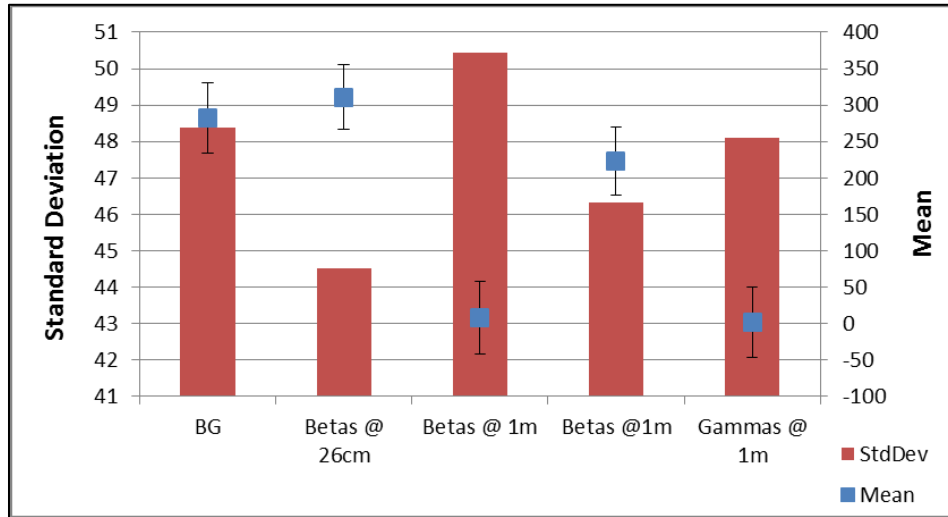


Figure 37. Mean and standard deviation of beta and gamma sources.

### *Distance*

The  $^{210}\text{Po}$  source was imaged at 26, 100, and 146 cm for 5-minute exposure times to observe how distance affects the image. The image at 26 cm was taken as shown in Figure 31. The 100 and 146 cm images were acquired with the  $^{210}\text{Po}$  source on a source stand perpendicular to the ground, similar to Figure 7. A montage of the 3 images is shown in Figure 38. The 100 and 146 cm images have extra light at the bottom of the image; this could be due to the fluorescence photons reflecting off the black plastic that lines the light-tight-black-box. Because these three images were not acquired in the same experimental set-up (the 26 cm image has the plastic cylinder around it and the reflected light in the 100 and 146 cm image), the yellow squares in the montage show a selection

that data was also acquired from. Table 13 gives the mean and standard deviation values for the whole image and the selection. The mean and standard deviation for the selection is graphed in Figure 39.

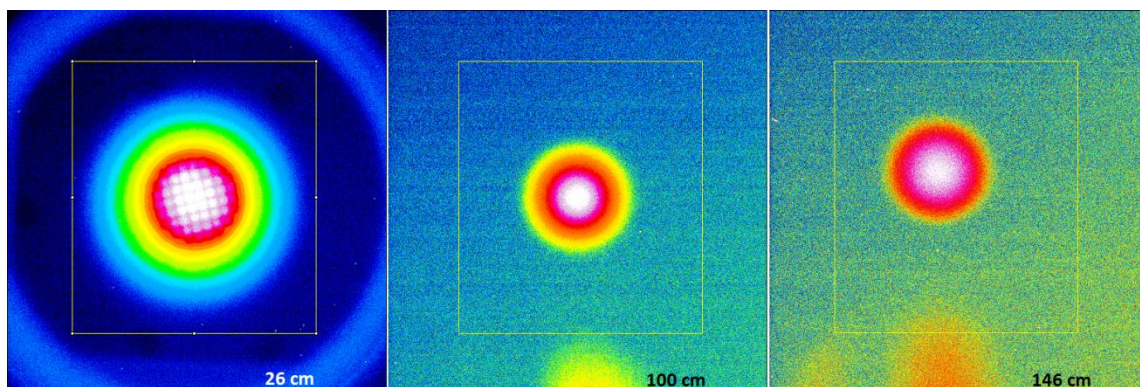


Figure 38. Montage of  $^{210}\text{Po}$  source at various distances.<sup>a</sup>

Table 13  
Mean and Standard Deviation Values for the  $^{210}\text{Po}$  Source at Various Distances

Distance (cm)	Mean Whole Image	StdDev Whole Image	Mean Selection	StdDev Selection
26	311.065	327.062	429.702	452.276
100	195.104	33.869	202.601	48.26
146	199.96	15.147	201.748	14.376

---

<sup>a</sup> The yellow boxes represent the selection area.

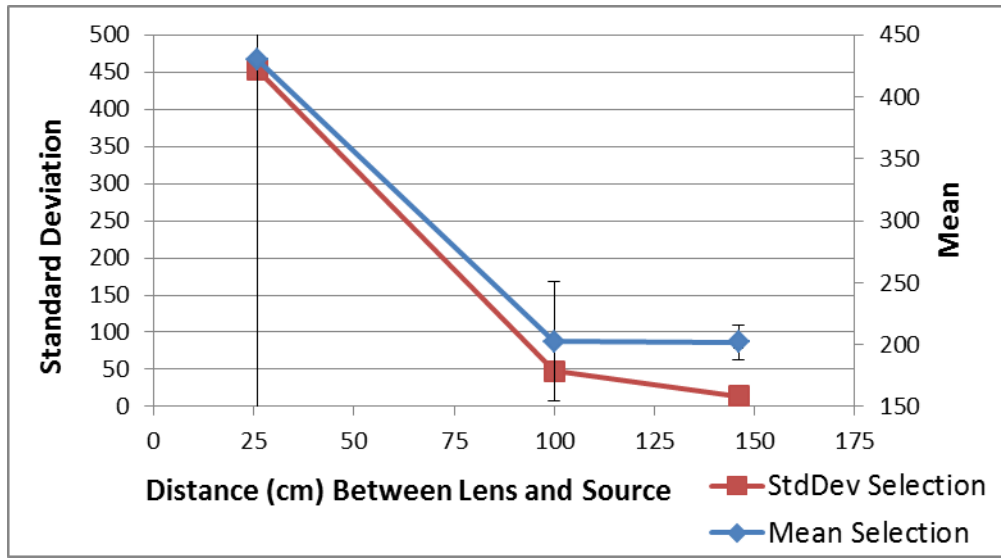


Figure 39. Mean and standard deviation of  $^{210}\text{Po}$  source at various distances. <sup>a</sup>

Because these are shorter exposure times with a strong source, it is expected that the mean would follow the data trend, decreasing with distance, better than the standard deviation. But the mean decreases insignificantly from the 100 to 146 cm distance while the standard deviation decreases fairly linearly with distance.

#### *Point Source to Surface Source Spoof*

To investigate whether a point source could be made to look like a surface source, the  $^{210}\text{Po}$  source was surrounded by polyethylene (poly) beads and imaged for an exposure time of 30 minutes at 100 cm from the camera lens. The aim of this setup was to see if the polyethylene beads could blur the point source enough to make it look like a surface source. The  $^{210}\text{Po}$  source was placed in a glass jar then placed in a glass beaker filled with polyethylene beads as shown in Figure 40.

---

<sup>a</sup> The standard deviation error bar on the mean at 26 cm extends beyond the graph.

A montage of the  $^{210}\text{Po}$  source imaged alone at 100 cm for 5 minutes (left) and in the polyethylene beads at 100 cm for 30 minutes (right) is shown in Figure 41. The black “x” shows the position of the source, and the white cylinder on the right represents the approximate location of the glass beaker. The polyethylene beads are successful at blurring the photons to make it look like a surface source, but they also decrease the intensity, thereby requiring a longer exposure time. This result shows that a point source can be made to look like a surface source, but the acquisition times will vary depending on the source strength and polyethylene bead thickness.



Figure 40. Photograph of  $^{210}\text{Po}$  source surrounded by polyethylene beads.

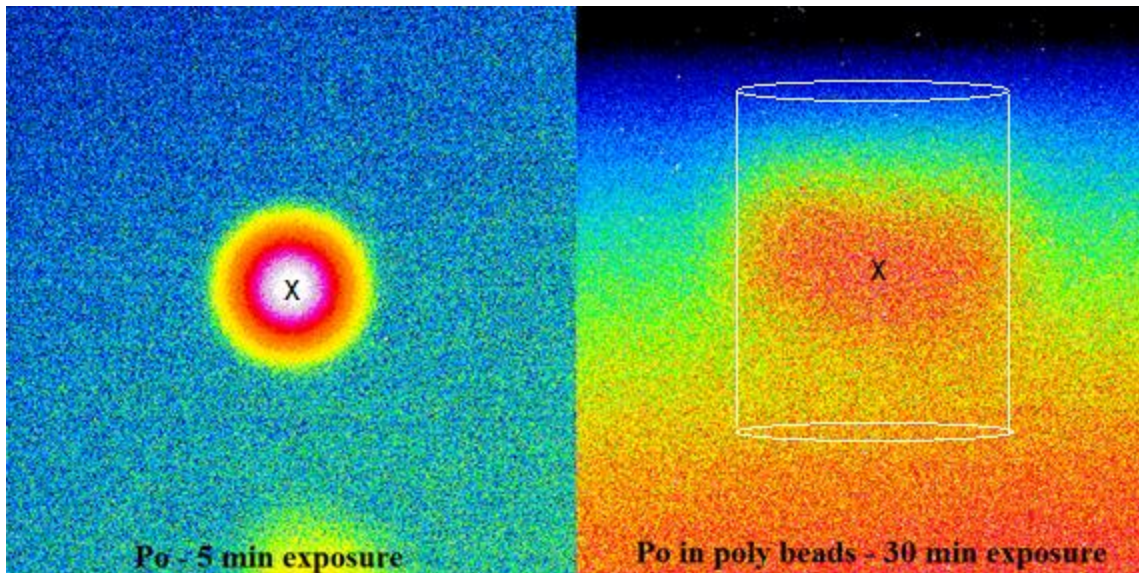


Figure 41. Montage of  $^{210}\text{Po}$  source images at 100 cm alone for 5 minute (left) and in polyethylene beads for 30 minutes (right).

### III.F. Experimental Conclusions Summary

While a limited number of experiments could be performed because of the limited time with the PIXIS camera and the number and types of sources available, enough information was collected to confirm the imaging system proof-of-concept. A number of conclusions can be made from the image data and what this data can tell about the material it is measuring.

First, in images with higher source strengths and shorter exposure times (less than 10 minutes), the mean does a better job of following data trends. In images with lower source strengths and longer exposure times (greater than 10 minutes), the standard deviation does a better job of following data trends. This behavior makes sense because, as the exposure time increases, the camera's dark current and background (that changes from day-to-day and image-to-image) has more effect on the image and therefore the

image mean. The standard deviation is taken relative to the mean; it is a measure of the variation of pixel values from the average. Therefore, even if the camera's behavior changes in a particular image, the greater number of UV photons from a source that hit the CCD will create a greater standard deviation. This result is true regardless of the intensity of the background and the dark image, as long as the background and dark image is evenly distributed across any one image or distributed the same when comparing two or more images.

Analysis has shown that the imaging system can generally discriminate between uranium of differing enrichments while not being able to provide isotopic data from the source. This result is expected because the fluorescence photons being imaged are secondary particles created by the nitrogen molecules de-exciting, which emit the same spectrum regardless of how they were excited. The image data follows material alpha particle source strength; therefore as long as the uranium was enriched via gaseous diffusion or gas centrifuge (and the  $^{234}\text{U}$  to  $^{235}\text{U}$  ratio reflects this) the imaging system can differentiate enrichment. Because the image data follows source strength, it is not able to differentiate between U metal and U oxide.

The U metal montages show that the 54% and higher enriched U metal specimen locations can be clearly identified by bright spots on the image. This is not true for the specimens at 20.8% enriched and below. This result indicates a visual detection limit between these two source strengths for the U metal in the experimental setup in which the images were taken. Once the image was analyzed, the image data was able to detect



the 4.7% enriched U metal and the depleted UO<sub>3</sub>, indicating a detection limit for analyzed images for U metal and oxide.

The material shape resolution depends on the source strength and the distance between lens and source. The resolution of the 93% enriched U metal specimen is approximately ~1 cm and detailed geometrical data ought not to be determined due to fuzzy edges around the specimen. On the contrary, for a strong source such as the <sup>210</sup>Po, the detailed shape of the metal grating could be seen at 26 cm indicating a resolution in the mm range. The image was blurred at 100 cm, showing that the resolution can be degraded by distance.

It was confirmed that the fluorescence photons can pass through translucent material and do not pass through non-translucent material. Thus, to acquire an image, the alpha particles from the material must be able to penetrate the air with no non-transparent material between the lens and the fluorescence photons being produced. Because it takes very little to shield alpha particles, the material will need to be uncanned when imaged. It was also determined that if the alpha particles can interact with a scintillating material, additional photons are created which can make the scintillating material light up. While some scintillating material can increase the signal, as the material thickens it will start attenuating more photons than it is producing, decreasing the overall signal. Translucent materials can also distort the shape of a source, making it possible to make a point source look like a surface source.



Lastly, the imaging system appears to be blind to beta particles and gamma-rays. Additional experiments with stronger beta particles and gamma-rays sources should be performed to confirm this conclusion.

## CHAPTER IV

### SIMULATIONS

#### IV.A. Simulation Overview

To simulate the fluorescence images and calculate the mean and standard deviation of these images, a combination of the GEANT4 Simulation Toolkit and a small computer code written in the Python Programming Language was used. GEANT4 was used to simulate all the U metal experimental set-ups, the UO<sub>3</sub> in the plastic petri dish, and the <sup>210</sup>Po source by itself. GEANT4 created and transported the fluorescence photons then collected the energy and location of the photons on a surface representative of the CCD field-of-view. The Python code then collected the photon data, sorted it into pixel values, calculated the mean and standard deviation, and produced the images.

#### *Alpha Particle Energy Distribution*

Alpha particles were simulated in GEANT4 to confirm their energy distribution in air was similar to experimental results. To do this, alpha particles were simulated in the U metal specimens with alpha energies and intensities according to the enrichment. The alpha particle energies were then collected in air as they were emitted from the surface of the specimen and at half cm increments from the surface. GEANT4 then output a comma separated variable (csv) file with the alpha particle energy at each surface it passed. Python read the csv file and summed the energy at each surface.

To compare to the experimental energy distribution, a plot profile of the 93% enriched U metal specimen sitting sideways was used. A plot profile displays a two-dimensional graph of the intensities of pixels along a line or rectangular selection. The

pixel intensities show where the fluorescence photons are originating from and thus where the alpha energy is deposited. Figure 42 shows a screen shot image of the 93% U metal specimen sitting sideways with the rectangular selection and the associated profile plot. With the rectangular selection, the profile plot displays a ‘column average plot,’ where the X axis represents the horizontal distance through the selection and the Y axis represents the vertically averaged pixel intensity.

The pixel numbers and intensities can then be exported to excel. Knowing the number of pixels per cm allows for the conversion of pixel numbers to length. The experimental pixel intensity data and the simulated summed alpha energy versus distance from source are shown in Figure 43.

The simulated alpha particle energy distribution matches well with the experimental results. Therefore, the alpha particle energy distribution was simulated for each U metal specimen, UO<sub>3</sub>, and the <sup>210</sup>Po source. This energy distribution was then used to create the fluorescence photon input for GEANT4.

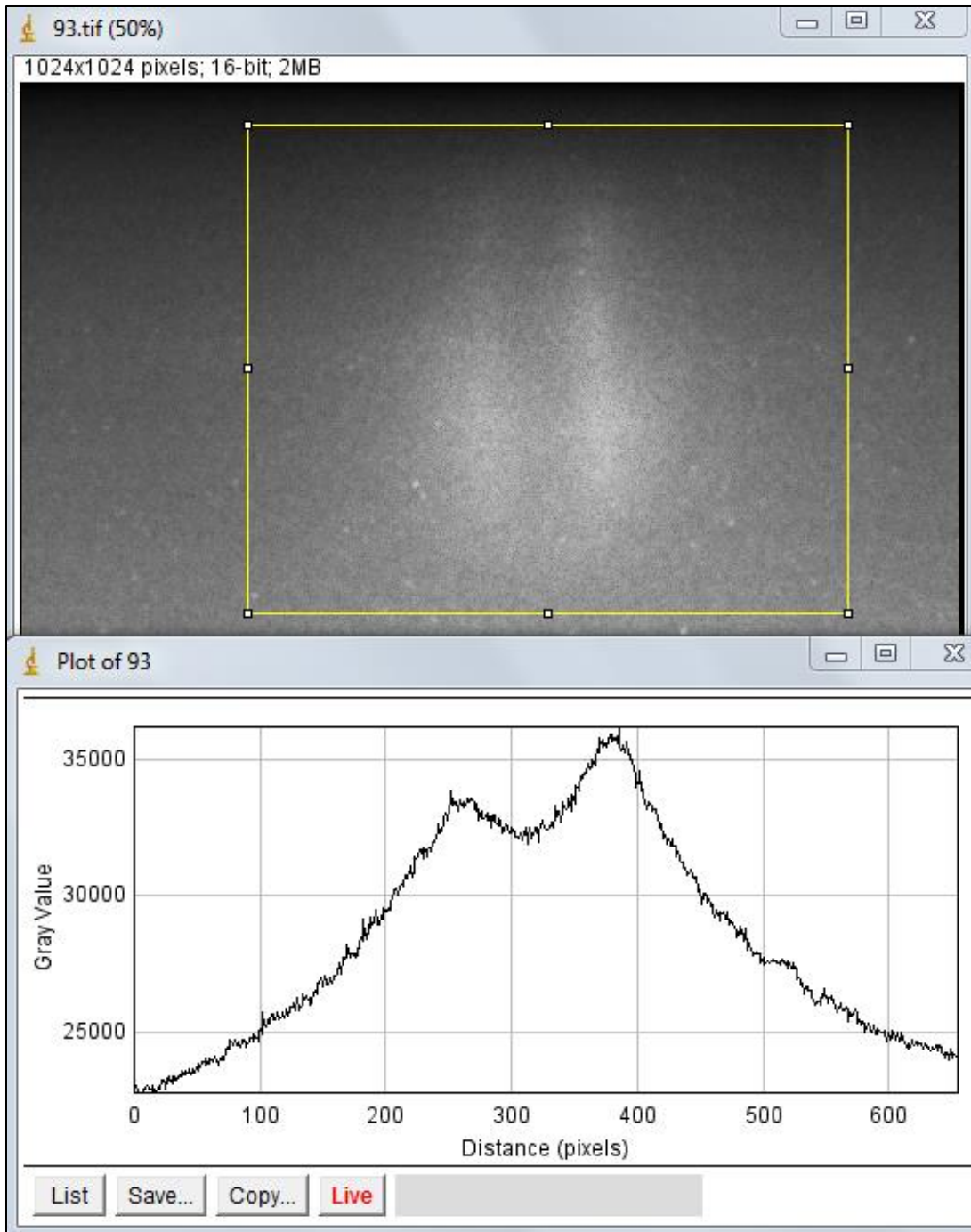


Figure 42. Screenshot of the 93% U metal specimen and associated plot profile.

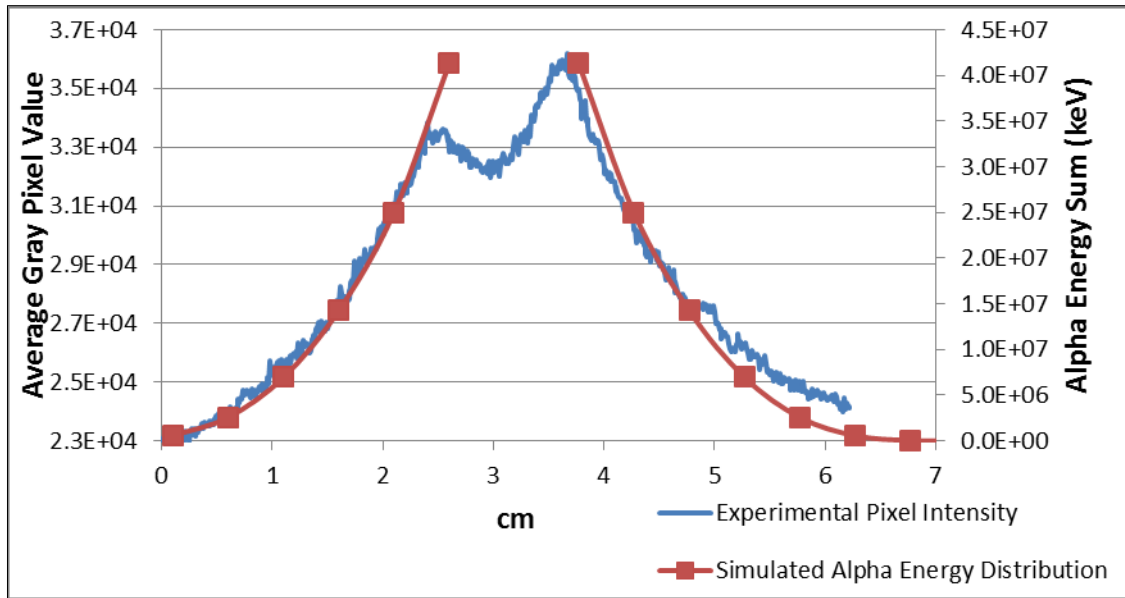


Figure 43. Alpha energy distribution comparison from GEANT4 and experimental result.

### *GEANT4 Fluorescence Simulation*

The General Particle Source (GPS) within GEANT4 was used to generate the initial particles from the source. GPS allows the specification of the spectral, spatial and angular distribution of the primary source particles.<sup>51</sup> Optical photons were used as the initial particles.<sup>a,52</sup> The spatial distribution was created from the simulated alpha particle energy distribution discussed in the previous section. The spectral distribution is made from the nitrogen fluorescence photon spectrum.<sup>b</sup> The optical photons are emitted in a beam towards the detector surface to simulate the intensity each CCD pixel observes.

<sup>a</sup> Simulations were also run with ‘gamma-rays’ to compare to the results from optical photons. There was no distinguishable difference in the results. This could be due to the fact that the distance traveled by the gamma-rays and optical photons is significantly smaller than their mean free path in air.

<sup>b</sup> Figure A2 shows a graph of the fluorescence spectrum used in the simulations.

The low energy electromagnetic Livermore physics list, 'G4EmLivermorePhysics,' was used to transport the optical photons through air. In the stepping action when a photon hit a surface that was non-translucent, such as the U metal, the particle was killed. When the photon hit the 'detector' surface, the x, y, and z location and energy of the photon was collected and saved in a csv file. The detector surface was sized to simulate the field-of-view of the CCD.

As the number of fluorescence photons is proportional to the number of alpha particles emitted, the number of photons created in each run is proportional to the number of alpha particles emitted over the experimental exposure time. The GPS file and header files for the 0.7% U metal simulation are given in Appendix B.

#### *Python Calculations*

The csv files created by GEANT4 are read by the Python code. Python first makes a matrix with 512 rows and 512 columns to represent the CCD pixels. The 512 rows and columns are half the 1024 by 1024 pixels in the camera CCD. Using half the actual experimental value was deemed acceptable as the simulations are representative, image quality is not compromised, and it decreased computational time. Each line of the csv file is read and the location where the photon hit the detector is sorted into its 'pixel' location and the energy of the photon is added to the array location.

The image mean is calculated by:

$$\bar{x} = \frac{\text{sum of all pixel values}}{N}$$

where  $N$  is the number of pixels. The standard deviation is calculated by:

$$s = \sqrt{\frac{1}{N-1} \sum_{i=1}^N (x_i - \bar{x})^2}$$

where  $x_i$  is the value at each array location. Lastly, Python creates a surface plot where the z axis is a representation of the value of the array points in a 2D array. The error in the mean and variance of the variance was also calculated, but the error bars are too small to be seen in the figures showing the mean and standard deviation results. A sample python code that was used to calculate the mean and standard deviation, create the simulated images, and calculate the error in the mean and deviation of the standard deviation is given in Appendix C.

#### **IV.B. Simulation Results**

In each set of the simulated results, a montage of the simulated images will be shown similar to the experimental results. When plots are shown, the first point is a background measurement/simulation unless otherwise specified. Normalized values are normalized to one.

##### *Single U Metal Specimens, Front Facing and Background Effects*

A montage of the single U metal specimens, front facing is shown in Figure 44. The enrichment of the specimen is labeled at the bottom of the image. Each image was scaled independently with the maximum value equal to the largest value in the matrix.

Each specimen looks very similar, while the pixel intensity scale varies significantly. This result is expected, as the alpha particle energy distribution varies little between the different enrichments making each specimen look the same, while the source strength varies by orders of magnitude like the intensity scale.

Figure 45 shows a montage of the same images, single U metal specimens, front facing, on a single intensity scale. The enrichment of the specimen is labeled at the bottom of the image. These simulated images look more like of the experimental images because the decreased intensity acts similar to the background in the experimental images, masking the lower enriched specimens. However, the lower enriched specimens can still be faintly seen because background was not simulated and does not mask the weak signal.

A plot of the normalized values of the standard deviation, mean, and source strength versus enrichment from simulated images is shown in Figure 46. The mean and standard deviation both follow the source strength fairly closely.

As in the experimental data, the standard deviation is a measure of the variation of pixel values from the average. Thus, the larger number of photons from the source that hit the detector surface will create a bright spot and increase the standard deviation. As there is no background in the simulated images, the mean also increases with source strength.



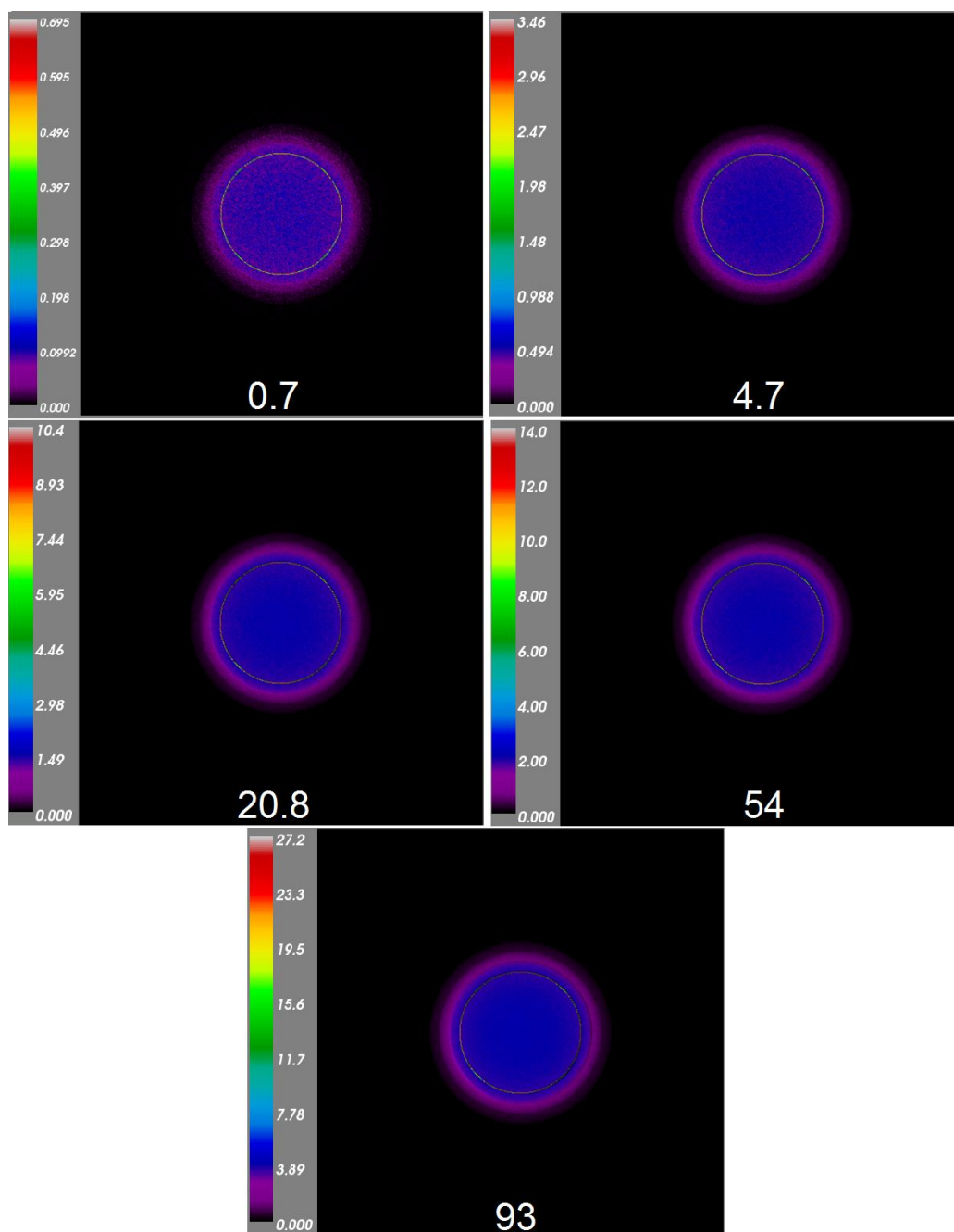


Figure 44. Montage of the simulated images from single U metal specimens, front facing – each image has individual intensity scale.

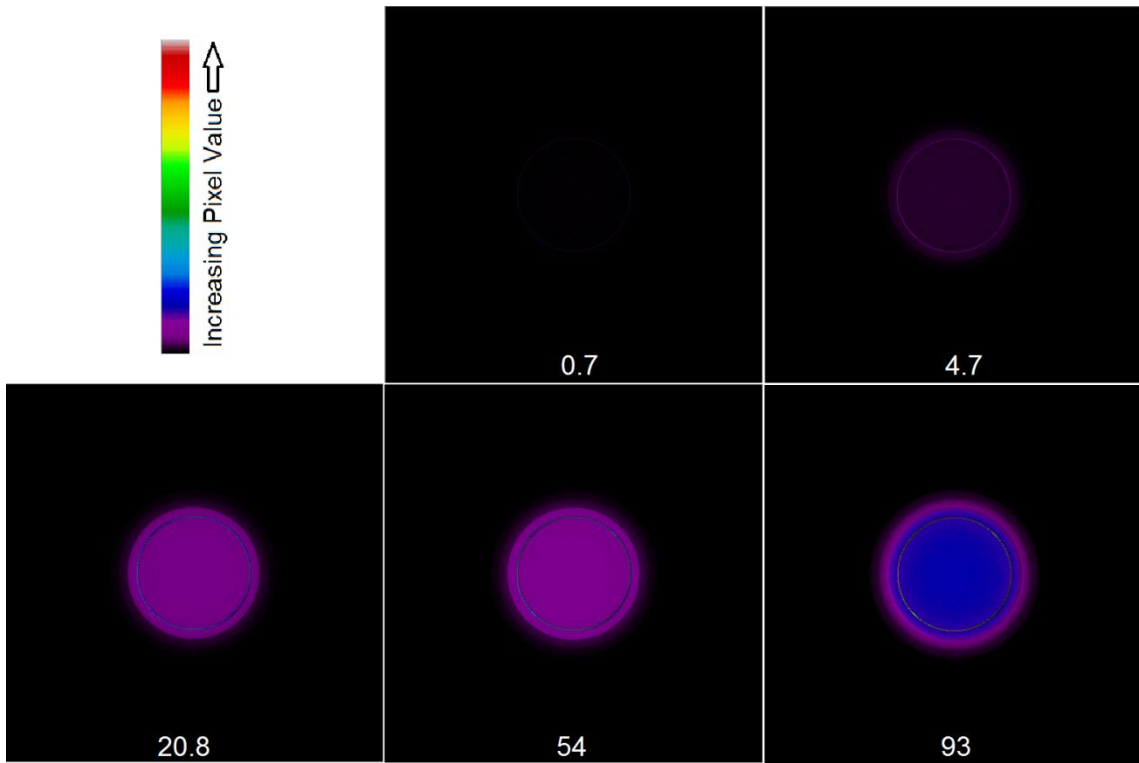


Figure 45. Montage of the simulated images from single U metal specimens, front facing – all images on the same intensity scale.

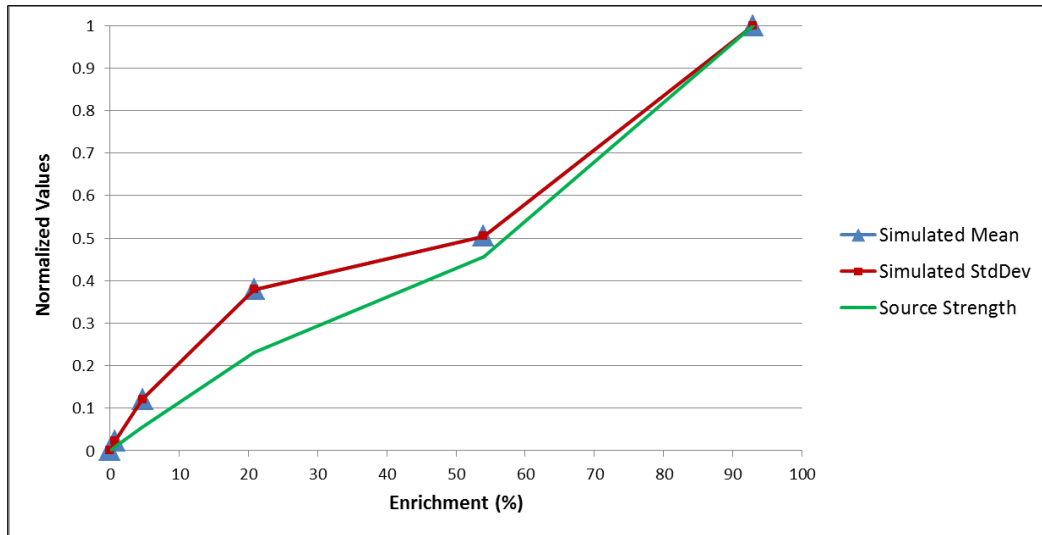


Figure 46. Normalized standard deviation, mean, and source strength versus enrichment from simulated images of single U metal specimens, front facing.<sup>a</sup>

To confirm the mean fluctuates with background while the standard deviation increases with source strength regardless of background, background was added to the 0.7% and 20.8% enriched simulations. The background was evenly distributed over the representative CCD matrix. The resulting plot of the normalized values of the standard deviation, mean, and source strength versus enrichment is shown in Figure 47. As expected, the mean varies with background while the standard deviation increases with source strength.

---

<sup>a</sup> Error bars on the simulated points are too small to be seen on graph.

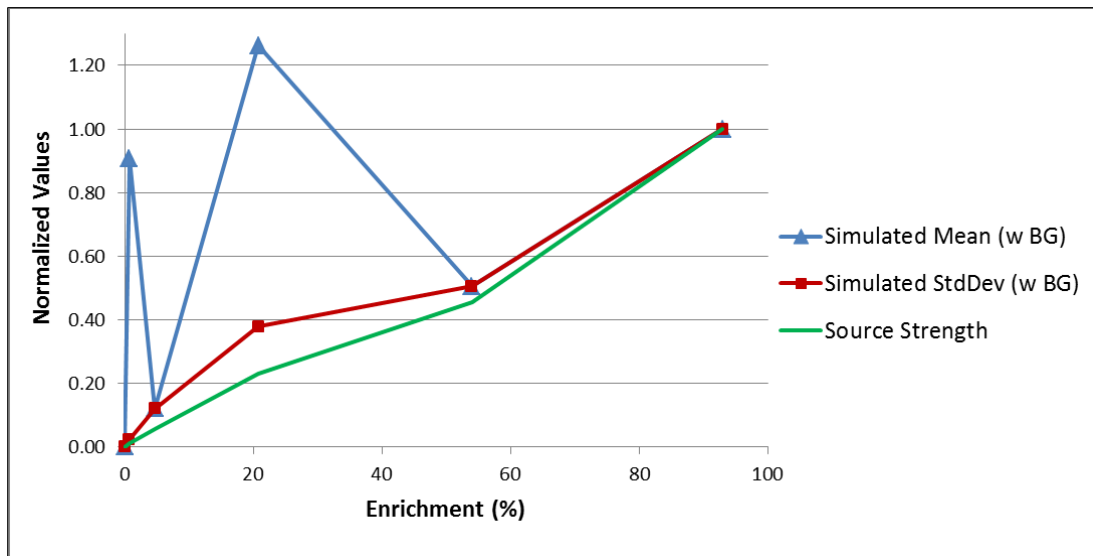


Figure 47. Normalized standard deviation, mean, and source strength with background added.<sup>a</sup>

It was also proposed in the experimental results that in images with higher source strengths (and shorter exposure times), the mean does a better job of following data trends. It then follows that the background has less effect on images with higher source strengths. To test this, two different intensities of background were added to the 0.7% and 20.8% enriched simulations, and the percent change in mean was recorded. These results are shown in Table 14. The amount of added background is equivalent to a photon with that energy in keV hitting each pixel. The percent change in the mean is less for the higher source strength (20.8% enriched source), confirming that background has less effect on sources with higher source strengths.

---

<sup>a</sup> Error bars on the simulated points are too small to be seen on graph.

Table 14

Percent Change in Mean for Different Values of Added Background

Enrichment (%)	Added Background	
	0.2 <sup>*</sup>	0.4 <sup>*</sup>
0.7	1906% ±19.08 <sup>**</sup>	3814% ±38.17 <sup>**</sup>
20.8	116.6% ±1.17 <sup>**</sup>	233.2% ±2.33 <sup>**</sup>

<sup>\*</sup> keV equivalent hitting each pixel

<sup>\*\*</sup> This is the average of the positive and negative deviation

To compare the experimental and simulated results of the single U metal specimens facing front, a plot of the experimental and simulated standard deviations is shown in Figure 48. Both increase fairly linearly with enrichment and thus source strength. Moreover, the curve of the simulated standard deviation is similar to the experimental curve.

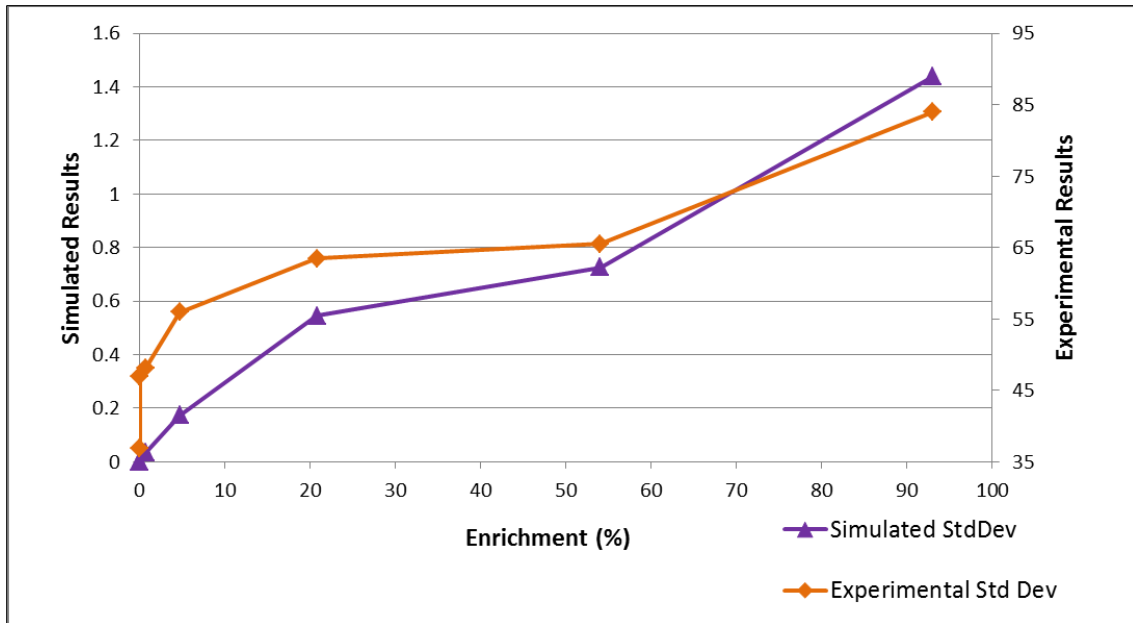


Figure 48. Simulated and experimental standard deviation versus enrichment for single U metal specimens, front facing.<sup>a</sup>

### *Multiple U Metal Specimens, Front Facing*

A montage of the multiple U metal specimens, front facing with each image scaled independently, is shown in Figure 49. Each image was scaled with the maximum value equal to the largest value in the matrix. The enrichment of each specimen is labeled, and the added enrichment of the specimens in the image is labeled at the bottom. Because the 114, 148.8, and 239.4 added enrichment images each have a 93% enriched specimen, the intensity scale values are comparable. The 4.7% enriched specimen in the added 4.9 image looks similar to the 93% enriched specimen in the other images. This

---

<sup>a</sup> Error bars on the simulated points are too small to be seen on graph.

result is expected, as both specimens are the most intense source in the image. However, the intensity scale values on the added 4.9 image are an order of magnitude less.

Figure 50 shows a montage of the multiple U metal specimens, front facing with a single intensity scale. The enrichment of each specimen is labeled, and the added enrichment of the specimens in the image is labeled at the bottom. These simulated images look more like the experimental images, with bright spots more clearly seen for enriched specimens at 54% and above. The specimens in the added 4.9 image are all but masked by the decreased intensity, similar to the background masking lower source strength specimens in the experimental images.

A plot of the normalized values of the standard deviation, mean, and source strength versus enrichment from simulated images is shown in Figure 51. As there is no background, the mean follows the source strength very closely while the standard deviation increases fairly linearly. To compare to experimental data, a plot of the simulated and experimental standard deviations versus enrichment is shown in Figure 52. Both increase proportionally.

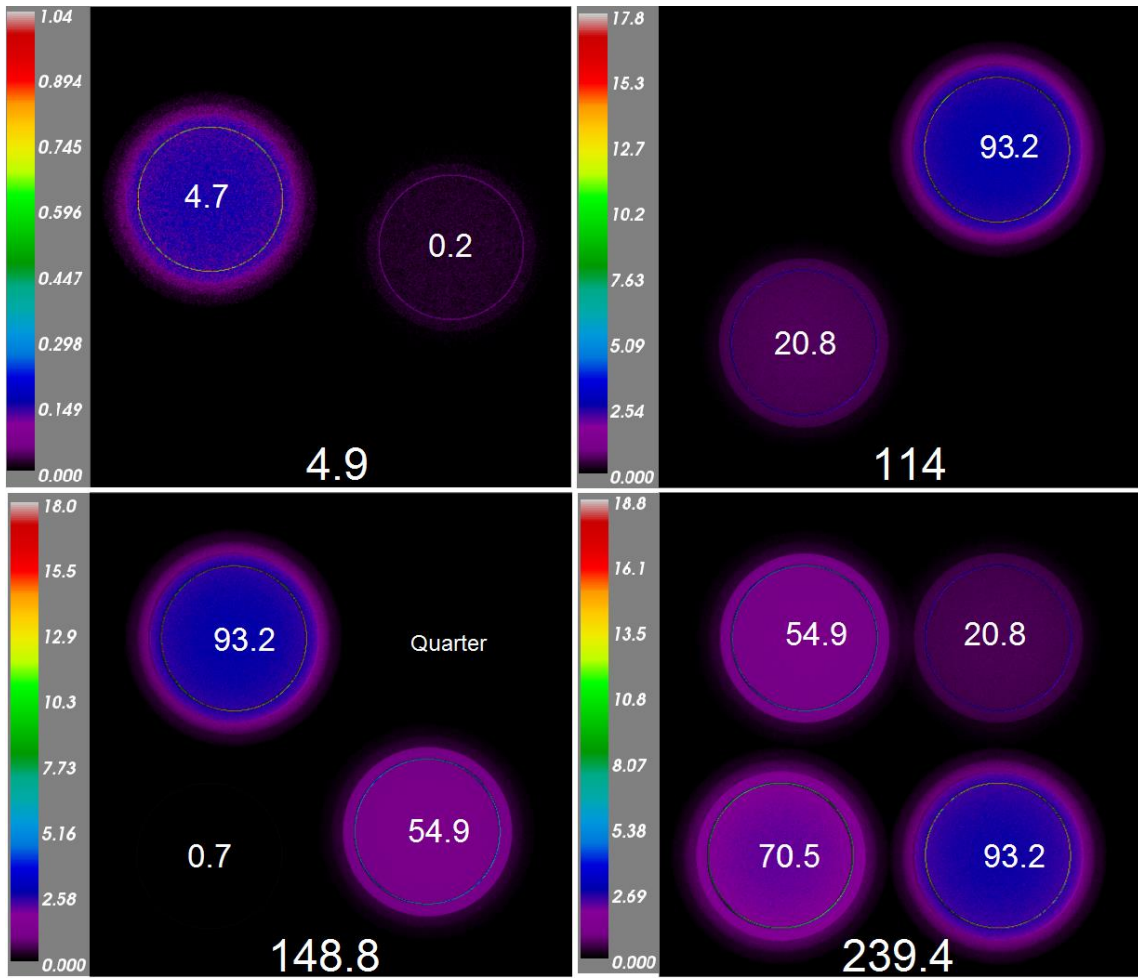


Figure 49. Montage of the simulated images from multiple U metal specimens, front facing - each image has individual intensity scale.



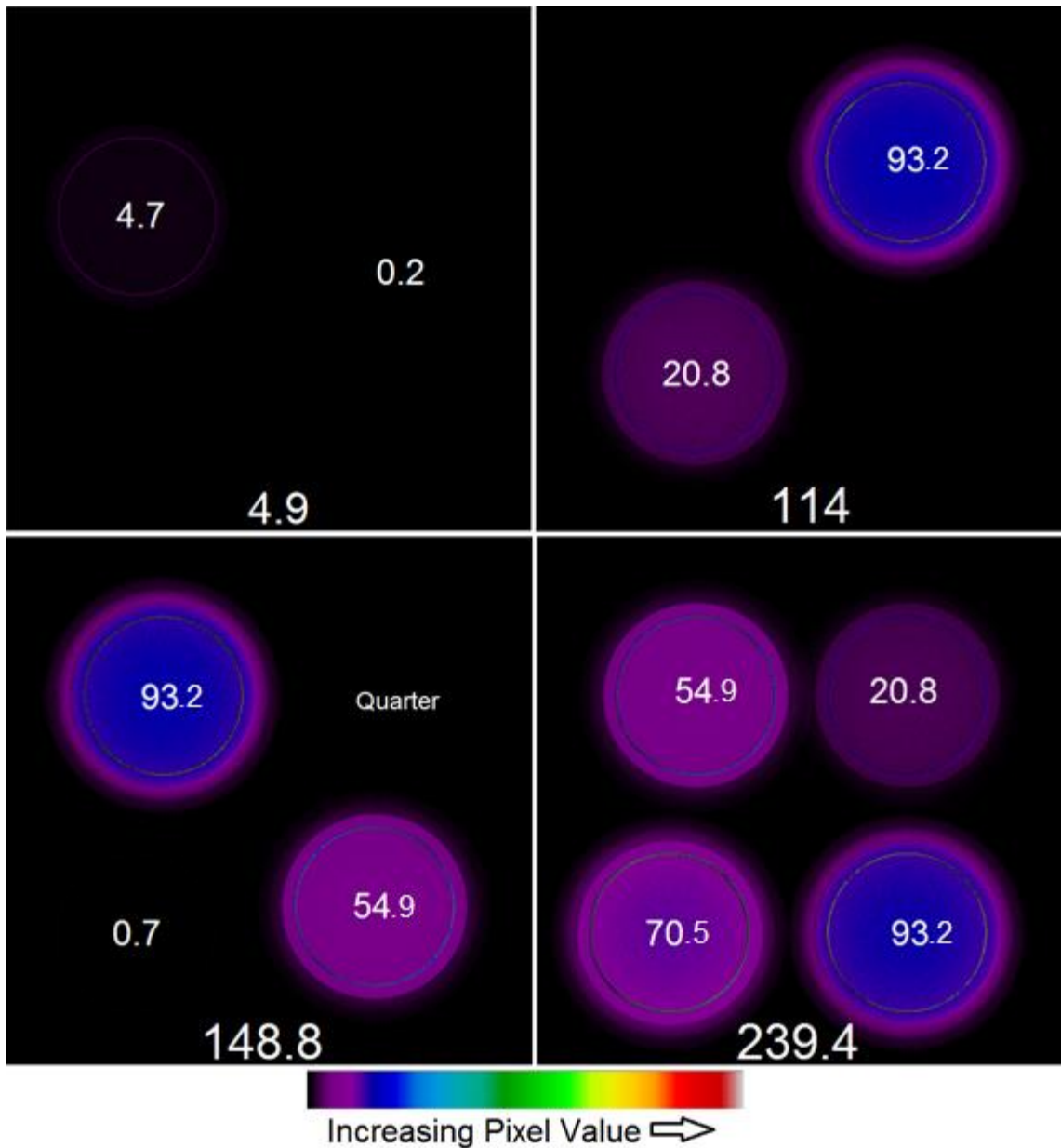


Figure 50. Montage of the simulated images from multiple U metal specimens, front facing - all images on the same intensity scale.

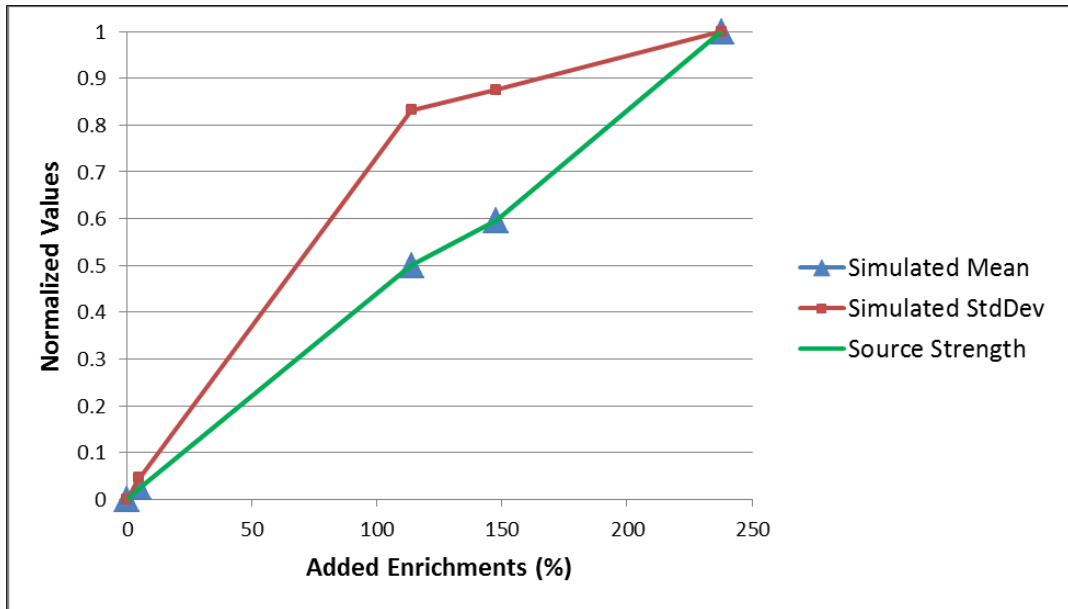


Figure 51. Normalized standard deviation, mean, and source strength versus enrichment from simulated images of multiple U metal specimens, front facing.<sup>a</sup>

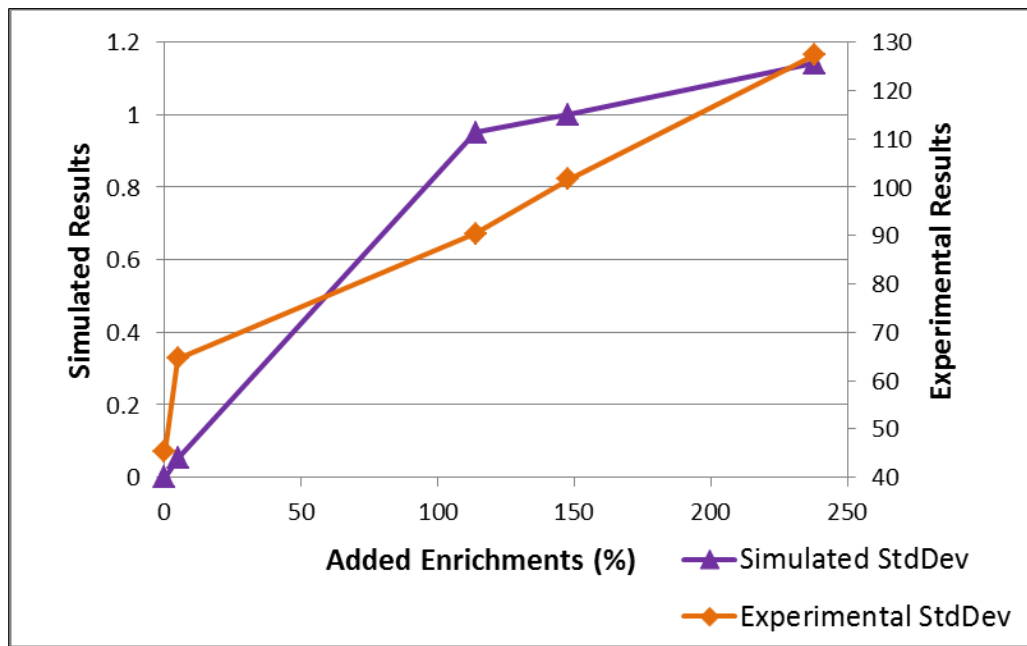


Figure 52. Simulated and experimental standard deviation versus enrichment for multiple U metal specimens, front facing.<sup>a</sup>

<sup>a</sup> Error bars on the simulated points are too small to be seen on graph.

### *Multiple U Metal Specimens, Side Facing*

A montage of the multiple U metal specimens, side facing, with each image scaled independently, is shown in Figure 53. Each image was scaled with the maximum value equal to the largest value in the matrix. The enrichment of each specimen is labeled, and the added enrichment of the specimens in the image is labeled at the bottom. Similar to the previous experimental set-up results, all specimens can be seen, and the intensity scale values are proportional to the most intense source strength in the image.

Figure 54 shows a montage of the multiple U metal specimens, side facing with a single intensity scale. The enrichment of each specimen is labeled, and the added enrichment of the specimens in the image is labeled at the bottom. These simulated images look more like the experimental images, because the decreased intensity acts similar to the background in the experimental images masking, the lower enriched specimens. However, the lower enriched specimens can still be faintly seen because background was not simulated and does not mask the weak signal.

A plot of the normalized values of the standard deviation, mean, and source strength versus enrichment from simulated images is shown in Figure 55. The mean and standard deviation follow the source strength, with the standard deviation exhibiting a larger jump between the added 75.2% and 75.7% enrichments. This result compares to the experimental data, where the standard deviations decrease proportionally between these two enrichments as shown in Figure 56. Differing from the experimental data, the added 40.2 image has a lower simulated standard deviation than the 75.7 image which is as expected because of its two similar but weak sources. Additionally, the 163.7 image

has the largest simulated standard deviation; showing that two stronger sources creating two bright spots will produce a greater standard deviation than one strong source with one bright spot.

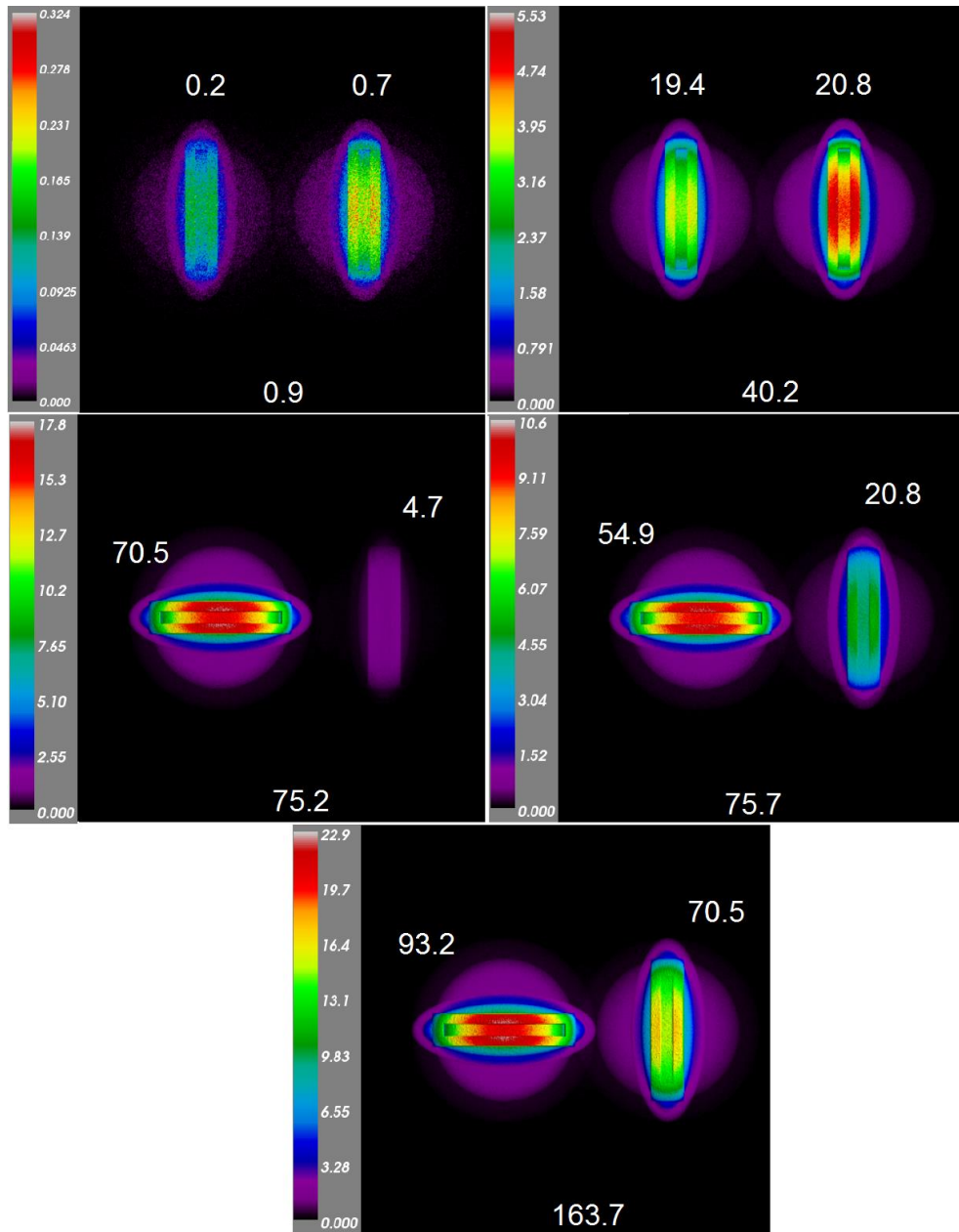


Figure 53. Montage of the simulated images from multiple U metal specimens, side facing - each image has individual intensity scale.

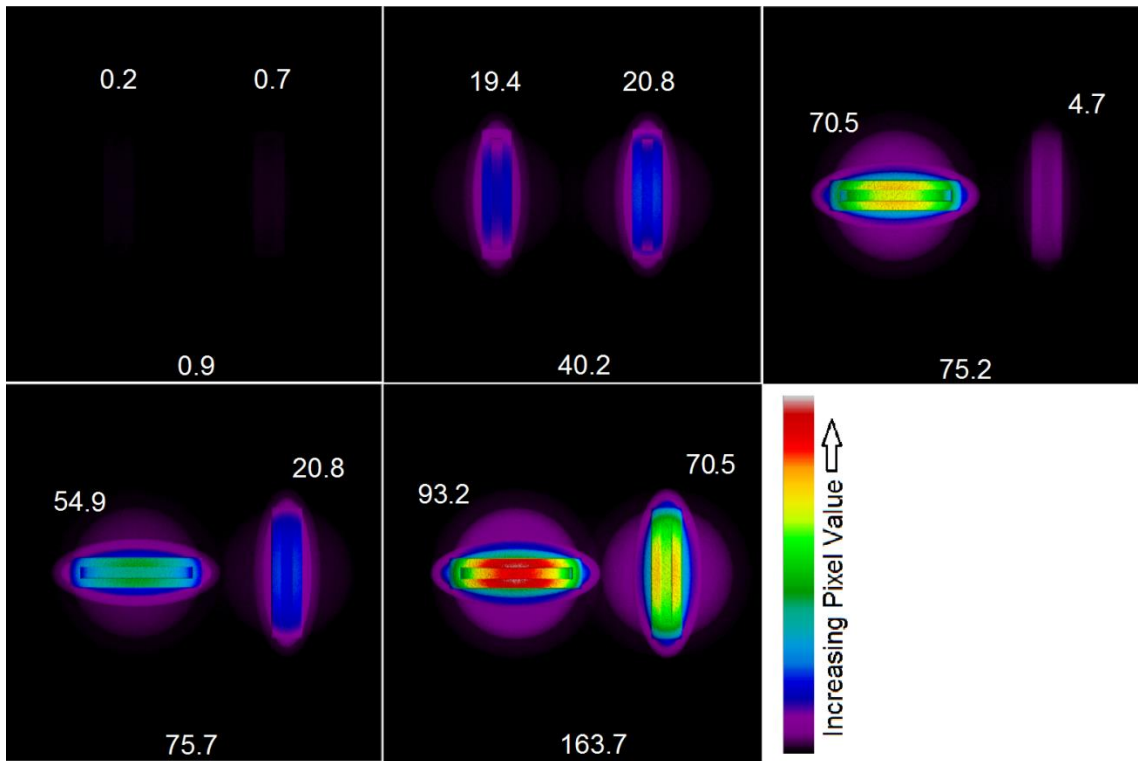


Figure 54. Montage of the simulated images from multiple U metal specimens, side facing - all images on the same intensity scale.

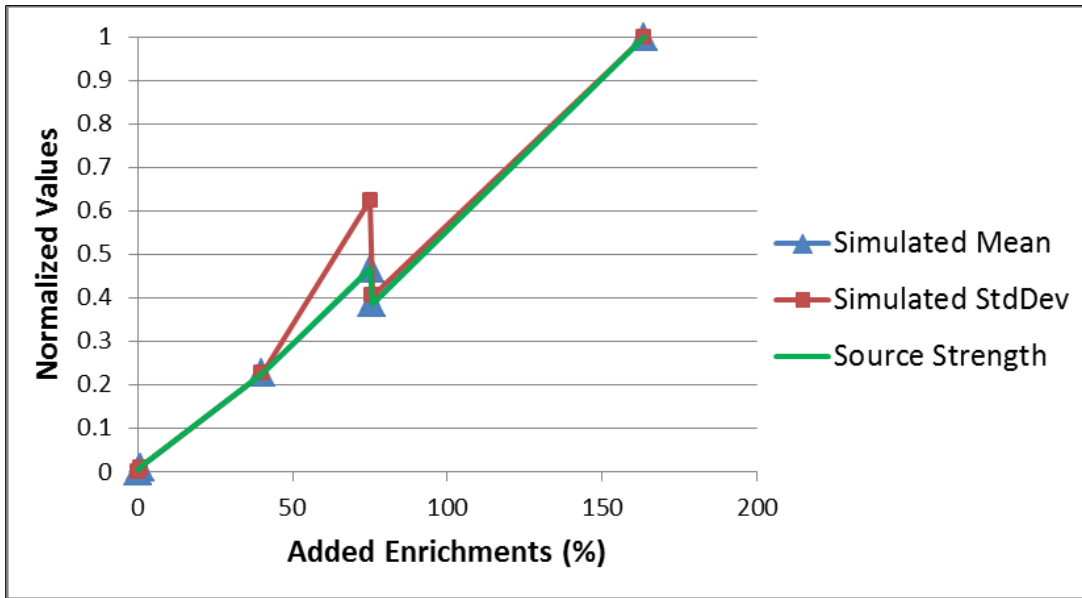


Figure 55. Normalized standard deviation, mean, and source strength versus enrichment from simulated images of multiple U metal specimens, side facing.<sup>a</sup>

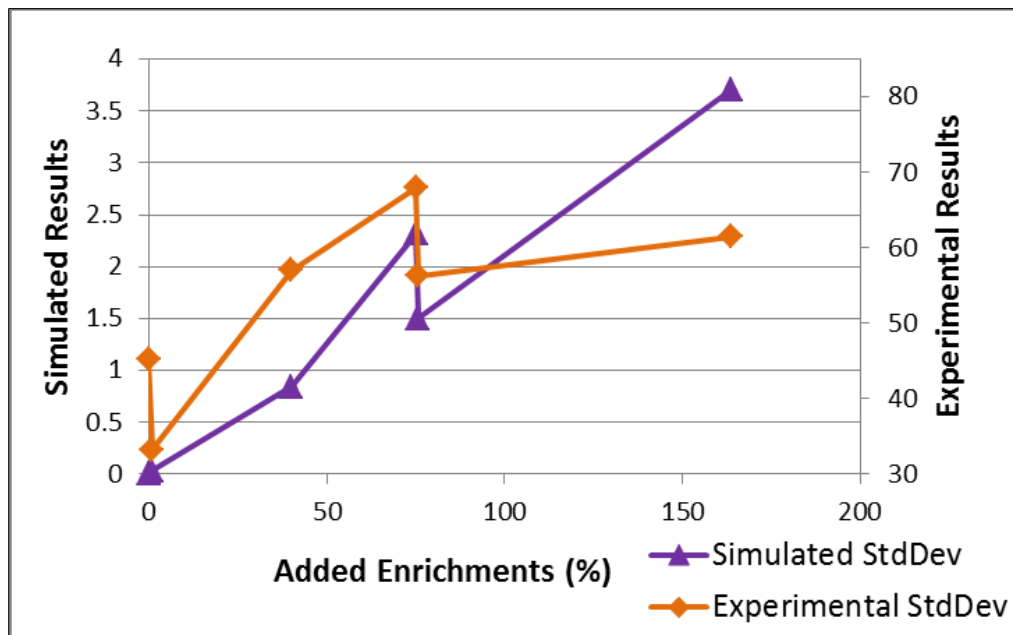


Figure 56. Simulated and experimental standard deviation versus enrichment for multiple U metal specimens, side facing.<sup>a</sup>

<sup>a</sup> Error bars on the simulated points are too small to be seen on graph.

### *UO<sub>3</sub> in Plastic Petri Dish*

To simulate the UO<sub>3</sub> in the plastic petri dish, the alpha particles that interact with the plastic of the petri dish are taken into account. Approximately 80 times more fluorescence photons are produced in polystyrene (plastic of the petri dish) than in air due to scintillation.<sup>18</sup> A montage of the depleted and natural UO<sub>3</sub> in a petri dish scaled individually is shown in Figure 57. Due to the increased fluorescence photons produced in polystyrene, the edge of the petri dish is significantly brighter than the actual UO<sub>3</sub>.

A plot of the normalized values of the standard deviation, mean, and source strength versus enrichment from simulated images is shown in Figure 58. Both the mean and standard deviation follow the source strength very closely. To compare to experimental data, a plot of the simulated and experimental standard deviations versus enrichment is shown in Figure 59. Both increase proportionally.

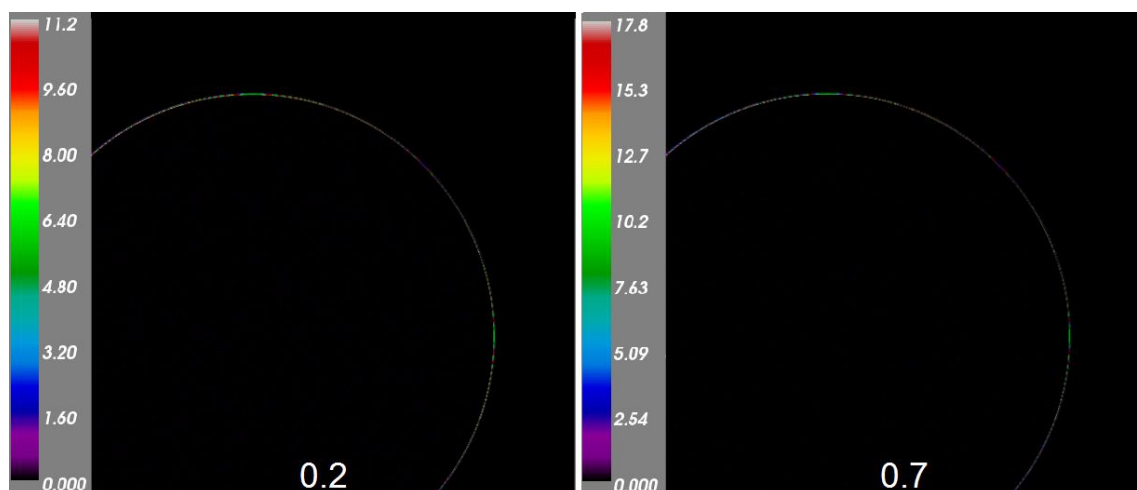


Figure 57. Montage of the simulated UO<sub>3</sub> in plastic petri dish.

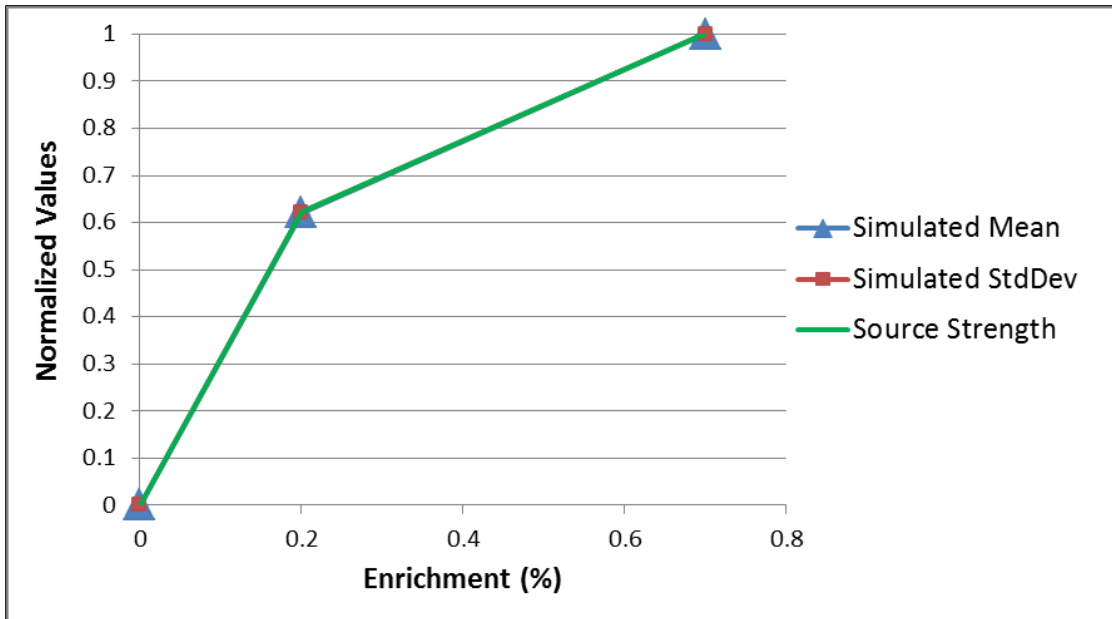


Figure 58. Normalized standard deviation, mean, and source strength versus enrichment from simulated images of  $\text{UO}_3$ .<sup>a</sup>

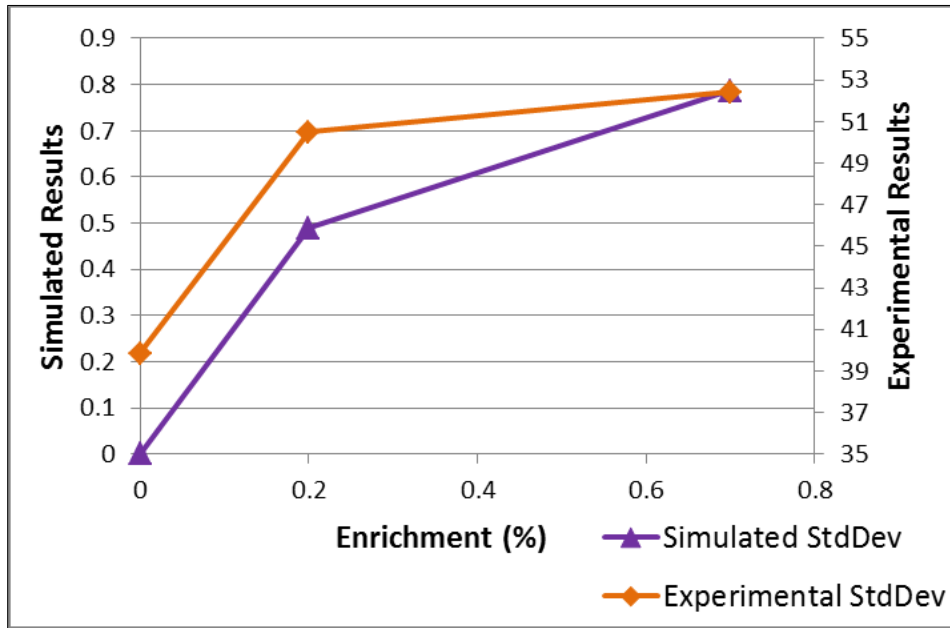


Figure 59. Simulated and experimental standard deviation versus enrichment for  $\text{UO}_3$ .<sup>a</sup>

<sup>a</sup> Error bars on the simulated points are too small to be seen on graph.



### $^{210}\text{Po}$ Source

To test the image resolution capability of the simulated images, the  $^{210}\text{Po}$  source was simulated. The  $^{210}\text{Po}$  source was chosen because the metal grating on top of the source could be seen in experimental images. Figure 60 shows a photograph of the  $^{210}\text{Po}$  source, the experimental result, the simulated source schematic, and the simulated result. The metal grating can clearly be seen in the simulated image and matches well with the experimental image.

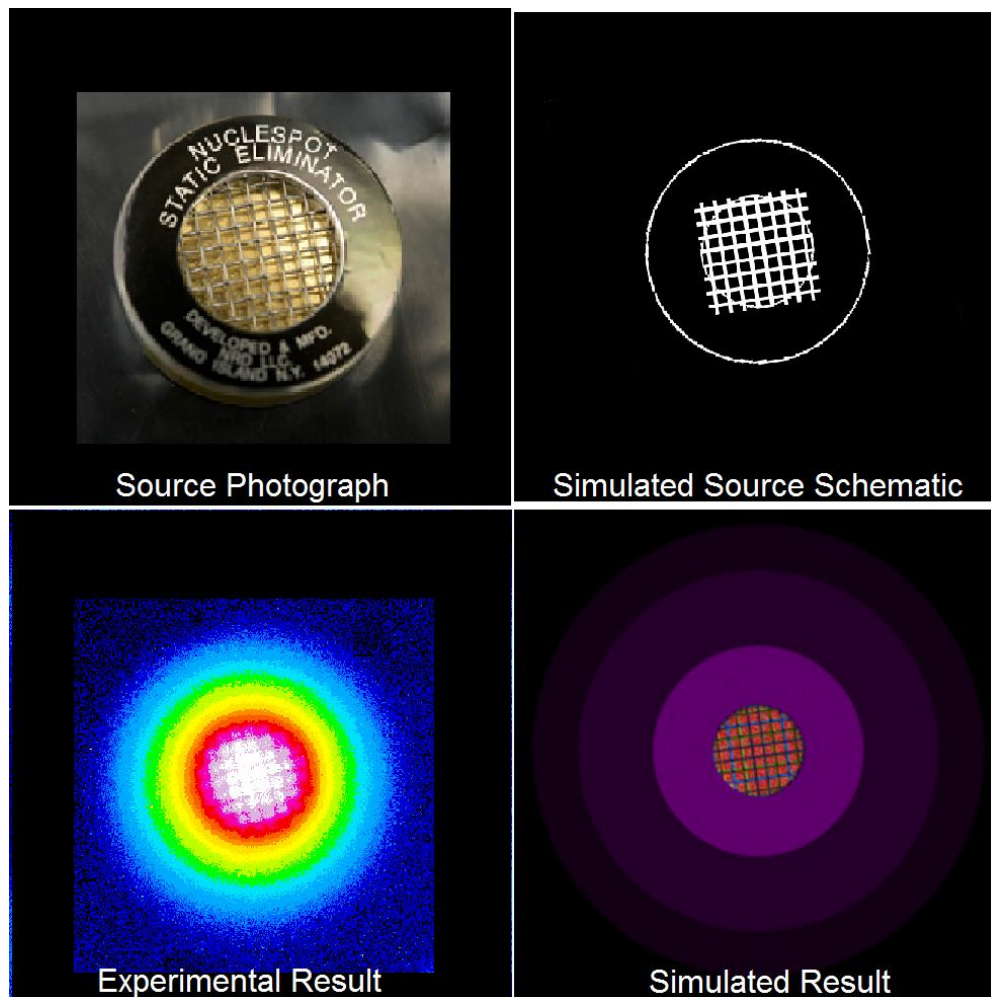


Figure 60. Comparison of  $^{210}\text{Po}$  source images.

#### **IV.C. Simulation Remarks and Summary**

The GEANT4 simulations performed here were done in two steps. The first step involved determining the alpha particle energy distribution for the fluorescence photon creation in step two. GEANT4 does have the ability to perform this calculation in one step. This one-step calculation can be performed if the user manually implements a number of calculations including the energy lost in each alpha particle step and inputs the number of photons generated per unit energy loss, the emission spectrum, and the material properties (photon characteristics in the material).<sup>53</sup> This methodology was tested, and the results were indistinguishable from the two step process implemented in this work. This result is expected, because the same information is input by the user in both cases. The difference is the computational time, which is significantly longer in the one step process, which is why the two step process was used.

The simulations confirm our understanding of the physics and that a computational procedure could be developed to be used in the future. Current simulations require the user to input much information, some of which is not well known or readily available. For example, the experimental setup testing UV photon transmission through translucent material was not simulated, because necessary input data was not found. This includes consistent information on the scintillation efficiency and emission spectrum of high density polyethylene when bombarded by alpha particles and the transmission of fluorescence photons through high density polyethylene. This difficulty in obtaining the necessary physics data is also why simulations of various spoofing scenarios were not simulated.

For the application presented in this research, a code that combined all the simulation steps and consolidated available information on scintillation properties and UV photon transmission data would be very useful and cut down on possible user error. Combining the simulation steps could include integrating a code such as SOURCES that can be used to calculate the source strength of alpha particles per unit area and the energies at which they are emitted from a specified source material.<sup>48</sup> This code could easily be expanded to take into account the source size and shape. Additionally, automatically calculating the energy deposited over the track length of the alpha particle and creating the fluorescence photon spectrum should be included.

The fluorescence photon spectrum is well-known for a number of materials, and its consolidation within a code would be convenient. Furthermore, known material properties should be included so that photon transmission is automatically and accurately taken into account. Combining these elements into a single code would allow a user to simply input the experimental setup and exposure time for an output of the fluorescence photons locations and energies on a specified detection plane.

Scintillation and transmission properties are not well known for all materials of interest. Work on consolidating known information and determining unknown characteristics would be useful. For arms control applications, determining this information for plastics used in high explosives would be especially useful. Other applications, such as ultra-high energy cosmic ray research, would also benefit from the consolidation of this information into a single code.

Even with the multi-step process and large amount of user input, the simulations done here provided valuable information and confirmed conclusions made in the experimental results. These conclusions include the confirmation that the image standard deviation follows the source strength, even with varying background, and that background has less effect on high intensity sources.

The next step is to do experimental tests and simulations on actual weapons-like objects. Future tests should include Pu and various masses and shapes of fissile material. This step would provide additional information on the capabilities and limitations of this imaging technique. Comparing additional experimental and simulated results may give further indications on where improvements in the simulations can be made.

## CHAPTER V

### SUMMARY AND CONCLUSIONS

The results from the experimental and simulated measurements were used to confirm the proof-of-concept of fluorescence imaging to determine if it could be a viable tool for nuclear arms control verification. Specifically, this work characterizes the fissile material attributes where fluorescence imaging would be useful in verifying an uncanned nuclear warhead or warhead component and to observe if it has the ability to reveal presumably sensitive information about these components.

As shown in the experimental results, fluorescence photons do not travel through non-translucent material, which is why an *uncanned* nuclear warhead is specified. More precisely, as non-translucent material blocks the signal, this technique could be used to verify bare pits and fissile material components in the dismantlement process.

It is generally agreed that sensitive information would include the mass and isotopics of the nuclear material, dimension of the nuclear cores, and detailed design of the engineered components. Measurements from this work have shown that fluorescence imaging does not have the ability to determine the mass and isotopics of the nuclear material, dimensions of the cores, or design of internal features of engineered components. The measurement technique may have the ability to image external fissile material components with too much detail. However, this will depend on the source strength of the fissile material, acquisition time, and distance between the lens and item being imaged.

The low source strength of HEU will prevent fluorescence imaging from obtaining detailed designs of any external HEU component. While Pu source strength is orders of magnitude higher than HEU, it is still orders of magnitude lower than the  $^{210}\text{Po}$  source from which a detailed image was obtained. While additional experiments should be performed with Pu to determine the amount of image detail that can be obtained, steps could be taken in a verification scenario to confirm detailed information is not revealed. This approach could include limiting the acquisition time or increasing the distance between the Pu component and camera lens.

Because fissile material is somewhat unique in the fact that it emits neutrons, gamma-rays, and alpha particles, combining non-sensitive measurements that account for each of these - gross neutron, gross gamma, and fluorescence imaging respectively - will have the greatest utility. Each measurement is able to confirm pieces of information about the item, leading to increased overall confidence that the item being verified is as declared, without the need for an information barrier. Many of the fissile material attributes can be assessed with strong assurance using these measurements. Table 15 summarizes these results with a discussion of each attribute below.

Table 15  
Fissile Material Attribute Verification Summary\*

Attribute	Fluorescence Imaging	Gross Neutron	Gross Gamma	All 3
Presence of fissile material (Pu or U)	+	+	+	++
Mass greater than threshold	+	++	~	++
<sup>239</sup> Pu to <sup>240</sup> Pu ratio	+	+	~	++
Symmetry	++	++	+	+++
U enrichment greater than threshold	+++	+	+	+++
Pu age	+	+	~	+
Absence of oxide	~	~	~	~

\*The values range from “~” meaning very limited utility/low confidence to “+++” meaning highly useful / high confidence.

The presence of fissile material, Pu, or U can be evaluated by confirming the material emits neutrons, gamma-rays, and alpha particles. Fluorescence imaging, gross neutron, and gross gamma would confirm that the material emits all three radiations in the appropriate proportions. The presence of Pu or U could be evaluated more precisely as their source strength (based on assumed isotopics) would be taken into account.

The mass of fissile material can be estimated by gross neutron counting and supported by fluorescence imaging. Fluorescence imaging supplements gross neutron counting in two ways. First, the size of the object can be predicted by fluorescence imaging and compared to the measured mass. Secondly, for metallic U and Pu, gross neutron counting is essentially an estimate of <sup>238</sup>U and <sup>240</sup>Pu mass due to their spontaneous fission dominance. In HEU metal, the small percentage of <sup>238</sup>U will

correlate to a small neutron production rate, but the larger percentage of  $^{235}\text{U}$  and  $^{234}\text{U}$  will correspond to a larger alpha production rate; thus providing an enhanced fluorescence image. Fluorescence imaging would also make it less probable that an overestimation of weapons grade Pu metal mass will occur from an excess of  $^{240}\text{Pu}$ , due to the size to mass comparison (mentioned above) and the difference in alpha specific activity of  $^{239}\text{Pu}$  and  $^{240}\text{Pu}$ . This factor leads to the fissile material attribute of the  $^{239}\text{Pu}$  to  $^{240}\text{Pu}$  ratio greater than a threshold.

The combination of experimental and simulated results shows it is possible for the standard deviation to discriminate between source strength differences as small as  $4 \times 10^3$  alphas per second over a 60 minute exposure. This result implies that a  $^{239}\text{Pu}$  to  $^{240}\text{Pu}$  ratio threshold could be verified by fluorescence imaging due to the specific activity difference ( $\sim 6.1 \times 10^9$  alphas per second) in these isotopes. Experiments imaging Pu specimens with different  $^{239}\text{Pu}$  and  $^{240}\text{Pu}$  ratios should be performed to confirm this assumption.

Similarly, the difference in specific activity of  $^{241}\text{Am}$  to  $^{239}\text{Pu}$  and  $^{240}\text{Pu}$  may be able to give some indication of Pu age. Pu age is determined by the  $^{241}\text{Am}$  content which has a specific activity two orders of magnitude greater than  $^{239}\text{Pu}$  or  $^{240}\text{Pu}$ . Again, experiments to assess the fluorescence imaging sensitivity to this parameter should be performed.

Symmetry of fissile material can be confirmed by comparing gross neutron measurements at incremental rotations accompanied by fluorescence imaging and gross



gamma. The neutrons confirm the material volume is symmetric while the alpha particles and gamma rays confirm the material surface is symmetric.

The combination of gross neutron, gross gamma, and fluorescence imaging may give some clues about the absence of oxide, but this attribute is complex due to the balance of production rates and material form. For example, for equal amounts of U, HEU metal and oxide have distinguishable neutron production rates, while HEU metal and LEU oxide both have equally small neutron production rates from the small percentage of  $^{238}\text{U}$  spontaneously fissioning and  $^{234}\text{U}$  causing  $(\alpha, n)$  reactions, respectively. Moreover, the decreased density of oxide will emit more alpha particles and gamma-rays than the same mass and isotopic content in metallic form. Fluorescence images may provide enough information through material size and alpha source strength that, when paired with gross neutron and gross gamma, inferences can be made about the presence or absence of oxide; but experiments with differing Pu quality and U enrichments with sintered oxide would need to be performed before such conclusions could be made.

Experimental and simulated results show that fluorescence imaging can generally discriminate between different enrichments of U, assuming that it was enriched via gaseous diffusion or gas centrifuge (where the  $^{234}\text{U}$  was also enriched). Thus, it is able to confirm the enrichment of U greater than a threshold. Fluorescence imaging can be accompanied by gross neutron and gross gamma to give supporting measurements of the U enrichment.

All the fissile material attributes cannot be confirmed using fluorescence imaging, gross neutron, and gross gamma. This is tolerable as it is still debated which of these attributes will need to be analyzed in a verification scenario. Measuring alpha particles, neutrons, and gamma-rays makes it more difficult to spoof the system, as the activity of each would need to match the declared item. Furthermore, making gross neutron measurements at incremental rotations, fluorescence images, and gamma images (without spectroscopy) would also mean the distribution of neutrons, alpha particles, and gamma-rays would need to match the declared item.

Assessing many fissile material attributes using non-sensitive measurements requires the assumption of knowing something about the material, such as assuming material form or general isotopics. For verification of a nuclear warhead or warhead components, such assumptions would be supported by other verification means such as tamper indicating tags and seals and national technical means.

The work performed in this dissertation verified the proof-of-concept of fluorescence imaging for use in nuclear arms control treaty verification. Further development of this technology would prove useful to fully understand what this technique is capable of. Because a great deal of work needs to go into the simulations, additional experiments may be the easiest way to confirm the assumptions made here and advance the utility of this technology.

## REFERENCES

- 1) U.S. Department of State, “New START Treaty Entry Into Force,” Fact Sheet, Office of the Spokesman, Washington, DC, February 5, 2011. Retrieved July 30, 2014, from <http://www.state.gov/r/pa/prs/ps/2011/02/156037.htm>
- 2) Office of the Press Secretary, U.S. President Barack Obama’s Speech, Prague, Czech Republic, April 5, 2009. Retrieved July 30, 2014, from [http://www.whitehouse.gov/the\\_press\\_office/Remarks-By-President-Barack-Obama-In-Prague-As-Delivered](http://www.whitehouse.gov/the_press_office/Remarks-By-President-Barack-Obama-In-Prague-As-Delivered)
- 3) G. P. Shultz, W. J. Perry, H. A. Kissinger, and S. Nunn, “A World Free of Nuclear Weapons,” *The Wall Street Journal*, January 4, 2007.
- 4) United Nations, “2010 Review Conference of the Parties to the Treaty on the Non-Proliferation of Nuclear Weapons,” Final Report, NPT/CONF.2010/50 (Vol. I), New York, NY, (2010).
- 5) C. L. Glaser, “The Flawed Case for Nuclear Disarmament,” *Survival*, Vol. 40 No. 1, pg 112-128, (1998).
- 6) D. Cliff, H. Elbahtimy and A. Persbo., “Verifying Warhead Dismantlement Past, Present, Future” *Vertic Research Reports*, Number 9, September 2010.
- 7) J. Davis, J. Browne, P. Lewis, C. Pura, A. Sessoms, T. Shea, F. Slakey, B. Tannenbaum, J. Tape, J. Taylor and P. D. Zimmerman, “Technical Steps to Support Nuclear Arsenal Downsizing,” A Report by the APS Panel on Public Affairs, February 2010.

- 8) A. Schaper, "Transparency and Secrecy in Nuclear Weapons," Weapons of Mass Destruction Commission, (2011). Retrieved July 30, 2014, from <http://www.blixassociates.com/wp-content/uploads/2011/03/No34.pdf>
- 9) A. L. Pregenzer, "Workshop on Technical Approaches to Support Nuclear Arms Control and Nonproliferation," The Carnegie Endowment for International Peace, Washington, D.C., April 8-9, 2009.
- 10) D. Spears, et. al., "Technology R&D for Arms Control," Arms Control and Nonproliferation Technologies, Spring 2001.
- 11) Union of Concerned Scientist, "Nuclear Weapons: How They Work," Fact Sheet, April 2009. Retrieved July 30, 2014, from <http://www.ucsusa.org/assets/documents/nwgs/nuclearweaponshowtheyworkfinal.pdf>
- 12) J. F. Morgan, "Transparency and Verification Options: An Initial Analysis of Approaches for Monitoring Warhead Dismantlement," Institute of Nuclear Material Management 38th Annual Conference Proceedings, Phoenix, AZ (1997).
- 13) U.S. Department of State, "Article-By-Article Analysis of New START Treaty Documents", Bureau of Arms Control, Verification and Compliance, May 5, 2010. Retrieved July 30, 2014, from <http://www.state.gov/t/avc/trty/141829.htm>
- 14) S. Drell, et. al., "Verification Technology: Unclassified Version," The MITRE Corporation, Report number: JSR-89-100A, McLean, VA, October 1990.
- 15) U.S. Arms Control and Disarmament Agency, "Field Test FT 34 Demonstrated Destruction of Nuclear Weapons," Final Report, Volume I, January 1969.

- 16) Executive Office of the President, “Verification of Nuclear Warhead Dismantlement and Special Nuclear Material Controls,” Report of Congress, July 1991.
- 17) National Research Council, *Monitoring Nuclear Weapons and Nuclear-Explosive Materials: An Assessment of Methods and Capabilities*, The National Academies Press, Washington, DC, 2005.
- 18) J. B. Burks, *The Theory and Practice of Scintillation Counting*, Pergamon Press LTD., New York, NY, 1964.
- 19) NIST ASTAR Database, Composition of Air, Dry (near sea level), National Institute of Standards and Technology. Retrieved July 30, 2014, from <http://physics.nist.gov/cgi-bin/Star/compos.pl?matno=104>
- 20) J. Rosado, F. Blanco and F. Arqueros, “Comparison of available measurements of the absolute fluorescence yield,” *Astropart. Phys.* 34, pg. 164-172, (2010).
- 21) T. Waldenmaier, J. Blumer, and H. Klages, “Spectral Resolved Measurement of the Nitrogen Fluorescence Emissions in Air Induced by Electrons,” *Astropart. Phys.* 29, pg. 205-222, (2008).
- 22) Portland State University, “Charge-Coupled Devices,” Physics Department Information Sheet, (2008). Retrieved July 30, 2014, from <http://web.pdx.edu/~d4eb/ccd/>
- 23) M. Nagano, K. Kobayakawa, N. Sakaki, K. Ando, “New Measurement on Photon Yields from Air and the Application to the Energy Estimation of Primary Cosmic Rays,” *Astropart. Phys.* 22, pg. 235-248, (2004).

- 24) AIRFLY Collaboration, “Measurement of the Pressure Dependence of Air Fluorescence Emission Induced by Electrons,” *Astropart. Phys*, 28, pg. 41-57, (2007).
- 25) F. Arqueros, F. Blanco, and J Rosado, “Analysis of the Fluorescence Emission From Atmospheric Nitrogen by Electron Excitation, and its Application to Fluorescence Telescopes,” *New Journal of Physics*, 11, (2009).
- 26) R. Abbasi, et al., “Air Fluorescence Measurements in the Spectral Range 300–420 nm Using a 28.5 GeV Electron Beam,” *Astropart. Phys*, 29, pg. 77–86, (2008).
- 27) NIST ASTAR Database, CSDA Range for 5 MeV alpha particles in Air, Dry (near sea level), National Institute of Standards and Technology.
- 28) L. Elterman, “UV, Visible, and IR Attenuation for Altitudes to 50 km, 1968,” *Environmental Research Papers*, No. 285, April 1968.
- 29) S. M. Baschenko, “Remote optical detection of alpha particle sources,” *J. Rad. Protect*, Vol. 24, pg. 75–82, (2004).
- 30) J. Sand, V. Hannuksela, S. Ihanola, K. Peräjärvi, H. Toivonen, and J. Toivonen, “Remote optical detection of alpha particle sources,” International Atomic Energy Agency Publication: IAEA-CN-184/23.
- 31) F. Lamadie, F. Delmas, C. Mahe, P. Gironès, C. Le Goaller, and J. R. Costes, “Remote Alpha Imaging in Nuclear Installations: New Results and Prospects,” *IEEE Transactions on Nuclear Science*, Vol. 52, No. 6, (2005).
- 32) J. Allison, et. al., “GEANT4 Developments and Applications,” *IEEE Transactions on Nuclear Science*, Vol. 53, February 2006.

- 33) Nuclear Threat Initiative (NTI) website, Treaties and Regimes, Nuclear Weapons.  
Retrieved July 30, 2014, from <http://www.nti.org/treaties-and-regimes/treaties/>
- 34) E. Corin, “Presidential Nuclear Initiatives: An Alternative Paradigm for Arms Control”, Nuclear Threat Initiative article, March 1, 2004. Retrieved July 30, 2014, from <http://www.nti.org/analysis/articles/presidential-nuclear-initiatives/>
- 35) Arms Control Association, “U.S.-Russian Nuclear Arms Control Agreements at a Glance,” August 2010. Retrieved July 30, 2014, from <http://www.armscontrol.org/factsheets/USRussiaNuclearAgreementsMarch2010>
- 36) U.S. Department of State, “Treaty on the Non-Proliferation of Nuclear Weapons,” signed in Washington, London, and Moscow, July 1, 1968. Retrieved July 30, 2014, from <http://www.state.gov/t/isn/trty/16281.htm>
- 37) G. Thielmann, “New START Verification: Fitting the Means to the Ends”, Threat Assessment Brief, The Arms Control Association, February 22, 2010.
- 38) U.S. Department of State, “Treaty Between The United States of America and the Russian Federation on Measures for the Further Reduction and Limitation of Strategic Offensive Arms,” Signed in Prague, April 8, 2010. Retrieved July 30, 2014, from <http://www.state.gov/documents/organization/140035.pdf>
- 39) United Nations Conference on Disarmament, Shannon Mandate; CD/1299, March 24, 1995.
- 40) J. Fuller, “Verification on the Road to Zero: Issues for Nuclear Warhead Dismantlement,” *Arms Control Today*, December 2010.

- 41) A. Glaser, B. Barak, R. Goldston, “A New Approach to Nuclear Warhead Verification Using a Zero-Knowledge Protocol,” Institute of Nuclear Material Management 53th Annual Conference Proceedings, Orlando, FL, (2012).
- 42) Kostenko, I., Rubanenko, N., Sokolov, Y., Terekhin, V., Yudov, A., Seager, K. “Multi-aspect System for Measurement of Attributes of Fissile Materials and Explosives,” Institute of Nuclear Material Management 48th Annual Conference Proceedings, Tucson, AZ, (2007).
- 43) D. K. Hauck and D. W. MacArther, “Benefits of a ‘Presence of Fissile Material’ Attribute for Warhead Confirmation in Treaty Verification,” Institute of Nuclear Material Management 54th Annual Conference Proceedings, Palm Desert, CA, (2013).
- 44) G. F. Knoll, *Radiation Detection and Measurement*, John Wiley & Sons, Inc., Hoboken, NJ, (2000).
- 45) D. Reilly, N. Ensslin, H. Smith, and S. Kreine, *Passive Nondestructive Assay of Nuclear Materials*, U.S. Nuclear Regulatory Commission, Washington, DC, (1991).
- 46) K. P. Ziock, “Gamma-Ray Imaging Spectrometry,” *Science & Technology Review*, October 1995.
- 47) Princeton Instruments PIXIS: 1024 Data Sheet. Retrieved July 30, 2014, from [http://www.princetoninstruments.com/Uploads/Princeton/Documents/Datasheets/PIXIS/Princeton\\_Instruments\\_PIXIS\\_1024\\_eXcelon\\_rev\\_N3\\_8.21.2012.pdf](http://www.princetoninstruments.com/Uploads/Princeton/Documents/Datasheets/PIXIS/Princeton_Instruments_PIXIS_1024_eXcelon_rev_N3_8.21.2012.pdf)



- 48) W. Wilson, et., al., "SOURCES 4A: A Code for Calculating ( $\alpha$ ,n), Spontaneous Fission, and Delayed Neutron Sources and Spectra," Los Alamos National Laboratory Report, LA-13639-MS, September 1999.
- 49) J. S. Feener and W. S. Charlton, "Preliminary Results of Nuclear Fluorescence Imaging of Alpha and Beta Emitting Sources," Advancements in Nuclear Instrumentation Measurement Methods and their Applications 3rd Conference Proceedings, Marseille, France, June (2013). Copyright 2013 IEEE.
- 50) W. S. Rasband, "ImageJ Image Processing and Analysis in Java," U. S. National Institutes of Health, Bethesda, MD. Retrieved July 30, 2014, from <http://imagej.nih.gov/ij/>
- 51) GEANT4 Users Guide, Section 2.7 General Particle Source, Geant4 Collaboration. Retrieved July 30, 2014, from <https://geant4.web.cern.ch/geant4/UserDocumentation/UsersGuides/ForApplicationDeveloper/html/ch02s07.html>
- 52) GEANT4 User Guide, Section 5.2.5 Optical Photon Processes, Geant4 Collaboration. Retrieved July 30, 2014, from <http://geant4.web.cern.ch/geant4/UserDocumentation/UsersGuides/ForApplicationDeveloper/html/ch05s02.html#sect.PhysProc.Photo>
- 53) P. Gumplinger, "Optical Photon Processes in GEANT4," GEANT4 Users' Workshop at SLAC, February 2002.

APPENDIX A

SUPPLEMENTAL INFORMATION

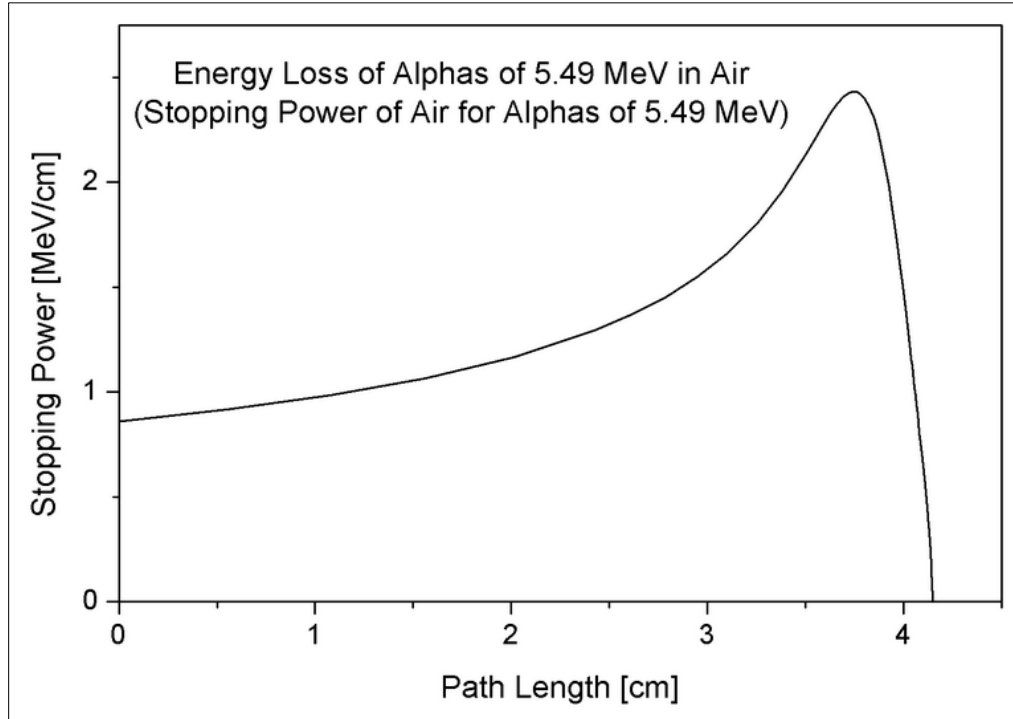


Figure A1. Example Bragg curve for a 5.49 MeV Alpha Particle in Air.

Table A1

Scintillation Photons per 4.6 MeV Alpha Particle in Nitrogen at Different Pressures<sup>18</sup>

Pressure (atm)	1	0.82	0.64	0.32
Total number of photons	1000	1060	1310	1970

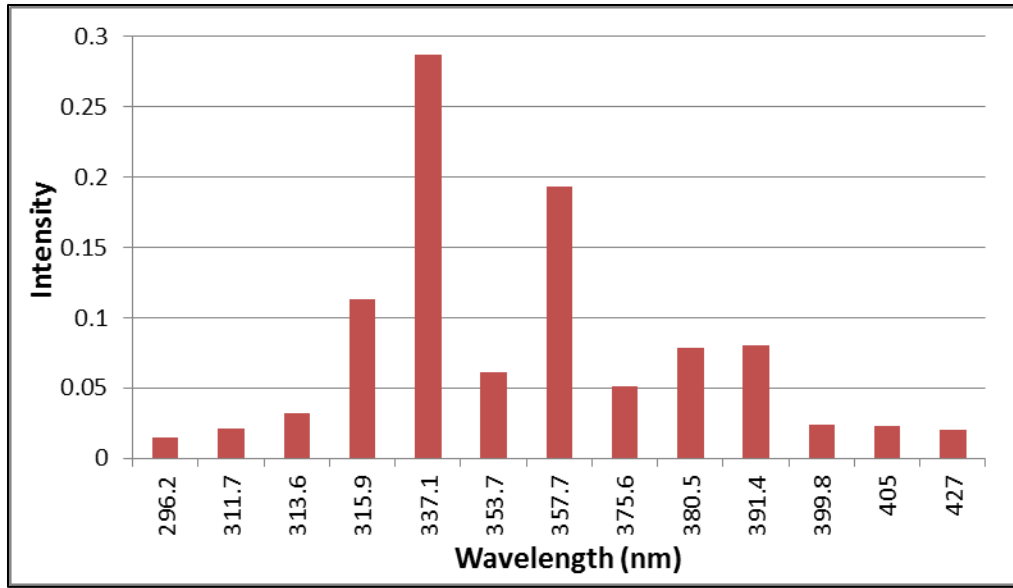


Figure A2. Fluorescence spectrum used in GEANT4 simulations.<sup>24</sup>

## APPENDIX B

### SAMPLE GEANT4 GPS AND HEADER FILES

#### GPS file

```
# Random particle generator in source
# U metal specimen flou input NAT
#
# at source
/gps/source/intensity 0.2340143
/gps/particle opticalphoton
/gps/pos/type Surface
/gps/pos/shape Cylinder
/gps/pos/centre 0. 0. 0. cm
/gps/pos/radius 1.5 cm
/gps/pos/halfz 0.15 cm
/gps/ang/type beam1d
/gps/ene/type User
/gps/hist/type energy # histogram for N Fluo above 5%
/gps/hist/point 0.0000029013 0
/gps/hist/point 0.0000029245 7.08
/gps/hist/point 0.0000030497 0
/gps/hist/point 0.0000030961 8.07
/gps/hist/point 0.0000031400 8.38
/gps/hist/point 0.0000031625 0
/gps/hist/point 0.0000031901 28
/gps/hist/point 0.0000032512 0
/gps/hist/point 0.0000032952 27.2
/gps/hist/point 0.0000033360 17.87
/gps/hist/point 0.0000034454 0
/gps/hist/point 0.0000034989 67.4
/gps/hist/point 0.0000035368 21.35
/gps/hist/point 0.0000036643 0
/gps/hist/point 0.0000037092 100
/gps/hist/point 0.0000039154 0
/gps/hist/point 0.0000039478 39.3
/gps/hist/point 0.0000039705 11.05
/gps/hist/point 0.0000040091 7.24
/gps/hist/point 0.0000041751 0
/gps/hist/point 0.0000042393 5.16
#
# 0.25 cylinder
/gps/source/add 0.1870903
/gps/particle opticalphoton
/gps/pos/type Volume
/gps/pos/shape Cylinder
/gps/pos/centre 0. 0. 0. cm
/gps/pos/radius 1.75 cm
/gps/pos/halfz 0.40 cm
/gps/ang/type beam1d
```

```

/gps/ene/type User
/gps/hist/type energy # histogram for N Fluo above 5%
/gps/hist/point 0.0000029013 0
/gps/hist/point 0.0000029245 7.08
/gps/hist/point 0.0000030497 0
/gps/hist/point 0.0000030961 8.07
/gps/hist/point 0.0000031400 8.38
/gps/hist/point 0.0000031625 0
/gps/hist/point 0.0000031901 28
/gps/hist/point 0.0000032512 0
/gps/hist/point 0.0000032952 27.2
/gps/hist/point 0.0000033360 17.87
/gps/hist/point 0.0000034454 0
/gps/hist/point 0.0000034989 67.4
/gps/hist/point 0.0000035368 21.35
/gps/hist/point 0.0000036643 0
/gps/hist/point 0.0000037092 100
/gps/hist/point 0.0000039154 0
/gps/hist/point 0.0000039478 39.3
/gps/hist/point 0.0000039705 11.05
/gps/hist/point 0.0000040091 7.24
/gps/hist/point 0.0000041751 0
/gps/hist/point 0.0000042393 5.16
# 0.5 cm out
/gps/source/add 0.1543769
/gps/particle opticalphoton
/gps/pos/type Volume
/gps/pos/shape Ellipsoid
/gps/pos/centre 0. 0. 0. cm
/gps/pos/halfx 2. cm
/gps/pos/halfy 2. cm
/gps/pos/halfz 0.65 cm
/gps/ang/type beam1d
/gps/ene/type User
/gps/hist/type energy
/gps/hist/point 0.0000029013 0
/gps/hist/point 0.0000029245 7.08
/gps/hist/point 0.0000030497 0
/gps/hist/point 0.0000030961 8.07
/gps/hist/point 0.0000031400 8.38
/gps/hist/point 0.0000031625 0
/gps/hist/point 0.0000031901 28
/gps/hist/point 0.0000032512 0
/gps/hist/point 0.0000032952 27.2
/gps/hist/point 0.0000033360 17.87
/gps/hist/point 0.0000034454 0
/gps/hist/point 0.0000034989 67.4
/gps/hist/point 0.0000035368 21.35
/gps/hist/point 0.0000036643 0
/gps/hist/point 0.0000037092 100
/gps/hist/point 0.0000039154 0
/gps/hist/point 0.0000039478 39.3
/gps/hist/point 0.0000039705 11.05

```

```

/gps/hist/point 0.0000040091 7.24
/gps/hist/point 0.0000041751 0
/gps/hist/point 0.0000042393 5.16
# 0.75 cm out
/gps/source/add 0.1145497
/gps/particle opticalphoton
/gps/pos/type Volume
/gps/pos/shape Ellipsoid
/gps/pos/centre 0. 0. 0. cm
/gps/pos/halfx 2.25 cm
/gps/pos/halfy 2.25 cm
/gps/pos/halfz 0.90 cm
/gps/ang/type beam1d
/gps/ene/type User
/gps/hist/type energy
/gps/hist/point 0.0000029013 0
/gps/hist/point 0.0000029245 7.08
/gps/hist/point 0.0000030497 0
/gps/hist/point 0.0000030961 8.07
/gps/hist/point 0.0000031400 8.38
/gps/hist/point 0.0000031625 0
/gps/hist/point 0.0000031901 28
/gps/hist/point 0.0000032512 0
/gps/hist/point 0.0000032952 27.2
/gps/hist/point 0.0000033360 17.87
/gps/hist/point 0.0000034454 0
/gps/hist/point 0.0000034989 67.4
/gps/hist/point 0.0000035368 21.35
/gps/hist/point 0.0000036643 0
/gps/hist/point 0.0000037092 100
/gps/hist/point 0.0000039154 0
/gps/hist/point 0.0000039478 39.3
/gps/hist/point 0.0000039705 11.05
/gps/hist/point 0.0000040091 7.24
/gps/hist/point 0.0000041751 0
/gps/hist/point 0.0000042393 5.16
# 1 cm out SPHERE
/gps/source/add 0.0729369
/gps/particle opticalphoton
/gps/pos/type Volume
/gps/pos/shape Sphere
/gps/pos/centre 0. 0. 0. cm
/gps/pos/radius 1.75 cm
/gps/ang/type beam1d
/gps/ene/type User
/gps/hist/type energy
/gps/hist/point 0.0000029013 0
/gps/hist/point 0.0000029245 7.08
/gps/hist/point 0.0000030497 0
/gps/hist/point 0.0000030961 8.07
/gps/hist/point 0.0000031400 8.38
/gps/hist/point 0.0000031625 0
/gps/hist/point 0.0000031901 28

```

```

/gps/hist/point 0.0000032512 0
/gps/hist/point 0.0000032952 27.2
/gps/hist/point 0.0000033360 17.87
/gps/hist/point 0.0000034454 0
/gps/hist/point 0.0000034989 67.4
/gps/hist/point 0.0000035368 21.35
/gps/hist/point 0.0000036643 0
/gps/hist/point 0.0000037092 100
/gps/hist/point 0.0000039154 0
/gps/hist/point 0.0000039478 39.3
/gps/hist/point 0.0000039705 11.05
/gps/hist/point 0.0000040091 7.24
/gps/hist/point 0.0000041751 0
/gps/hist/point 0.0000042393 5.16
# 1.5 cm out SPHERE
/gps/source/add 0.0341884
/gps/particle opticalphoton
/gps/pos/type Volume
/gps/pos/shape Sphere
/gps/pos/centre 0. 0. 0. cm
/gps/pos/radius 2.25 cm
/gps/ang/type beam1d
/gps/ene/type User
/gps/hist/type energy
/gps/hist/point 0.0000029013 0
/gps/hist/point 0.0000029245 7.08
/gps/hist/point 0.0000030497 0
/gps/hist/point 0.0000030961 8.07
/gps/hist/point 0.0000031400 8.38
/gps/hist/point 0.0000031625 0
/gps/hist/point 0.0000031901 28
/gps/hist/point 0.0000032512 0
/gps/hist/point 0.0000032952 27.2
/gps/hist/point 0.0000033360 17.87
/gps/hist/point 0.0000034454 0
/gps/hist/point 0.0000034989 67.4
/gps/hist/point 0.0000035368 21.35
/gps/hist/point 0.0000036643 0
/gps/hist/point 0.0000037092 100
/gps/hist/point 0.0000039154 0
/gps/hist/point 0.0000039478 39.3
/gps/hist/point 0.0000039705 11.05
/gps/hist/point 0.0000040091 7.24
/gps/hist/point 0.0000041751 0
/gps/hist/point 0.0000042393 5.16
# 2 cm out SPHERE
/gps/source/add 0.0126649
/gps/particle opticalphoton
/gps/pos/type Volume
/gps/pos/shape Sphere
/gps/pos/centre 0. 0. 0. cm
/gps/pos/radius 2.75 cm
/gps/ang/type beam1d

```

```

/gps/ene/type User
/gps/hist/type energy
/gps/hist/point 0.0000029013 0
/gps/hist/point 0.0000029245 7.08
/gps/hist/point 0.0000030497 0
/gps/hist/point 0.0000030961 8.07
/gps/hist/point 0.0000031400 8.38
/gps/hist/point 0.0000031625 0
/gps/hist/point 0.0000031901 28
/gps/hist/point 0.0000032512 0
/gps/hist/point 0.0000032952 27.2
/gps/hist/point 0.0000033360 17.87
/gps/hist/point 0.0000034454 0
/gps/hist/point 0.0000034989 67.4
/gps/hist/point 0.0000035368 21.35
/gps/hist/point 0.0000036643 0
/gps/hist/point 0.0000037092 100
/gps/hist/point 0.0000039154 0
/gps/hist/point 0.0000039478 39.3
/gps/hist/point 0.0000039705 11.05
/gps/hist/point 0.0000040091 7.24
/gps/hist/point 0.0000041751 0
/gps/hist/point 0.0000042393 5.16
# 2.5 cm out SPHERE
/gps/source/add 0.0028307
/gps/particle opticalphoton
/gps/pos/type Volume
/gps/pos/shape Sphere
/gps/pos/centre 0. 0. 0. cm
/gps/pos/radius 3.25 cm
/gps/ang/type beam1d
/gps/ene/type User
/gps/hist/type energy
/gps/hist/point 0.0000029013 0
/gps/hist/point 0.0000029245 7.08
/gps/hist/point 0.0000030497 0
/gps/hist/point 0.0000030961 8.07
/gps/hist/point 0.0000031400 8.38
/gps/hist/point 0.0000031625 0
/gps/hist/point 0.0000031901 28
/gps/hist/point 0.0000032512 0
/gps/hist/point 0.0000032952 27.2
/gps/hist/point 0.0000033360 17.87
/gps/hist/point 0.0000034454 0
/gps/hist/point 0.0000034989 67.4
/gps/hist/point 0.0000035368 21.35
/gps/hist/point 0.0000036643 0
/gps/hist/point 0.0000037092 100
/gps/hist/point 0.0000039154 0
/gps/hist/point 0.0000039478 39.3
/gps/hist/point 0.0000039705 11.05
/gps/hist/point 0.0000040091 7.24
/gps/hist/point 0.0000041751 0

```



```
/gps/hist/point 0.0000042393 5.16  
#  
/control/execute run.mac
```

## GEANT4 Header Files

### *DetectorConstruction*

```
//  
//  
#include "DetectorConstruction.hh"  
#include "G4Box.hh"  
#include "G4Colour.hh"  
#include "G4LogicalVolume.hh"  
#include "G4Material.hh"  
#include "G4NistManager.hh"  
#include "G4PVPlacement.hh"  
#include "G4RunManager.hh"  
#include "G4Tubs.hh"  
#include "G4Ellipsoid.hh"  
#include "G4VisAttributes.hh"  
  
#include "G4Sphere.hh"  
  
#include "G4SDManager.hh"  
  
DetectorConstruction::DetectorConstruction()  
  :fpWorldLogical(0)  
  ,fpWorldPhysical(0)  
{  
  
DetectorConstruction::~~DetectorConstruction() {}  
  
G4VPhysicalVolume* DetectorConstruction::Construct()  
{  
  // Material Definition  
  DefineMaterials();  
  
  // Geometry Definition  
  SetupGeometry();  
  
  // Return world volume  
  return fpWorldPhysical;  
}  
  
void DetectorConstruction::DefineMaterials()  
{  
  G4String symbol;  
  G4double a, z, density;  
  G4int ncomponents;  
  G4double fractionmass;
```

```

// Define materials

// U metal (all U-238)
G4Material* lU = new G4Material("Umetal",z = 92,a = 238.0507847*g/mole,density
    = 18.9*g/cm3);

// Define elements
G4Element* C = new G4Element("carbon",symbol="C",z=6,a=12.01073589*g/mole);
G4Element* H = new G4Element("hydrogen",symbol="H",z=1,a=1.007940754*g/mole);
G4Element* N = new G4Element("Nitrogen",symbol="N",z=7.,a=14.01*g/mole);
G4Element* O = new G4Element("Oxygen",symbol="O",z=8.,a=16.00*g/mole);
//
// Define air
G4Material* air = new G4Material("Air",density= 1.290*mg/cm3, ncomponents=2);
air->AddElement(N, fractionmass=0.7);
air->AddElement(O, fractionmass=0.3);

// Define vacuum
G4Material* vacuum = new G4Material("Galactic",z=1.,a=1.01*g/mole,
    density=universe_mean_density, kStateGas, 0.1*kelvin, 1.e-19*pascal);

// Dump material information
G4cout << *(G4Material::GetMaterialTable()) << G4endl;
}

void DetectorConstruction::SetupGeometry()
{
//G4Material* air = G4Material::GetMaterial("Air");
G4Material* air = G4NistManager::Instance()->FindOrBuildMaterial("G4_AIR");
G4Material* vacuum = G4Material::GetMaterial("Galactic");

// World volume
G4Box* worldSolid = new G4Box("World_Solid", // Name
    5.0*cm, 5.0*cm, 5.0*cm); // Half lengths

fpWorldLogical = new G4LogicalVolume(worldSolid, // Solid
    air, // Material
    "World_Logical"); // Name

fpWorldPhysical = new G4PVPlacement(0, // Rotation matrix pointer
    G4ThreeVector(), // Translation vector
    fpWorldLogical, // Logical volume
    "World_Physical", // Name
    0, // Mother volume
    false, // Unused boolean parameter
    0); // Copy number

////////////////////////////////////
G4Material* Umetal = G4Material::GetMaterial("Umetal");

    G4VSolid* UmetalSolid = new G4Tubs("Umetal_solid", 0, 1.49*cm,
        0.149*cm, 0, 360*degree);

```

```

G4LogicalVolume* UmetalLogical = new G4LogicalVolume(UmetalSolid, // Solid
Umetal, // Material
"Umetal_Logical"); // Name

new G4PVPlacement(0, // Rotation matrix pointer
G4ThreeVector(0, 0, 0), // Translation vector
UmetalLogical, // Logical volume
"Solid_Physical", // Name
fpWorldLogical, // Mother volume
false, // Unused boolean parameter
0); // Copy number

////////////////////////////////////

// Detector Volume
G4double detectorhalflength = 5.0*cm;
G4double detectorthickness = 0.025*cm; // detector half thickness
G4double detectorplacement = 4.025*cm;

G4VSolid* DetectorSolidY = new G4Box("Detector_SolidY", detectorhalflength,
detectorthickness, detectorhalflength);

G4VSolid* DetectorSolidZ = new G4Box("Detector_SolidZ", detectorhalflength,
detectorhalflength, detectorthickness);

G4LogicalVolume* DetectorLogicalY =
new G4LogicalVolume(DetectorSolidY, air, "Detector_LogicalY");

G4LogicalVolume* DetectorLogicalZ =
new G4LogicalVolume(DetectorSolidZ, air, "Detector_LogicalZ");

new G4PVPlacement(0, G4ThreeVector(0.,0.,-detectorplacement), DetectorLogicalZ,
"Detector_Physical-Z", fpWorldLogical, false, 0);

////////////////////////////////////
// Visualisation attributes

// Invisible world volume.
fpWorldLogical->SetVisAttributes(G4VisAttributes::Invisible);

// Detector - Green with transparency
G4VisAttributes* detectorAttributes =
new G4VisAttributes(G4Colour::Green());
detectorAttributes->SetVisibility(true);
// DetectorLogicalX->SetVisAttributes(detectorAttributes);
DetectorLogicalY->SetVisAttributes(detectorAttributes);
DetectorLogicalZ->SetVisAttributes(detectorAttributes);

// Umetal
G4VisAttributes* OuterAttributes = new G4VisAttributes(G4Colour::Yellow());//
OuterAttributes->SetForceSolid(true);
UmetalLogical->SetVisAttributes(OuterAttributes);

```

## *PhysicsList*

```
// *****
//In LowerEcutoff
// $Id: G4EmLivermorePhysics.cc,v 1.12 2010-10-10 15:18:34 vnivanch Exp $
// GEANT4 tag $Name: geant4-09-05

#include "G4EmLivermorePhysics.hh"
#include "PhysicsList.hh"
#include "G4ParticleDefinition.hh"
#include "G4ProcessManager.hh"
#include "G4Decay.hh"

// *** Processes and models

// gamma
#include "G4PhotoElectricEffect.hh"
#include "G4LivermorePhotoElectricModel.hh"

#include "G4ComptonScattering.hh"
#include "G4LivermoreComptonModel.hh"

#include "G4GammaConversion.hh"
#include "G4LivermoreGammaConversionModel.hh"

#include "G4RayleighScattering.hh"
#include "G4LivermoreRayleighModel.hh"

#include "G4SynchrotronRadiation.hh"
#include "G4TransitionRadiation.hh"
#include "G4Cerenkov.hh"
#include "G4Scintillation.hh"
#include "G4OpAbsorption.hh"
#include "G4OpRayleigh.hh"
#include "G4OpMieHG.hh"
#include "G4OpBoundaryProcess.hh"
// e+-
#include "G4eMultipleScattering.hh"
#include "G4UniversalFluctuation.hh"

#include "G4eIonisation.hh"
#include "G4LivermoreIonisationModel.hh"

#include "G4eBremsstrahlung.hh"
#include "G4LivermoreBremsstrahlungModel.hh"

// e+
#include "G4eplusAnnihilation.hh"

// mu+-
#include "G4MuMultipleScattering.hh"
#include "G4MuIonisation.hh"
#include "G4MuBremsstrahlung.hh"
```

```

#include "G4MuPairProduction.hh"

// hadrons
#include "G4hMultipleScattering.hh"
#include "G4MscStepLimitType.hh"

#include "G4hBremsstrahlung.hh"
#include "G4hPairProduction.hh"

#include "G4hIonisation.hh"
#include "G4ionIonisation.hh"
#include "G4alphaIonisation.hh"
#include "G4IonParametrisedLossModel.hh"
#include "G4NuclearStopping.hh"

// msc models
#include "G4UrbanMscModel95.hh"
#include "G4WentzelVIModel.hh"
#include "G4GoudsmitSaundersonMscModel.hh"
#include "G4CoulombScattering.hh"

// interfaces
#include "G4LossTableManager.hh"
#include "G4EmProcessOptions.hh"
#include "G4UAtomicDeexcitation.hh"

// particles

#include "G4Gamma.hh"
#include "G4Electron.hh"
#include "G4Positron.hh"
#include "G4MuonPlus.hh"
#include "G4MuonMinus.hh"
#include "G4PionPlus.hh"
#include "G4PionMinus.hh"
#include "G4KaonPlus.hh"
#include "G4KaonMinus.hh"
#include "G4Proton.hh"
#include "G4AntiProton.hh"
#include "G4Deuteron.hh"
#include "G4Triton.hh"
#include "G4He3.hh"
#include "G4Alpha.hh"
#include "G4GenericIon.hh"

//
#include "G4PhysicsListHelper.hh"
#include "G4BuilderType.hh"

//...ooo0000ooo.....ooo0000ooo.....ooo0000ooo.....ooo0000ooo.....

PhysicsList::PhysicsList()
  :G4VUserPhysicsList()
{

```

```

    G4LossTableManager::Instance();
    // SetPhysicsType(bElectromagnetic); // 'SetPhysicsType' identifier mpt found
                                        // make: *** [tmp/WIN32-
VC/Main/PhysicsList.o] Error 2
}

//....ooo0000ooo.....ooo0000ooo.....ooo0000ooo.....ooo0000ooo.....

PhysicsList::~PhysicsList() {}

//....ooo0000ooo.....ooo0000ooo.....ooo0000ooo.....ooo0000ooo.....

void PhysicsList::ConstructParticle()
{
    // gamma
    G4Gamma::Gamma();
    G4OpticalPhoton::OpticalPhotonDefinition();
    // leptons
    G4Electron::Electron();
    G4Positron::Positron();
    G4MuonPlus::MuonPlus();
    G4MuonMinus::MuonMinus();

    // mesons
    G4PionPlus::PionPlusDefinition();
    G4PionMinus::PionMinusDefinition();
    G4KaonPlus::KaonPlusDefinition();
    G4KaonMinus::KaonMinusDefinition();

    // baryons
    G4Proton::Proton();
    G4AntiProton::AntiProton();

    // ions
    G4Deuteron::Deuteron();
    G4Triton::Triton();
    G4He3::He3();
    G4Alpha::Alpha();
    G4GenericIon::GenericIonDefinition();
}

//....ooo0000ooo.....ooo0000ooo.....ooo0000ooo.....ooo0000ooo.....

void PhysicsList::ConstructProcess()
{
    AddTransportation();
    G4PhysicsListHelper* ph = G4PhysicsListHelper::GetPhysicsListHelper();

    // Add Livermore EM Processes

    theParticleIterator->reset();

    while( (*theParticleIterator)() ){

```

```

G4ParticleDefinition* particle = theParticleIterator->value();
G4String particleName = particle->GetParticleName();

G4double LivermoreHighEnergyLimit = GeV;

if (particleName == "gamma") {

    G4PhotoElectricEffect* thePhotoElectricEffect = new G4PhotoElectricEffect();
    G4LivermorePhotoElectricModel* theLivermorePhotoElectricModel =
        new G4LivermorePhotoElectricModel();
    theLivermorePhotoElectricModel-
>SetHighEnergyLimit(LivermoreHighEnergyLimit);
    thePhotoElectricEffect->AddEmModel(0, theLivermorePhotoElectricModel);
    ph->RegisterProcess(thePhotoElectricEffect, particle);

    G4ComptonScattering* theComptonScattering = new G4ComptonScattering();
    G4LivermoreComptonModel* theLivermoreComptonModel =
        new G4LivermoreComptonModel();
    theLivermoreComptonModel->SetHighEnergyLimit(LivermoreHighEnergyLimit);
    theComptonScattering->AddEmModel(0, theLivermoreComptonModel);
    ph->RegisterProcess(theComptonScattering, particle);

    G4GammaConversion* theGammaConversion = new G4GammaConversion();
    G4LivermoreGammaConversionModel* theLivermoreGammaConversionModel =
        new G4LivermoreGammaConversionModel();
    theLivermoreGammaConversionModel-
>SetHighEnergyLimit(LivermoreHighEnergyLimit);
    theGammaConversion->AddEmModel(0, theLivermoreGammaConversionModel);
    ph->RegisterProcess(theGammaConversion, particle);

    G4RayleighScattering* theRayleigh = new G4RayleighScattering();
    G4LivermoreRayleighModel* theRayleighModel = new G4LivermoreRayleighModel();
    theRayleighModel->SetHighEnergyLimit(LivermoreHighEnergyLimit);
    theRayleigh->AddEmModel(0, theRayleighModel);
    ph->RegisterProcess(theRayleigh, particle);

} else if (particleName == "e-") {

    G4eMultipleScattering* msc = new G4eMultipleScattering();
    msc->AddEmModel(0, new G4UrbanMscModel195());
    //msc->AddEmModel(0, new G4GoudsmitSaundersonMscModel());
    msc->SetStepLimitType(fUseDistanceToBoundary);
    ph->RegisterProcess(msc, particle);

    // Ionisation
    G4eIonisation* eIoni = new G4eIonisation();
    G4LivermoreIonisationModel* theIoniLivermore = new
        G4LivermoreIonisationModel();
    theIoniLivermore->SetHighEnergyLimit(1*MeV);
    eIoni->AddEmModel(0, theIoniLivermore, new G4UniversalFluctuation() );
    eIoni->SetStepFunction(0.2, 100*um); //
    ph->RegisterProcess(eIoni, particle);

    // Bremsstrahlung

```

```

G4eBremsstrahlung* eBrem = new G4eBremsstrahlung();
G4LivermoreBremsstrahlungModel* theBremLivermore = new
    G4LivermoreBremsstrahlungModel();
theBremLivermore->SetHighEnergyLimit(LivermoreHighEnergyLimit);
eBrem->AddEmModel(0, theBremLivermore);
ph->RegisterProcess(eBrem, particle);

} else if (particleName == "e+") {

    // Identical to G4EmStandardPhysics_option3

    G4eMultipleScattering* msc = new G4eMultipleScattering();
    msc->AddEmModel(0, new G4UrbanMscModel195());
    //msc->AddEmModel(0, new G4GoudsmitSaundersonMscModel());
    msc->SetStepLimitType(fUseDistanceToBoundary);
    G4eIonisation* eIoni = new G4eIonisation();
    eIoni->SetStepFunction(0.2, 100*um);

    ph->RegisterProcess(msc, particle);
    ph->RegisterProcess(eIoni, particle);
    ph->RegisterProcess(new G4eBremsstrahlung(), particle);
    ph->RegisterProcess(new G4eplusAnnihilation(), particle);

} else if (particleName == "mu+" ||
           particleName == "mu-" ) {

    // Identical to G4EmStandardPhysics_option3

    G4MuMultipleScattering* msc = new G4MuMultipleScattering();
    msc->AddEmModel(0, new G4WentzelVIModel());
    G4MuIonisation* muIoni = new G4MuIonisation();
    muIoni->SetStepFunction(0.2, 50*um);

    ph->RegisterProcess(msc, particle);
    ph->RegisterProcess(muIoni, particle);
    ph->RegisterProcess(new G4MuBremsstrahlung(), particle);
    ph->RegisterProcess(new G4MuPairProduction(), particle);
    ph->RegisterProcess(new G4CoulombScattering(), particle);

} else if (particleName == "alpha" ||
           particleName == "He3" ) {

    // Identical to G4EmStandardPhysics_option3

    G4ionIonisation* ionIoni = new G4ionIonisation();
    ionIoni->SetStepFunction(0.1, 10*um);

    ph->RegisterProcess(new G4hMultipleScattering(), particle);
    ph->RegisterProcess(ionIoni, particle);
    ph->RegisterProcess(new G4NuclearStopping(), particle);

} else if (particleName == "GenericIon") {

    // Identical to G4EmStandardPhysics_option3

```



```

G4ionIonisation* ionIoni = new G4ionIonisation();
ionIoni->SetEmModel(new G4IonParametrisedLossModel());
ionIoni->SetStepFunction(0.1, 1*um);

ph->RegisterProcess(new G4hMultipleScattering(), particle);
ph->RegisterProcess(ionIoni, particle);
ph->RegisterProcess(new G4NuclearStopping(), particle);

} else if (particleName == "pi+" ||
           particleName == "pi-" ||
           particleName == "kaon+" ||
           particleName == "kaon-" ||
           particleName == "proton" ) {

// Identical to G4EmStandardPhysics_option3

G4hIonisation* hIoni = new G4hIonisation();
hIoni->SetStepFunction(0.2, 50*um);

ph->RegisterProcess(new G4hMultipleScattering(), particle);
ph->RegisterProcess(hIoni, particle);
ph->RegisterProcess(new G4hBremsstrahlung(), particle);
ph->RegisterProcess(new G4hPairProduction(), particle);

} else if (particleName == "B+" ||
           particleName == "B-" ||
           particleName == "D+" ||
           particleName == "D-" ||
           particleName == "Ds+" ||
           particleName == "Ds-" ||
           particleName == "anti_He3" ||
           particleName == "anti_alpha" ||
           particleName == "anti_deuteron" ||
           particleName == "anti_lambda_c+" ||
           particleName == "anti_omega-" ||
           particleName == "anti_proton" ||
           particleName == "anti_sigma_c+" ||
           particleName == "anti_sigma_c++" ||
           particleName == "anti_sigma+" ||
           particleName == "anti_sigma-" ||
           particleName == "anti_triton" ||
           particleName == "anti_xi_c+" ||
           particleName == "anti_xi-" ||
           particleName == "deuteron" ||
           particleName == "lambda_c+" ||
           particleName == "omega-" ||
           particleName == "sigma_c+" ||
           particleName == "sigma_c++" ||
           particleName == "sigma+" ||
           particleName == "sigma-" ||
           particleName == "tau+" ||
           particleName == "tau-" ||
           particleName == "triton" ||

```

```

        particleName == "xi_c+" ||
        particleName == "xi-" ) {

    // Identical to G4EmStandardPhysics_option3

    ph->RegisterProcess(new G4hMultipleScattering(), particle);
    ph->RegisterProcess(new G4hIonisation(), particle);

}
}

// Em options
//
G4EmProcessOptions opt;
opt.SetFluo(true);
opt.SetPIXE(true);
opt.SetVerbose(verbose);

// Multiple Coulomb scattering
//
opt.SetPolarAngleLimit(0.2);

// Physics tables
//

opt.SetMinEnergy(0.1*eV);
opt.SetMaxEnergy(1*GeV);
opt.SetDEDXBinning(220);
opt.SetLambdaBinning(220);

// Ionization
//
//opt.SetSubCutoff(true);

// Deexcitation
//
G4VAtomDeexcitation* de = new G4UAtomicDeexcitation();
G4LossTableManager::Instance()->SetAtomDeexcitation(de);
de->SetFluo(true);

}

//...ooo0000ooo.....ooo0000ooo.....ooo0000ooo.....ooo0000ooo.....

void PhysicsList::ConstructGeneral()
{
    // Add Decay Process
    G4Decay* theDecayProcess = new G4Decay();

    theParticleIterator->reset();

    while( (*theParticleIterator)() ){
        G4ParticleDefinition* particle = theParticleIterator->value();
        G4ProcessManager* pmanager = particle->GetProcessManager();

```

```

    if (theDecayProcess->IsApplicable(*particle)) {
        pmanager ->AddProcess(theDecayProcess);

        // Set ordering for PostStepDoIt and AtRestDoIt
        pmanager ->SetProcessOrdering(theDecayProcess, idxPostStep);
        pmanager ->SetProcessOrdering(theDecayProcess, idxAtRest);
    }
}

void PhysicsList::SetCuts()
{
    if (verboseLevel > 0){
        G4cout << "PhysicsList::SetCuts:";
        G4cout << "CutLength : " << G4BestUnit(defaultCutValue,"Length") << G4endl;
    }

    // Set cut values for gamma first since some e+/e- processes
    // need gamma cut values
    SetCutValue(10e-6*mm, "gamma");
    SetCutValue(10e-6*mm, "e-");
    SetCutValue(10e-6*mm, "e+");

    if (verboseLevel > 0) DumpCutValuesTable();
}

```

### *PrimaryGeneratorAction*

```

// $Id:$
// GEANT4 tag $Name:$
//
// T. Aso          Original author
//
#include "PrimaryGeneratorAction.hh"
#include "G4Event.hh"
#include "G4GeneralParticleSource.hh"
#include "G4ParticleTable.hh"
#include "G4ParticleDefinition.hh"

PrimaryGeneratorAction::PrimaryGeneratorAction()
{
    particleGun = new G4GeneralParticleSource();
}

PrimaryGeneratorAction::~~PrimaryGeneratorAction()
{
    delete particleGun;
}

void PrimaryGeneratorAction::GeneratePrimaries(G4Event* anEvent)
{

```

```

    particleGun->GeneratePrimaryVertex(anEvent) ;
}

```

### *EventAction*

```

#include "EventAction.hh"
#include "G4Event.hh"
#include "G4Timer.hh"
#include "G4UnitsTable.hh"

```

```

EventAction::EventAction():drawFlag("all")
{
    //timer = new G4Timer;
}

```

```

EventAction::~EventAction()
{
    //delete timer;
}

```

```

void EventAction::BeginOfEventAction(const G4Event* evt)
{
    G4int evtNb = evt->GetEventID();
    if(evtNb%1000000 == 0) {
        G4cout << "EV: " << evt->GetEventID() << G4endl;
    }
}

```

```

void EventAction::EndOfEventAction(const G4Event* evt)
{ }

```

### *RunAction*

```

#include "RunAction.hh"
//#include "Run.hh"
#include "G4Run.hh"
#include "G4RunManager.hh"
#include "G4UnitsTable.hh"
#include <assert.h>
#include "G4VTouchable.hh"
#include <fstream>

```

```

RunAction::RunAction()
{
    G4cout << "Opening output file..." << G4endl;
    outfile.open("output.csv");
}

```

```

RunAction::~RunAction()
{
    outfile.close();
}

```

```

void RunAction::BeginOfRunAction(const G4Run*)
{
}

```

### *SteppingAction*

```
#include "SteppingAction.hh"
```

```
#include "G4Track.hh"
#include "DetectorConstruction.hh"
// #include "EventAction.hh"
#include "RunAction.hh"
```

```
#include "G4Step.hh"
```

```
#include "G4StepPoint.hh"
#include "G4TrackStatus.hh"
#include "G4VTouchable.hh"
#include "G4SteppingManager.hh"
#include "G4RunManager.hh"
```

```
SteppingAction::SteppingAction(DetectorConstruction* det, RunAction* run)
    : detector(det), runaction(run)
{
    hitNumber = 0;
}

```

```
SteppingAction::~SteppingAction()
{ }

```

```
void SteppingAction::UserSteppingAction(const G4Step* aStep)
{

```

```

    // G4cout << "Stepping Action..." << G4endl;
    G4double X, Y, Z;

    G4StepPoint * thePrePoint = aStep->GetPreStepPoint();
    G4VPhysicalVolume * thePrePV = thePrePoint->GetPhysicalVolume();
    G4double pEnergy = aStep->GetTrack()->GetKineticEnergy();
    G4String pName = aStep->GetTrack()->GetParticleDefinition()-
>GetParticleName();
    G4String thePrePVname = thePrePV->GetName();

    // Kills particle passing through "Solid_Physical"
    if((thePrePVname.find("Solid_Physical") != std::string::npos )
        && thePrePoint->GetStepStatus() == fGeomBoundary) {
        aStep->GetTrack()->SetTrackStatus(fStopAndKill);
    }
}

```

```

    }

    if((thePrePVname.find("Detector_Physical") != std::string::npos )
        && thePrePoint->GetStepStatus() == fGeomBoundary) {
        hitNumber++;
        //G4cout << "Particle name: " << pName << G4endl;
        X = aStep->GetPreStepPoint()->GetPosition().x();
        Y = aStep->GetPreStepPoint()->GetPosition().y();
        Z = aStep->GetPreStepPoint()->GetPosition().z();

        //runaction->AddHit(pName,X,Y,Z,pEnergy);
        runaction-
>AddHit(hitNumber,pName,X,Y,Z,pEnergy,thePrePVname);

        aStep->GetTrack()->SetTrackStatus(fStopAndKill);
    }
}

```

### *Main*

```

//
#include "DetectorConstruction.hh"
#include "PhysicsList.hh"
#include "PrimaryGeneratorAction.hh"
// User defined run action
#include "RunAction.hh"
#include "G4RunManager.hh"
#include "G4UImanager.hh"
#include "G4UIterminal.hh"
#include "Randomize.hh"
#include "EventAction.hh"

#include "SteppingAction.hh"
#include "RunAction.hh"

#ifdef G4UI_USE
#include "G4UIExecutive.hh"
#endif

#ifdef G4VIS_USE
#include "G4VisExecutive.hh"
#endif

int main(int argc, char** argv) {

    // Seed the random number generator manually
    //
    //G4long myseed = 4921974514;
    //CLHEP::HepRandom::setTheSeed(myseed);
    // Run manager

```

```

G4RunManager * runManager = new G4RunManager;

// Mandatory initialization classes
DetectorConstruction* detector = new DetectorConstruction;
runManager->SetUserInitialization(detector);
runManager->SetUserInitialization(new PhysicsList);

// User action classes
runManager->SetUserAction(new PrimaryGeneratorAction());

RunAction* run_action = new RunAction();
runManager->SetUserAction(run_action);

EventAction* event_action = new EventAction();
runManager->SetUserAction(event_action);

G4UserSteppingAction* stepping_action =
    new SteppingAction(detector, run_action);
runManager->SetUserAction(stepping_action);

// User defined run action
//runManager->SetUserAction(new RunAction);
// Initialize G4 kernel
runManager->Initialize();

#ifdef G4VIS_USE
// Visualization manager
G4VisManager* visManager = new G4VisExecutive;
visManager->Initialize();
#endif

G4UImanager* UImanager = G4UImanager::GetUIpointer();

if (argc!=1) // batch mode
{
    G4String command = "/control/execute ";
    G4String fileName = argv[1];
    UImanager->ApplyCommand(command+fileName);
}
else
{ // interactive mode :define UI session
#ifdef G4UI_USE
G4UIExecutive* ui = new G4UIExecutive(argc, argv);
#ifdef G4VIS_USE
UImanager->ApplyCommand("/control/execute volsrc.mac");
#endif
if (ui->IsGUI())
    UImanager->ApplyCommand("/control/execute visTutor/gui.mac");
ui->SessionStart();
delete ui;
#endif
}
// Job termination
#ifdef G4VIS_USE

```

```
    delete visManager;  
#endif  
  
    delete runManager;  
return 0;  
}
```



## APPENDIX C

### SAMPLE PYTHON FILES

#### *Mean and Standard Deviation Calculation + Simulated Images*

```
from mayavi import mlab
import csv
from math import sqrt
import numpy as np
import matplotlib.pyplot as plt
from mpl_toolkits.mplot3d import Axes3D
import matplotlib.cm as cm
import matplotlib as mpl
import os

Nbins = 512 # number of pixels
MatrixNegZ = [[0 for x in xrange(Nbins)] for x in xrange(Nbins)]
MatrixPosZ = [[0 for x in xrange(Nbins)] for x in xrange(Nbins)]
MatrixNegY = [[0 for x in xrange(Nbins)] for x in xrange(Nbins)]
MatrixPosY = [[0 for x in xrange(Nbins)] for x in xrange(Nbins)]
MatrixNegX = [[0 for x in xrange(Nbins)] for x in xrange(Nbins)]
MatrixPosX = [[0 for x in xrange(Nbins)] for x in xrange(Nbins)]

HalfLength = 50.00 #half length of FoV
BinLength = 2*HalfLength/Nbins #camera pixel bin size

text_file = open("Results.txt", "w")
text_file.write("Camera FOV half length = " + str(HalfLength) + "\n")
text_file.write("# Pixels in calculation = " + str(Nbins) + "\n")
#text_file1.close()

Totalrownum = 0
files = [file for file in os.listdir('.') if file.endswith(".csv")]
print files
n=0
while n<len(files):
    fname = files[n]
    print fname
    ifile = open(fname,"rb")
    reader = csv.reader(ifile)
    rownum = 0
    for row in reader:
        if row[6] == "Detector_Physical-Z":
            X = float(row[2])
            Y = float(row[3])
            for i in xrange(0, Nbins):
                A = -HalfLength + i* BinLength
                B = -HalfLength + (i + 1)* BinLength
                if X > A and X < B:
```

```

        Xbin = i
        break
        i += 1
    for j in xrange(0, Nbins):
        C = -HalfLength + j * BinLength
        D = -HalfLength + (j + 1) * BinLength
        if Y > C and Y < D:
            Ybin = j
            break
        j += 1
    currentE = MatrixNegZ[Xbin][Ybin]
    E = float(row[5])
    MatrixNegZ[Xbin][Ybin]=currentE + E

elif row[6] == "Detector_Physical+Z":
    X = float(row[2])
    Y = float(row[3])
    for i in xrange(0, Nbins):
        A = -HalfLength + i * BinLength
        B = -HalfLength + (i + 1) * BinLength
        if X > A and X < B:
            Xbin = i
            break
            i += 1
    for j in xrange(0, Nbins):
        C = -HalfLength + j * BinLength
        D = -HalfLength + (j + 1) * BinLength
        if Y > C and Y < D:
            Ybin = j
            break
        j += 1
    currentE = MatrixPosZ[Xbin][Ybin]
    E = float(row[5])
    MatrixPosZ[Xbin][Ybin]=currentE + E

elif row[6] == "Detector_Physical-Y":
    X = float(row[2])
    Z = float(row[4])
    for i in xrange(0, Nbins):
        A = -HalfLength + i * BinLength
        B = -HalfLength + (i + 1) * BinLength
        if X > A and X < B:
            Xbin = i
            break
            i += 1
    for j in xrange(0, Nbins):
        C = -HalfLength + j * BinLength
        D = -HalfLength + (j + 1) * BinLength
        if Z > C and Z < D:
            Zbin = j
            break
        j += 1
    currentE = MatrixNegY[Xbin][Zbin]

```

```

E = float(row[5])
MatrixNegY[Xbin][Zbin]=currentE + E

elif row[6] == "Detector_Physical+Y":
    X = float(row[2])
    Z = float(row[4])
    for i in xrange(0, Nbins):
        A = -HalfLength + i* BinLength
        B = -HalfLength + (i + 1)* BinLength
        if X > A and X < B:
            Xbin = i
            break
        i += 1
    for j in xrange(0, Nbins):
        C = -HalfLength + j * BinLength
        D = -HalfLength + (j + 1)* BinLength
        if Z > C and Z < D:
            Zbin = j
            break
        j += 1
    currentE = MatrixPosY[Xbin][Zbin]
    E = float(row[5])
    MatrixPosY[Xbin][Zbin]=currentE + E

elif row[6] == "Detector_Physical-X":
    Y = float(row[3])
    Z = float(row[4])
    for i in xrange(0, Nbins):
        A = -HalfLength + i* BinLength
        B = -HalfLength + (i + 1)* BinLength
        if Y > A and Y < B:
            Ybin = i
            break
        i += 1
    for j in xrange(0, Nbins):
        C = -HalfLength + j * BinLength
        D = -HalfLength + (j + 1)* BinLength
        if Z > C and Z < D:
            Zbin = j
            break
        j += 1
    currentE = MatrixNegX[Ybin][Zbin]
    E = float(row[5])
    MatrixNegX[Ybin][Zbin]=currentE + E

elif row[6] == "Detector_Physical+X":
    Y = float(row[3])
    Z = float(row[4])
    for i in xrange(0, Nbins):
        A = -HalfLength + i* BinLength
        B = -HalfLength + (i + 1)* BinLength
        if Y > A and Y < B:
            Ybin = i

```

```

        break
        i += 1
    for j in xrange(0, Nbins):
        C = -HalfLength + j * BinLength
        D = -HalfLength + (j + 1) * BinLength
        if Z > C and Z < D:
            Zbin = j
            break
        j += 1
    currentE = MatrixPosX[Ybin][Zbin]
    E = float(row[5])
    MatrixPosX[Ybin][Zbin]=currentE + E

    rownum+=1
ifile.close()
print "ifile close"
Totalrownum = Totalrownum + rownum
n+=1

def MatrixAddition (a,b):
    d=[]
    n=0
    while n<len(a):
        c=[]
        k=0
        while k<len(a[0]):
            c.append(a[n][k]+b[n][k])
            k+=1
        n+=1
        d.append(c)
    return (d)

def MatrixSum(a):
    numrows = len(a)
    numcols = len(a[0])
    total = 0

    for i in range(numrows):
        for j in range(numcols):
            total = total + a[i][j]
    return(total)
TotalEnergySumNegZ = MatrixSum(MatrixNegZ)
TotalEnergySumPosY = MatrixSum(MatrixPosY)

def MatrixMean(a):
    numrows = len(a)
    numcols = len(a[0])
    total = 0

    for i in range(numrows):
        for j in range(numcols):
            total = total + a[i][j]

```

```

    return(total/(numrows*numcols))

meanNegZ = MatrixMean(MatrixNegZ)

meanPosY = MatrixMean(MatrixPosY)

def MatrixStdDev(a):
    numrows = len(a)
    numcols = len(a[0])
    N = numrows*numcols
    s = 0
    Mean = MatrixMean(a)

    for i in range(numrows):
        for j in range(numcols):
            s = s + (a[i][j]-Mean)**2
    return(sqrt(s/(N-1)))

StdDevNegZ = MatrixStdDev(MatrixNegZ)

StdDevPosY = MatrixStdDev(MatrixPosY)

text_file.write("Total # of rows = " + str(Totalrownum) + "\n")
text_file.write("Total Energy Sum NegZ = " + str(TotalEnergySumNegZ) + "\n")
text_file.write("\n")
text_file.write("Total # of rows = " + str(Totalrownum) + "\n")
text_file.write("Total Energy Sum PosY = " + str(TotalEnergySumPosY) + "\n")
text_file.write("\n")
text_file.write("Mean NegZ = " + str(meanNegZ) + "\n")
text_file.write("StdDev NegZ = " + str(StdDevNegZ) + "\n")
text_file.write("\n")
text_file.write("Mean PosY = " + str(meanPosY) + "\n")
text_file.write("StdDev PosY = " + str(StdDevPosY) + "\n")

text_file.close()

# images
f = mlab.figure(size = (900,800))
mlab.view(0,0)
mlab.surf(MatrixNegZ, colormap = 'spectral')
mlab.colorbar(orientation='vertical')
mlab.savefig('NegZcolorbar.tiff')
mlab.surf(MatrixNegZ, colormap = 'spectral', vmax=27.2, vmin=0)
mlab.colorbar(orientation='vertical')
mlab.savefig('NegZcolorScale.tiff')
mlab.surf(MatrixNegZ, colormap = 'gray')
mlab.colorbar(orientation='vertical')
mlab.savefig('NegZgray.tiff')
mlab.close()

print "done"

```

## Sample Error and Variance of Variance Calculation

```
#VoV

from mayavi import mlab
import csv
from math import sqrt
import numpy as np
import matplotlib.pyplot as plt
from mpl_toolkits.mplot3d import Axes3D
import matplotlib.cm as cm
import matplotlib as mpl
import os

text_file = open("VoV.txt", "w")

M = 0
Esum = 0
files = [file for file in os.listdir('.') if file.endswith(".csv")]
print files
n=0
while n<len(files):
    fname = files[n]
    print fname
    ifile = open(fname,"rb")
    reader = csv.reader(ifile)
    rownum = 0
    for row in reader:
        if row[6] == "Detector_Physical-Z":
            currentE = Esum
            E = float(row[5])
            Esum = currentE + E
            M = M + 1
        elif row[6] == "Detector_Physical+Z":
            currentE = Esum
            E = float(row[5])
            Esum = currentE + E
            M = M + 1
        rownum+=1
    ifile.close()
    print "ifile close"

    n+=1

print Esum
print M
mean = Esum / M
mean = float(mean)
print mean

n = 0
X = 0
```

```

Y = 0
U = 0
T = 0
currentY = 0
currentU = 0
while n<len(files):
    fname = files[n]
    print fname
    ifile = open(fname,"rb")
    reader = csv.reader(ifile)
    rownum = 0
    for row in reader:
        if row[6] == "Detector_Physical-Z" :
            currentY = Y
            currentU = U
            E = float(row[5])
            X = (E - mean)**2
            Y = currentY + X
            T = (E - mean)**4
            U = currentU + T
        elif row[6] == "Detector_Physical+Z":
            currentY = Y
            currentU = U
            E = float(row[5])
            X = (E - mean)**2
            Y = currentY + X
            T = (E - mean)**4
            U = currentU + T
        rownum+=1
    ifile.close()
    print "ifile close"

    n+=1

N = M * 1.000000000000
Z = (1/(N-1))

error = sqrt(Y*Z)
print error

VoV = ((U/(Y**2))-(1/N))
print VoV

text_file.write("Total # of rows = " + str(M) + "\n")
text_file.write("Total # of rows 2 = " + str(N) + "\n")
text_file.write("E sum = " + str(Esum) + "\n")
text_file.write("Mean = " + str(mean) + "\n")
text_file.write("\n")
text_file.write("Error = " + str(error) + "\n")
text_file.write("\n")
text_file.write("VoV = " + str(VoV) + "\n")
text_file.close()
print "done"

```